NPS ARCHIVE
1964
LEWIS, S.

MORPHOLOGY OF UNSTABLE WAVES IN A BAROCLINIC JET

STANLEY P. LEWIS

DUDLEY KNOX LIBRARY
NAVAL POSTGRADUATE SCHOOL
MONTEREY, CA 93943-5101

LIBRARY
U.S. NAVAL POSTGRADUATE SCHOOL
MONTEREY, CALIFORNIA

MORPHOLOGY OF UNSTABLE WAVES IN A BAROCLINIC JET

* * * * *

STANLEY P. LEWIS

MORPHOLOGY OF UNSTABLE WAVES IN A BAROCLINIC JET

by

Stanley P. Lewis
Captain, United States Marine Corps

Submitted in partial fulfillment of
the requirements for the degree of

MASTER OF SCIENCE
IN
METEOROLOGY

United States Naval Postgraduate School
Monterey, California

1 9 6 4

PS Archive
364
Lewis, S.

LIBRARY
U.S. NAVAL POSTGRADUATE SCHOOL
MONTEREY, CALIFORNIA

MORPHOLOGY OF UNSTABLE WAVES IN A BAROCLINIC JET

by

Stanley P. Lewis

This work is accepted as fulfilling
the thesis requirements for the degree of
MASTER OF SCIENCE
IN
METEOROLOGY
from the
United States Naval Postgraduate School

ABSTRACT

Solution of a system of second-order partial differential equations obtained from linearized approximations to the vorticity and thermodynamic equations yields phase velocities and amplitude functions which are utilized to compute particular solutions of the perturbation stream function field over a net of grid points. These values are combined linearly to obtain general solutions over the entire wave which describe the three-dimensional structure of the perturbations for selected time intervals. Equations for the particular and general perturbation vertical pressure velocities are set forth. A selection of cases representing various vertical and lateral wind profiles and static stability fields, wave lengths, and latitudes are pictured in three dimensions over a 72-hour period. These preliminary results indicate unexpected retrogression of waves of moderate wave length imposed upon a current exhibiting vertical and horizontal jet-like flow.

TABLE OF CONTENTS

LIST OF ILLUSTRATIONS

TABLE OF SYMBOLS

R -- the gas constant for dry air

T -- the absolute temperature

C_p -- the coefficient of specific heat for constant pressure

f -- the coriolis parameter: $f = 2\Omega \sin\phi$

$\bar{f}$ -- the coriolis parameter at latitude 45N

g -- the vertical component of the acceleration due to gravity

t -- time

p -- the atmospheric pressure

P -- the pressure across a vertical layer

ω -- the pressure velocity: $\omega = dp/dt$

β -- the Rossby parameter: $\beta = \partial f/\partial y$

σ -- a static stability parameter (defined in text)

σ' -- a static stability parameter (defined in text)

λ -- the wave length

μ -- $\mu = 2\pi/\lambda$

c -- the phase velocity of a wave

r -- as a subscript, the real component of a complex quantity

i -- as a subscript, the imaginary component of a complex quantity

d -- a linear coefficient

$\mathbb{V}$ -- the wind velocity vector

∇ -- the gradient operator

ϕ -- the latitude

Φ -- the geopotential

Ψ -- the stream function

$\overline{\Psi}$ -- the basic stream function

Ψ' -- the perturbation stream function

Ψ' -- the general perturbation stream function

Ψ_{oo} -- the amplitude function of Ψ'

ω' -- the perturbation pressure velocity

W -- the amplitude function of ω'

U -- the basic wind flow

A -- the amplitude function of Ψ'

Ω -- the scalar angular velocity of the earth's rotation

f -- the relative vorticity

1. Introduction.

The behavior of atmospheric waves under the multitude of conditions occurring in nature has long been a primary field of interest for the dynamic meteorologist. Various authors have dealt with different aspects of the subject, including energy relationships, phase velocities, stability characteristics, and the three-dimensional structure. Each author has in turn defined a mathematical model with its associated boundary conditions and described some of its physical characteristics. It is the purpose of this paper to enlarge upon the knowledge of a particular model atmosphere, specifically the one utilized by Haltiner (1963) in his exploratory study of dynamic instability in a baroclinic jet as determined by certain finite-difference approximations. Haltiner described the effects of varying grid mesh size, wind profile, latitude, and static stability upon the occurrence of unstable phase velocities. At one point he stated that it would be possible to construct a complete solution to his particular system of equations although the phase velocities themselves, as indicators of dynamic instability, were the area of primary interest of his paper.

The aim of this study is to depict the three-dimensional structure of the waves described by Haltiner, both in the general sense and in terms of the particular contribution of each component of the phase velocity.

The amplification or damping of the waves with time is treated, as is the phase relationship of the thermal wave and the 500-mb contour wave.

Finite-difference approximations are utilized for both vertical and horizontal derivatives. The effects of a jet-like wind profile upon wave structure and development are deemed to be of primary interest; however variations in other parameters such as static stability, latitude, and grid mesh size are considered to some extent also. For comparative purposes, barotropic and simplified baroclinic cases are included for a selected wave length.

2. Derivation of the basic equations.

The vorticity equation in the following form is used:

$$\frac{\partial f}{\partial t} + \mathbf{V}\cdot\nabla(f+f) = \bar{f}\frac{\partial \omega}{\partial p} \tag{1}$$

where $\mathbf{V} = \hat{k} \times \nabla \Psi$, i.e. the flow is non-divergent.

The first law of thermodynamics for adiabatic motion is expressed as:

$$\frac{\partial T}{\partial t} + \mathbf{V}\cdot\nabla T - \sigma'\omega = 0 \tag{2}$$

where

$$\sigma' = \frac{RT}{pC_p} - \frac{\partial T}{\partial p} \tag{3}$$

Utilizing the approximation $\frac{\partial \Phi}{\partial p} \doteq \bar{f}\frac{\partial \Psi}{\partial p}$, the hydrostatic relationship, and the equation of state for a perfect gas, (2) may be expressed in terms of the stream function as follows:

$$\frac{\partial}{\partial t}\left(\frac{\partial \Psi}{\partial p}\right) + \mathbf{V}\cdot\nabla\frac{\partial \Psi}{\partial p} + \sigma\omega = 0 \tag{4}$$

where

$$\sigma = \frac{R}{p\bar{f}}\sigma' \tag{5}$$

The system of equations composed of (1) and (4) are then linearized by the perturbation method, with $\Psi = \bar{\Psi}(y,p) + \Psi'(x,y,p,t)$ and $\omega = \omega'(x,y,p,t)$, giving

$$\frac{\partial \Psi'}{\partial t} + U\frac{\partial}{\partial x}\nabla^2\Psi' + \frac{\partial \Psi'}{\partial x}\left(\beta - \frac{\partial^2 U}{\partial y^2}\right) = \bar{f}\frac{\partial \omega'}{\partial p} \tag{6}$$

and

$$\frac{\partial}{\partial t}\left(\frac{\partial \psi'}{\partial p}\right)+U\frac{\partial}{\partial x}\left(\frac{\partial \psi'}{\partial p}\right)-\frac{\partial \psi'}{\partial x}\frac{\partial U}{\partial p}+\sigma\,\omega'=0 \tag{7}$$

where U(y,p) represents the basic flow.

Substitution of the assumed harmonic solutions $\psi' = A\, e^{i\mu(x-ct)}$ and $\omega' = W\, e^{i\mu(x-ct)}$ into (6) and (7) results in the following equations in A, W, and c:

$$(U-c)\frac{\partial^2 A}{\partial y^2}+\left[\beta-\frac{\partial^2 U}{\partial y^2}-\mu^2(U-c)\right]A+\frac{i\bar{f}}{\mu}\frac{\partial W}{\partial p}=0 \tag{8}$$

$$(U-c)\frac{\partial A}{\partial p}-\frac{\partial U}{\partial p}A-\frac{i\sigma}{\mu}W=0 \quad . \tag{9}$$

The boundary conditions assumed are A=0 at the lateral bounds and W=0 at the vertical bounds. The form of the amplitude function A may be specified at the upper and lower boundaries by substituting the vertical boundary conditions into (9), yielding

$$(U-c)\frac{\partial A}{\partial p}-\frac{\partial U}{\partial p}A=0 \tag{10}$$

at p=0 and $p=p_0$=1000 mb. At this point, Haltiner [1] eliminated W from the system of (8) and (9) by differentiating (9) in respect to p, yielding an equation in A:

$$(U-c)\left(\frac{\partial^2 A}{\partial y^2}+\frac{\bar{f}}{\sigma}\frac{\partial^2 A}{\partial p^2}\right)-\frac{\bar{f}(U-c)}{\sigma^2}\frac{\partial \sigma}{\partial p}\frac{\partial A}{\partial p}+$$

$$\left[\beta-\frac{\partial^2 U}{\partial y^2}-\mu^2(U-c)-\frac{\bar{f}}{\sigma}\frac{\partial^2 U}{\partial p^2}+\frac{\bar{f}}{\sigma^2}\frac{\partial \sigma}{\partial p}\frac{\partial U}{\partial p}\right]A=0 \quad . \tag{11}$$

Centered difference approximations were then used to write (11) as a system of algebraic equations, with forward and backward differences applied as necessary at the boundaries. The atmosphere was divided into N layers of thickness P, with k=0 at 0 mb and k=N at 1000 mb. It was assumed that the perturbations were laterally symmetrical with respect to the center of the basic flow, so that computations might be restricted to one-half of the current laterally. This half was divided into M bands with j=0 at the center of the basic current and j=M at the northern bound.

Solution of the difference equation

$$\frac{(U_{j,k}-c)}{d^2}A_{j-1,k}+\left\{-(U_{j,k}-c)\left[\frac{2}{d^2}+\frac{2\bar{f}}{P^2\bar{\sigma}_{j,k}}+\left(\frac{2\pi}{\lambda}\right)^2\right]+\beta-\right.$$

$$\frac{(U_{j+1,k}-2U_{j,k}+U_{j-1,k})}{d^2}-\frac{\bar{f}}{P^2\bar{\sigma}_{j,k}}\left(U_{j,k+1}-2U_{j,k}+U_{j,k-1}\right)+$$

$$\left.\frac{\bar{f}}{4P^2\bar{\sigma}_{j,k}}\left(\bar{\sigma}_{j,k+1}-\bar{\sigma}_{j,k-1}\right)\left(U_{j,k+1}-U_{j,k-1}\right)\right\}A_{j,k}+\frac{(U_{j,k}-c)}{d^2}A_{j+1,k}+$$

$$\frac{\bar{f}(U_{j,k}-c)}{P^2\bar{\sigma}_{j,k}}\left[1-\frac{(\bar{\sigma}_{j,k+1}-\bar{\sigma}_{j,k-1})}{4\bar{\sigma}_{j,k}}\right](A_{j,k-1}+A_{j,k+1})=0,$$

$$j=0,1,\ldots(M-1)\;;\quad k=1,2,\ldots(N-1)\;. \tag{12}$$

with lateral boundary conditions

$$A_{M,k}=0,\ (k=0,1,\ldots N)\;;\ A_{-j,k}=A_{1,k} \tag{12a}$$

and vertical boundary conditions

$$A_{j,N} = A_{j,N-1}\frac{(U_{j,N}-c)}{(U_{j,N-1}-c)} \quad , \quad A_{j,0} = A_{j,1}\frac{(U_{j,0}-c)}{(U_{j,1}-c)} \tag{12b}$$

for c, the phase velocity, led to Haltiner's findings concerning the occurrence of dynamic instability under various conditions. Slight modification of the digital computer program utilized for computation yields the values of the A's, the amplitude functions, as well. For any given root c there are associated values of A for each and every grid point being considered. These known values of amplitude and phase velocity, both of which are complex, can be used to evaluate the harmonic solution

$$\psi' = A\, e^{i\mu(x-ct)} \tag{13}$$

for each value of c computed. The solution may be expanded into the form

$$\psi_r' + i\psi_i' = (A_r + iA_i)\left[\cos\mu(x-c_r t) + i\sin\mu(x-c_r t)\right] e^{\mu c_i t} \tag{14}$$

yielding the real particular solutions

$$\psi_r' = \left[A_r \cos\mu(x-c_r t) - A_i \sin\mu(x-c_r t)\right] e^{\mu c_i t} \tag{15}$$

The particular solutions for ω', the perturbation vertical motion, can now be obtained by returning first to equation (9) and solving for W:

$$W = \frac{\mu}{i\sigma}\left[(U-c)\frac{\partial A}{\partial p} - A\frac{\partial U}{\partial p}\right] \tag{16}$$

Expanding W, A, and c into real and imaginary portions and equating corresponding terms on the right and left yields the first order partial differential equations

$$W_r = \frac{\mu}{\sigma}\left[\frac{\partial A_i}{\partial p}(U - c_r) - c_i \frac{\partial A_r}{\partial p} - A_i \frac{\partial U}{\partial p}\right] \tag{17a}$$

and

$$W_i = \frac{\mu}{\sigma}\left[\frac{\partial A_r}{\partial p}(c_r - U) - c_i \frac{\partial A_i}{\partial p} + A_r \frac{\partial U}{\partial p}\right] . \tag{17b}$$

These amplitude functions can be computed from the corresponding linear difference equations

$$W_{r_{j,k}} = \frac{\mu}{2P\sigma_{j,k}}\left[(A_{i_{j,k+1}} - A_{i_{j,k-1}})(U_{j,k} - c_r) - c_i(A_{r_{j,k+1}} - A_{r_{j,k-1}}) - A_{i_{j,k}}(U_{j,k+1} - U_{j,k-1})\right] \tag{18a}$$

and

$$W_{i_{j,k}} = \frac{\mu}{2P\sigma_{j,k}}\left[(A_{r_{j,k+1}} - A_{r_{j,k-1}})(c_r - U_{j,k}) - c_i(A_{i_{j,k+1}} - A_{i_{j,k-1}}) + A_{r_{j,k}}(U_{j,k+1} - U_{j,k-1})\right] . \tag{18b}$$

At the vertical bounds, forward differences are substituted for the central difference approximations; for example, at the upper bound

$$\frac{A_{j,k+1} - A_{j,k}}{P} \tag{19}$$

and at the lower bound,

$$\frac{A_{j,N} - A_{j,N-1}}{P} \tag{20}$$

where the range of k is from 1 to N, from top to bottom.

With the phase velocities and their associated "W's" now known, the particular ω's can be calculated from the harmonic form

$$\omega' = W e^{i\mu(x-ct)} \tag{21}$$

in the same fashion that Ψ' was computed from (13). Thus we have

$$\omega'_r = [W_r \cos\mu(x-c_r t) - W_i \sin\mu(x-c_r t)] e^{\mu c_i t} \tag{22}$$

The physical appearance of the perturbation wave and its associated vertical motions are now described explicitly for each particular value of the phase velocity c. However, the general form of the wave represents a sum of all these solutions, each contributing to the total wave form in some way. Thus, the general solution Ψ' can be expressed as a linear combination of the particular solutions:

$$\Psi'(x,y,p,t) = \sum_{n=1}^{N} d_n A_n e^{i\mu(x-c_n t)} \tag{23}$$

where there are N different roots c to the frequency equation, and where d, A, and c are complex. Since the A's and c's are known, it is possible to calculate the values of the linear coefficients, the d's, if an initial wave form

is specified.

The initial wave form chosen herein decreases in amplitude laterally as

$$\sin \frac{\pi}{2}\left(1-\frac{j-1}{3}\right),\ j=1 \text{ at the jet axis.} \tag{24}$$

In the vertical, the initial wave has a tilt of $\lambda/8$ from 1000 mb to 0 mb, i.e. forty-five degrees of tilt in phase, as described by

$$e^{i\mu(x+\alpha)} \tag{25}$$

where

$$\alpha = \frac{\lambda(P_o - p)}{8 P_o}\ , \quad P_o = 1000 \text{ mb}. \tag{26}$$

Thus, the initial assumed wave form varies vertically as

$$e^{\frac{i\pi(P_o-(k-1)P)}{4P_o}}\ , \quad P = 250 \text{ mb}\ , \ P_o = 1000 \text{ mb} \tag{27}$$

for a four-layer model, with k=1 to 5 from top to bottom.

Let the initial wave be referred to as $\Psi'_{x,o}$ where

$$\Psi'_{x,o} = \Psi_{oo}\, e^{i\mu x} \tag{28}$$

Now, by expanding Ψ_{oo} into its real and imaginary portions, the following expressions result:

$$\Psi_{oo_r} = \sin\frac{\pi}{2}\left(1-\frac{j-1}{3}\right)\cos\frac{\pi}{4P_o}\left(P_o-(k-1)P\right) \tag{29a}$$

$$\Psi_{oo_i} = \sin\frac{\pi}{2}\left(1-\frac{j-1}{3}\right)\sin\frac{\pi}{4P_o}\left(P_o-(k-1)P\right) \tag{29b}$$

The form of the initial wave over the entire wave length is given by

$$\Psi'_{x,o} = \Psi_{oo}\, e^{i\mu x} = (\Psi_{oo_r} + i\,\Psi_{oo_i})(\cos\mu x + i \sin\mu x) \tag{30}$$

or

$$\Psi'_{x,o_r} = \Psi_{oo_r} \cos\mu x - \Psi_{oo_i} \sin\mu x \tag{31a}$$

$$\Psi_{x,o_i} = \Psi_{oo_i} \cos\mu x + \Psi_{oo_r} \sin\mu x \,. \tag{31b}$$

The general solution of the form of the perturbation stream function for all x and t can now be obtained by evaluating the coefficients of the general solution (23) necessary to give this initial wave form. Expansion of (23) yields

$$\Psi'_{x,t} = \sum_{n=1}^{N} \left\{ \left[(d_{n_r} A_{n_r} - d_{n_i} A_{n_i}) + i\,(d_{n_r} A_{n_i} + d_{n_i} A_{n_r}) \right] e^{i\mu (x - c_{n_r} t - i\, c_{n_i} t)} \right\} \tag{32}$$

from whence

$$\Psi'_{x,t} = \sum_{n=1}^{N} \left\{ \left[(d_{n_r} A_{n_r} - d_{n_i} A_{n_i}) + i\,(d_{n_r} A_{n_i} + d_{n_i} A_{n_r}) \right] \left[\cos\mu(x - c_{n_r} t) + i \sin\mu (x - c_{n_r} t) \right] e^{\mu c_{n_i} t} \right\} \tag{33}$$

Equating real and imaginary portions leads to

$$\Psi'_{x,t_r} = \sum_{n=1}^{N} \left\{ \left[\cos\mu(x - c_{n_r} t)(d_{n_r} A_{n_r} - d_{n_i} A_{n_i}) - \sin\mu (x - c_{n_r} t)\, (d_{n_r} A_{n_i} + d_{n_i} A_{n_r}) \right] e^{\mu c_{n_i} t} \right\} \tag{34a}$$

and

$$\Psi'_{x,t_i} = \sum_{n=1}^{N} \left\{ \left[\sin\mu(x - c_{n_r} t)\left(d_{n_r} A_{n_r} - d_{n_i} A_{n_i}\right) + \cos\mu(x - c_{n_r} t)\right.\right.$$

$$\left.\left.\left(d_{n_r} A_{n_i} + d_{n_i} A_{n_r}\right)\right] e^{\mu c_{n_i} t} \right\} \tag{34b}$$

Setting x and t equal to zero, these reduce to

$$\Psi'_r = \sum_{n=1}^{N} \left(d_{n_r} A_{n_r} - d_{n_i} A_{n_i}\right) \tag{35a}$$

$$\Psi'_i = \sum_{n=1}^{N} \left(d_{n_r} A_{n_i} + d_{n_i} A_{n_r}\right) \tag{35b}$$

Equations (35a) and (35b) comprise a system of thirty linear equations with thirty unknowns when three bands are considered laterally and four levels vertically. This system can be expressed as a product of matrices

$$A X = B \tag{36}$$

where

$$A = \begin{array}{c} n=1,\ldots \qquad\qquad ,N;1,\ldots \qquad N \\ \left[\begin{array}{c|c} A_{n_r} & -A_{n_i} \\ \hline A_{n_i} & A_{n_r} \end{array}\right] \end{array} \tag{37}$$

$$X = \begin{bmatrix} dn_r \\ \hline dn_i \end{bmatrix} \begin{matrix} n=1 \\ \vdots \\ N \\ n=1 \\ \vdots \\ N \end{matrix} \qquad (38)$$

and

$$B = \begin{bmatrix} \Psi_{oo_r} \\ \\ \Psi_{oo_i} \end{bmatrix} . \qquad (39)$$

This matrix equation can now be solved by multiplying both sides by A inverse, yielding the solution

$$X = A^{-1} B . \qquad (40)$$

In the present case, the elements of the X column matrix are the real and imaginary linear coefficients dn_r and dn_i. Thus, the complete general perturbation stream function can now be obtained from equations (34a) and (34b).

Computation of the d's also makes possible calculation of the vertical motion in this rather general wave. Equations (18a) and (18b) gave the particular values of W_r and W_i for each component phase velocity. These

amplitude functions may be substituted into the expression

$$\omega' = \sum_{n=1}^{N} dn\, Wn\, e^{i\mu(x-cnt)} \tag{41}$$

to yield the general solution for ω', since the vertical motions are dependent upon the stream function both initially and with increasing time. Expanding (41) into its complex components and equating the real portions leads to

$$\omega'_r = \sum_{n=1}^{N} \Big\{ \Big[\cos\mu(x-c_{n_r}t)(dn_r Wn_r - dn_i Wn_i) - \sin\mu(x-c_{n_r}t)(dn_r Wn_i + dn_i Wn_r) \Big] e^{\mu c_{n_i} t} \Big\} \tag{42}$$

which describes the general perturbation pressure velocity at all points for all time.

All the equations necessary to describe both the perturbation stream function and the vertical notion for the various component phase velocities and for the total wave have now been written. The thermal wave between 250 mb and 500 mb can be obtained by simple subtraction of computed general stream function values at those respective levels.

An incidental bit of information concerning the amplification rate of a particular wave component can be gleaned from the harmonic solution; setting the exponential $e^{\mu c_i t}$ equal to two and solving for t gives the time

required for that particular component to double (or halve) its amplitude.

3. Programming and computation.

All computation was performed on a Control Data Corporation 1604 digital computer. FORTRAN 60 was used exclusively as the programming medium.

Calculation of the phase velocities and amplitude functions was accomplished by a standard matrix inversion scheme, described in some detail by Haltiner [1]. Storage limitations precluded enlarging on that basic program for further computation, so a binary tape output was utilized to feed subsequent operations, a regretable but necessary expedient. Solution of equation (36) was accomplished with COOP subroutine MATINV, a Jordan matrix inversion routine which is quite economical with space. However, solution of the system for a five-by-three grid involves inversion and multiplication of 30 by 30 matrices; it can be seen that computations involving the full nine-by-six grid described by Haltiner would require similar manipulation of 108 by 108 matrices, which is beyond the capability of the installation. For this reason, the five-by-three grid with Δp=250 mb and a lateral grid mesh of 500 km was selected for all computation. Variations in results would be expected if other grid intervals were used; it is an unfortunate attribute of finite-difference methods that numerical results are determined not only by the dynamics of the system but also to some degree by the characteristics of the grid employed. It is hoped that the omission of

higher order roots has been of relatively minor importance in the portrayal of the subject perturbations.

4. Results.

Although Haltiner [1] in his original investigation dealt with a system with up to 54 grid points at which solutions could be obtained in any one vertical cross section, computer storage limits associated with the solution of equation (36) restricted computation to a net with five vertical levels and three grid points laterally, no calculations being performed at the fourth, northernmost grid point. Thus alternate values were taken from Haltiner's tables of zonal wind and static stability parameter for use in this study. The latitude in all cases, save one, was assumed to be 45 degrees, with $\bar{f}=1.03\times10^{-4}$ sec^{-1}, $\beta=1.63\times10^{-13}$ $sec^{-1}cm^{-1}$; and the total width of the basic current in all cases was taken to be 3000 km, resulting in a lateral grid mesh of 500 km. The vertical grid spacing is 250 mb. The wind profile of Table 1 is described by the expression U=B(1-cos2 y/D), with B=30 m sec^{-1} at the level of maximum wind, 250 mb, which profile has been previously employed by Wiin-Nielsen [2] and Haltiner [1]. The σ values Haltiner obtained from a temperature field based upon mean soundings near a jet core over a 12-day period in December, 1946 and the geostrophic thermal wind, with subsequent smoothing. The right-marginal column of Table 2 shows the average value of for each pressure level. These average values were used in the computation of the first six cases.

Table 1. Zonal wind velocity U in m sec^{-1}.

1	0	0	0	0
2	0	15.00	45.00	60.00
3	0	4.50	13.50	18.00
4	0	1.75	5.25	7.00
5	0	0	0	0
k/j	4	3	2	1

Table 2. Static stability in MTS units ($sec^3 ton^{-2}$)

1	-	10^3	10^3	10^3	10^3
2	-	52.70	41.40	21.90	42.54
3	-	4.79	5.12	5.65	5.08
4	-	2.00	2.15	2.01	2.08
5	-	1.05	1.15	1.25	1.13
k/j	4	3	2	1	

The initial wave is identical in structure for all cases. The horizontal scale of the illustrations varies from case to case, and in all cases spans one complete wave length. The lateral scale is fixed, each diagram at each individual pressure level extending northward from the jet axis a distance of 1500 km. Contours in the illustrations are labeled in MTS units; in most instances, the highest (lowest) central values of ridges (troughs) are also furnished. It should be noted however that these values may or may not

be absolute maxima or minima, but represent only the value of the grid point nearest the enclosed maximum or minimum. These values may be somewhat misleading, as can be seen for all cases at time t=0, where the central values of all troughs and ridges should be unity but do in fact vary from $\pm$ 1 to $\pm$.92 due to grid-point spacing. Therefore, only the general magnitude of the perturbations and the form of the wave should be considered by the reader. The absolute magnitudes of the perturbations are meaningless, since the assumed amplitude of the initial wave is completely arbitrary; relative magnitudes, with the restrictions just mentioned, between different cases and different time intervals are quite significant, however. The units of the perturbations presented in the figures and discussed in the text are those normally associated with the stream function, $m^2\ sec^{-1}$; however, since only the relative magnitudes of the perturbations have physical significance they will be referred to henceforth simply as numbers, omitting the units, to avoid possible confusion in the mind of the reader with more familiar synoptic values of the stream function. The depicted values will be more meaningful if it is noted that the initial maximum (minimum) at each level is +1 (-1), or +.5 (-.5) for the thermal wave. Thus, a Ψ' maximum of 3.0 at 1000 mb after 72 hours indicates a three-fold increase in the intensity of the ridge at that level, while a maximum of 3.0 in the thermal

wave after the same time lapse would represent a six-fold amplification of the thermal ridge.

In viewing the illustrations, the reader should bear in mind that they represent only perturbations of the stream function, not the complete wave. A true picture of the wave could be easily obtained by adding the perturbation quantities to the basic stream function values at each level as determined from the wind velocity-contour gradient relationship. Thus a closed negative perturbation center represents a trough in the total stream function field.

Before delving into the effects of the baroclinic three-dimensional jet structure upon the perturbation field, let us consider some simpler models as a basis for comparison.

Case 1 represents a barotropic situation with a stability parameter of 20 MTS units at all grid points and the basic flow constant in the vertical, having the value of the wind at the level of maximum wind, 250 mb. The horizontal jet structure remains; the wave length of the perturbation is 6000 km. Figure 1 shows that the wave is progressive at all levels, moving approximately 3500 km in 72 hours at 500 mb. The ridges and troughs amplify nearly five-fold during that time, growth being nearly uniform at all levels. The tilt of the troughs and ridges becomes nearly vertical over the interval. The thermal wave as measured between the 250-mb and 750-mb levels is very flat throughout the period, damping to a low of $\pm.23$ at t=48 hours

and increasing to only $\pm.29$ at t=72 hours. Its movement relative to the 500-mb wave is interesting; the thermal wave moves rapidly from its lagging position to a point directly under the 500-mb wave at t=12 hours and thence well ahead of the upper wave at t=24 hours. The rapid movement continues until at 72 hr it appears that a complete 360-degree phase change has been accomplished, for the thermal troughs and ridges occupy much the same position relative to the 500-mb wave as they did initially. At 36 hr , the maximum and minimum centers in the thermal wave appear to move northward away from the center of the flow; this is most likely due to grid point placement, although there is some deformation noticeable in the 250-mb and 750-mb waves with increasing time.

Case 2 utilizes the same wave length and wind field as Case 1 but represents an atmosphere with lower static stability, σ =2 MTS units. Movement of the wave at 500 mb appears to be slightly more rapid than the previous case. Amplification at 500 mb is very nearly the same as that of Case 1, but increased amplification at 250 mb and decreased development at 750 mb lead to a thermal wave with steady growth, more than doubling in intensity in 72 hr. The tilt of the wave is vertical after 72 hr; the thermal wave is directly in phase with the contour wave, having progressed steadily from its initial lagging position to a point directly under the 500-mb wave.

Case 3 represents a pure baroclinic atmosphere with the σ of the jet axis, j=1 in Table 2, constant horizontally at each level. The basic flow is jet-like vertically, having the profile of column j=1 in Table 1 at all points; the wave length is 6000 km. The wave is progressive, moving approximately 1700 km in 72 hr, less than half the movement of the barotropic cases. Amplification of the wave is moderate at 500 mb, the perturbation tripling in intensity in 72 hr, but the growth at the 250-mb level is nearly seven-fold. This, coupled with the rather small growth at 750 mb, gives a rapidly amplifying thermal wave which moves smoothly from its initial following position to a point directly in phase with the 500-mb contour wave. At this time, the wave shows a more complicated vertical structure than the preceding cases, tilting westward from 1000 mb to 500 mb, then rising vertically to 250 mb, and finally tilting eastward sharply to the top. This last feature should be regarded with suspicion since the development of the wave is erratic at the top in the figures. The most striking feature of Case 3 is the marked lack of deformation of the wave form at all levels throughout the period.

The next three cases considered utilize the zonal winds (U) of Table 1 and the average static stability parameter ($\bar{\sigma}$) of Table 2.

Case 4 represents a wave length of 2000 km. As might be expected of so short a wave, it is progressive, but only very slightly so at 500 mb. At the two lower levels the behavior of the wave is rather complicated and its shape badly deformed; the progression at 1000 mb is extremely rapid and the resulting vertical shear undoubtedly contributes to the complication at 750 mb. Because of the splitting of the low and high centers and the lateral skewing of troughs and ridges the life history of the wave's tilt is difficult to describe; however, the general picture after 72 hr is an eastward tilt above 250 mb and a tilt westward from 1000 mb up to that level, although the wave is nearly vertical in the middle layers. The perturbations vary widely in magnitude between different levels and time intervals, showing a steady growth only at 1000 mb. The thermal wave is fairly flat, reaching its maximum intensity at 48 hr and then damping somewhat by the end of the period. Its position relative to the 500-mb wave shifts rather rapidly rearward, apparently undergoing a 360-degree movement by t=60 hr and ending the three-day period 180° out of phase with the upper wave.

Case 5 has a wave length of 6000 km, but its behavior differs radically from that of the 6000-km waves previously discussed. It is more deformed in many instances; its perturbations have grown only slightly or have diminished by the end of the period, in most cases having reached an

intermediate maximum; but above all, it is retrogressive in movement, proceeding westward nearly 6000 km during the three-day period. The tilt is still generally westward after 72 hours, although the three middle levels are more or less vertically oriented. The thermal wave first moves through the 500-mb wave to a slightly leading position, then returns to lie approximately in phase with the upper wave at the end of the period. The retrogression of the contour perturbations in this case is unexpected in view of the behavior of synoptic waves of like wave length. Eliasen [3] has shown that atmospheric waves at approximately the same latitude and with wave lengths between 5000 and 6000 km generally progress in an easterly direction with a speed of about nine degrees of longitude per day, with occasional quasi-stationary periods of a week or so. Shorter waves seemed to move consistently toward the east.

Case 6 is a longer wave, 14,000 km, which exhibits only slight deformation, steady, moderate amplification, and moderate retrogression, moving westward some 2500 km in three days. The tilt is simple in its history, becoming vertical with time with a very slight eastward tilt above 250 mb. The thermal wave development is fairly strong, increasing from $\pm.5$ to ±3.5 over the period, due to the rather marked intensification at 250 mb; it moves toward the position of the 500-mb wave, lagging only very slightly after 72 hr. Eliasen [3] has indicated that actual waves of

this length in the atmosphere generally fluctuate about a mean position, only in a few cases moving more than a quarter of a wave length in either direction.

To further delineate the effects of the three-dimensional jet structure, the same three wave lengths were imposed upon an atmosphere with a linearly increasing wind in the vertical. The basic flow increases linearly from 1000 mb to the level of maximum wind of Table 1 and continues in the same fashion to the 0-mb level. The model has stability $\overline{\sigma}$ of Table 2, and a horizontally jet-like flow.

Case 7, with wave length 2000 km, is progressive at 500 mb and below, but the movement is erratic and hard to follow in 12-hour increments in the two top levels because of the extreme deformation. The amplification is extreme at 1000 mb and rather large at the top and at 500 mb; the 250-mb and 750-mb waves alternately weaken and intensify but never to any great degree, resulting in a fairly flat thermal wave which reaches its greatest proportions at 72 hr where it lies behind the 500-mb wave.

Case 8 represents a wave length of 6000 km and is slowly retrogressive in comparison with Case 5. It exhibits strange growth characteristics, intensifying for 36 hr above 1000 mb, then weakening for another 36 hr. The 1000-mb level shows alternate weakening and building in a pattern out of phase with the overlying layers. The final

result is a wave slightly intensified at 500 mb and below, slightly weakened in the two top levels, and approximately vertical in tilt. The thermal wave moves slowly forward through the 500-mb wave, traveling eastward rapidly in the last 12 hr and weakening to its lowest values; after 72 hr, the weak thermal troughs underlie the 500-mb ridges.

Case 9, wave length 14,000 km, is also slowly retrogressive and intensifies strongly at the top level, decreasing in strength with decreasing height at the end of the period. The wave after 72 hr tilts eastward from 1000 mb to 750 mb and thence rises vertically to the top. The thermal wave amplifies steadily from $\pm.36$ to ±3, and moves eastward relative to the 500-mb wave to a position just slightly to its rear. The waves in Cases 8 and 9 show very little deformation, the greatest occurring at 1000 mb.

As a matter of practical interest, an example was run using some data from actual soundings, an example also treated by Haltiner [1]. Table 3 lists the basic flow and stability pattern, which is based upon averages for 12 instances in December, 1946; the values for the top layer were taken by Haltiner from tabulated 100-mb and 150-mb figures, although the top level is treated mathematically as 0 mb. The data were originally obtained from "Jet Streams of the Atmosphere", published by the U. S. Navy.

Table 3. Average zonal wind (m sec^{-1}) and static stability parameter (MTS units) from actual data.

1	10/23.0	16/23.0	20/23.2	40/20.0	22.7
2	5/22.8	11/22.9	25/23.2	67/20.9	22.7
3	4/4.25	6/4.25	17/4.55	49/4.10	4.32
4	3/2.62	5/2.41	13/2.12	16/2.20	2.31
5	3/1.95	4/1.74	5/1.44	5/1.10	1.57
k/j	4	3	2	1	$\bar{\sigma}$

Case 10 represents the basic flow and average static stability parameter of Table 3 with a wave length of 6000 km. Above 1000 mb, the wave initially retrogresses slowly for about 12 hr and then moves eastward to approximately its starting point at the end of three days, although its exact behavior varies slightly from level to level. The 1000-mb wave is rather deformed and appears to progress through 360 degrees during the same period. The greatest amplification lies at 250 mb, the perturbation increasing to $\pm$10.47 after 72 hr, the greatest value noted in any of the cases. As a result, the thermal wave is extremely magnified also and progresses rapidly through the 500-mb wave, moving nearly 300 degrees relative to the upper wave.

Case 11 illustrates the effects of a moderate change in latitude. Here the latitude is taken to be 60N, with $\bar{f}=1.26\times10^{-4}$ sec^{-1} and $\beta=1.14\times10^{-13}$ sec^{-1} cm^{-1}; the wave length of the perturbation is 6000 km. Figure 11 shows that the general wave form, the retrogressive motion, the vertical tilt, and the phase relationship of the thermal and 500-mb waves all agree closely with those respective characteristics of Case 5 (latitude 45N), and that only slight differences are exhibited in the degree of amplification. The differences noted are all an order of magnitude smaller than the perturbations themselves and do not appear to be systematic from one level to the next. The thermal wave at t=72 hr is stronger at the higher latitude than in Case 5.

Case 12 represents a perturbation of wavelength 4000 km imposed upon the previously employed baroclinic jet structure of Tables 1 and 2. This example is included to show the development of a supposedly stable wave. The largest component imaginary phase velocities noted for this case are approximately zero and the fifteen real component phase velocities are, with one exception, positive, which would lead one to expect a stable, progressive wave at all levels. In fact, the wave is progressive at 1000 mb but undergoes moderate but nevertheless significant changes in intensity; at all other levels, the wave retrogresses rapidly and generally exhibits slightly greater amplification and damping. The wave form is badly deformed throughout its

development at the top, but the other levels show relatively little deformation.

Case 13 possesses the wave length (6000 km) and wind and stability profiles of Case 5, but the perturbation initially has greater tilt, exhibiting a phase shift of 90° to the west from 1000 mb to 0 mb. The initial wave form is given by

$$\sin \frac{\pi}{2}\left(1 - \frac{k-1}{3}\right) e^{\frac{i\pi(P_0 - (k-1)P)}{2P_0}} . \qquad (43)$$

The similarities of the behavior of this wave with that of the more vertical wave of Case 5 are generally more striking than the differences. The horizontal wave forms are quite similar at all levels and at all time intervals; the variations in intensity parallel each other in the two cases; the thermal waves move similarly in relation to the 500-mb waves, but the thermal wave is more intense throughout the development of Case 13. Whereas the perturbations in Case 5 retrogress rapidly at all levels, this is not true of Case 13, where the wave is progressive at 1000 mb but retrogressive at all other levels. The tilt after 72 hr closely resembles that of the earlier case, however. At time t=60 hr, the perturbations of Case 13 are the more highly amplified of the two at all levels; this is true at 72 hr also, with the exception of the 750-mb level which is very slightly weaker than that of Case 5. The most

interesting of these various features is the progressive lower wave, which more closely resembles in behavior synoptic waves of 6000-km wave length than do the wholly retrogressive perturbations of Case 5 and the upper levels of Case 13.

5. Conclusions and Acknowledgements.

The perturbation wave structures for a representative variety of unstable wavelengths have been presented for a model featuring a baroclinic atmosphere with a three-dimensional jet-like wind profile, and comparisons have been made for one of the wave lengths, 6000 km, with similar waves in a wide selection of other models. The jet structure appears to slow the progression of the waves or induce retrogression, even in cases where an eastward motion would appear intuitively likely from inspection of the component phase velocities. It is early in the study to try to reach any definite conclusions concerning the model. Further work is definitely needed to discern the effects of variation of grid interval, for instance, upon the wave structure. Observing the waves over longer time intervals might lead to knowledge concerning the existence of limiting phase angles between the thermal and 500-mb waves, as has been discussed by Wiin-Nielsen [4] for a different model. This paper does depict in some detail the form and development of a number of interesting cases, and has brought into existence some flexible computer programs suitable for further study into other aspects of the model.

The writer wishes to express his appreciation to Professor George J. Haltiner, Chairman of the Meteorology and Oceanography Department, U. S. Naval Postgraduate School, for his guidance, contributions, and encouragement

in this work.

Appreciation is also expressed to the personnel of the Computer Facility, U. S. Naval Postgraduate School, for their aid and advice in programming and performing the machine computations, and Samuel K. Bowman, AG 2, U. S. Navy, for his contribution in plotting the computed data. Thanks are expressed to Mrs. Christine Bowman for her efforts in typing this thesis.

BIBLIOGRAPHY

1. Haltiner, G. J. Finite difference approximations for the determination of dynamic instability. Tellus, v. 15, 1963: 230-240.

2. Wiin-Nielsen, A. On short and long term variations in quasi-barotropic flow. Monthly Weather Review, v. 89, 1961: 461-476.

3. Eliasen, E. A study of the long atmospheric waves on the basis of zonal harmonic analysis. Tellus, v. 10, 1958: 206-215.

4. Joint Numerical Weather Prediction Unit, Washington, D. C. A note on the structure of waves in a simple baroclinic model, by A. Wiin-Nielsen. May, 1960. Technical memorandum no. 17.

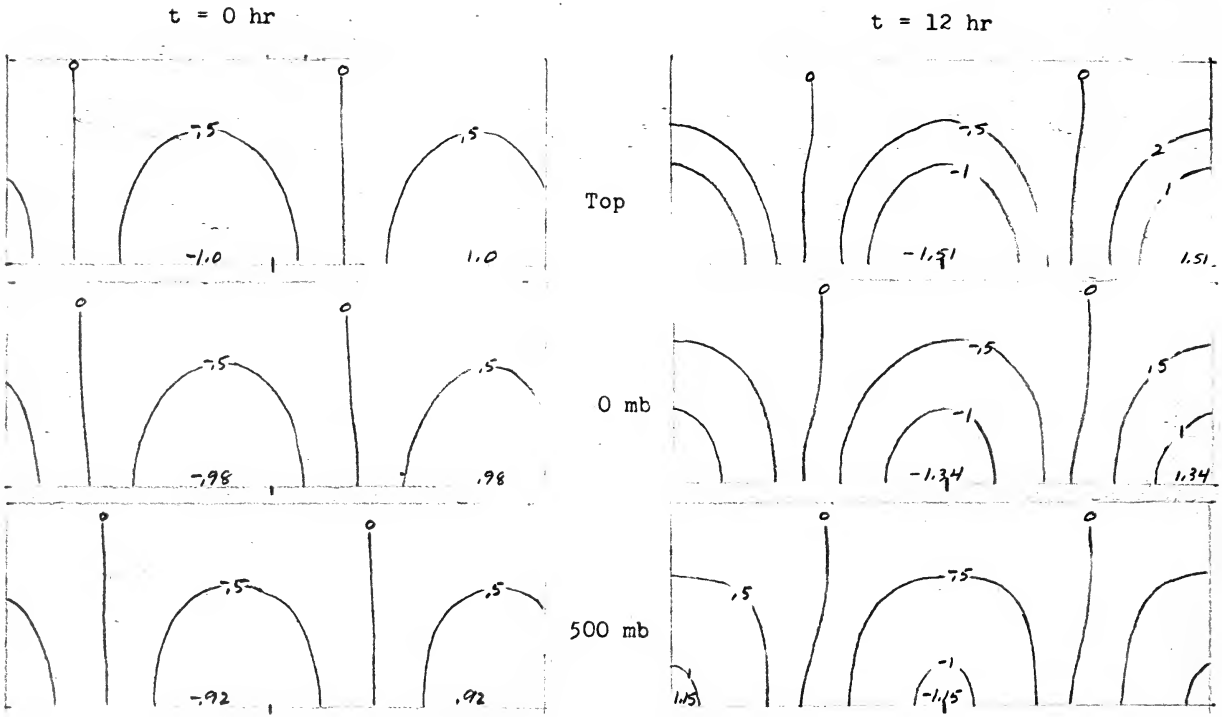
t = 0 hr
t = 12 hr
Top
0 mb
500 mb
0
.5
1.0
-.5
-1.0
.98
-.98
.92
-.92
1
2
1.51
-1.51
1.34
-1.34
1.15
-1.15

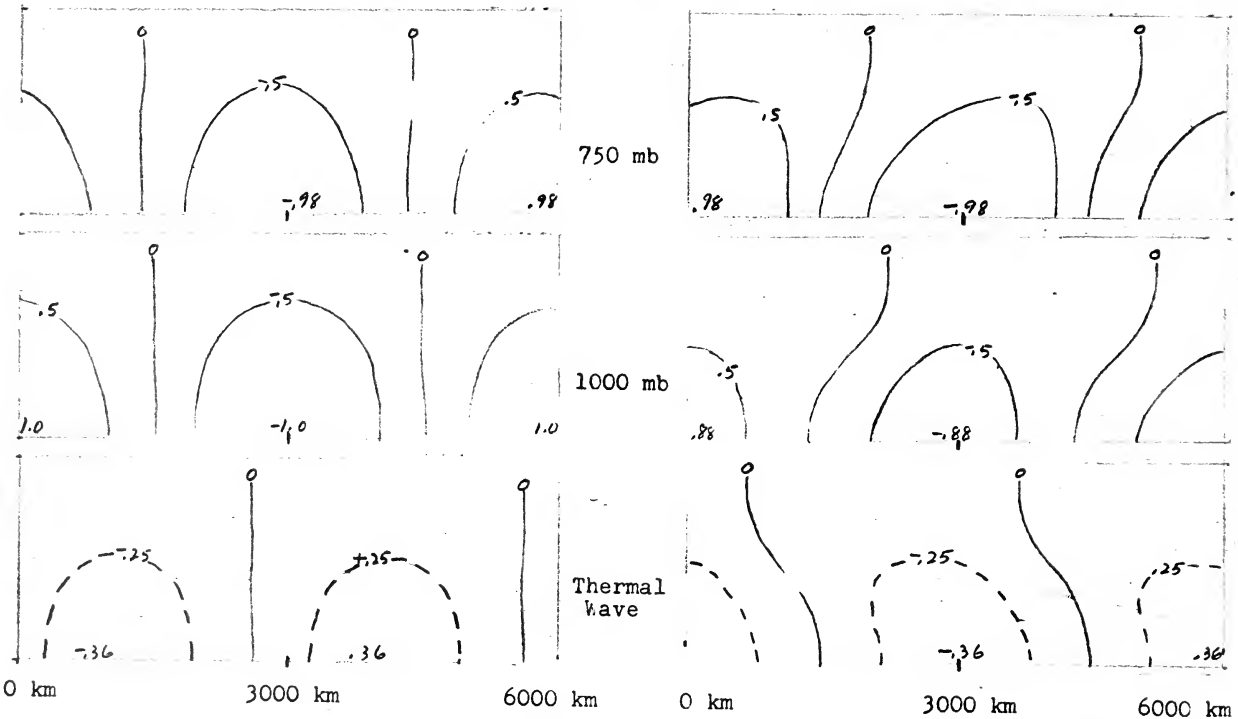

Figure 1.1. Case 1 (λ = 6000 km), Perturbation Stream Function (Ψ').

t = 24 hr

t = 36 hr

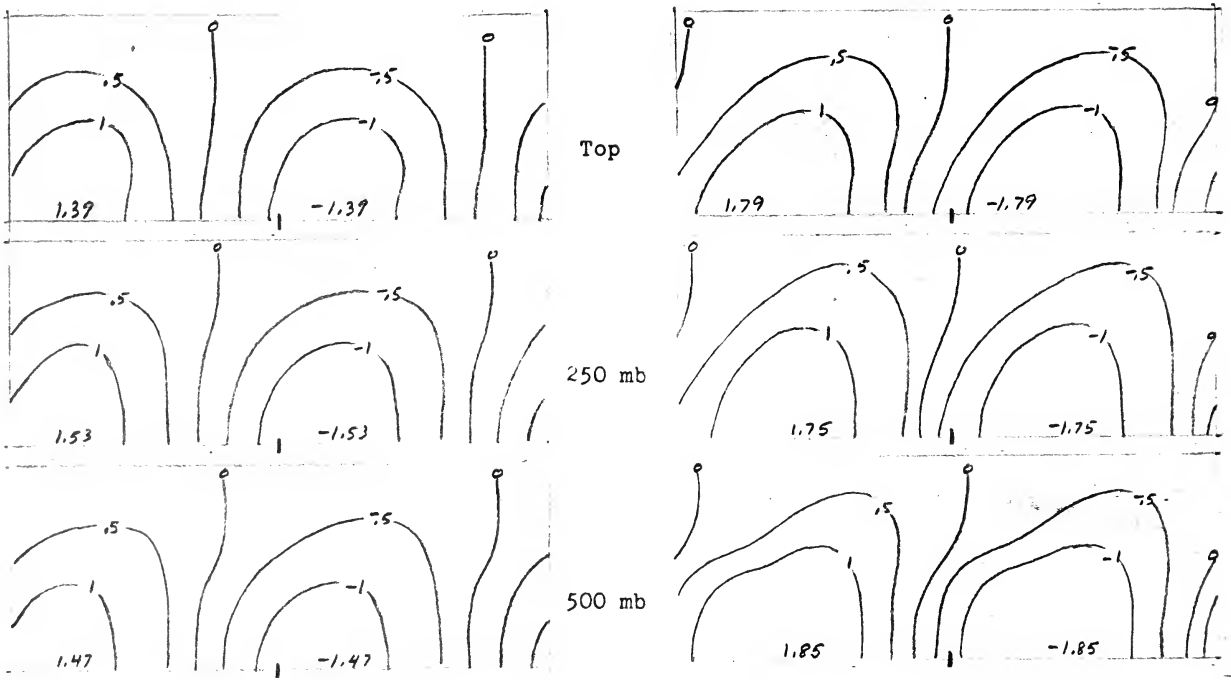
Top
250 mb
500 mb
0
.5
1
.75
-1
1.39
-1.39
1.53
-1.53
1.47
-1.47
1.79
-1.79
1.75
-1.75
1.85
-1.85

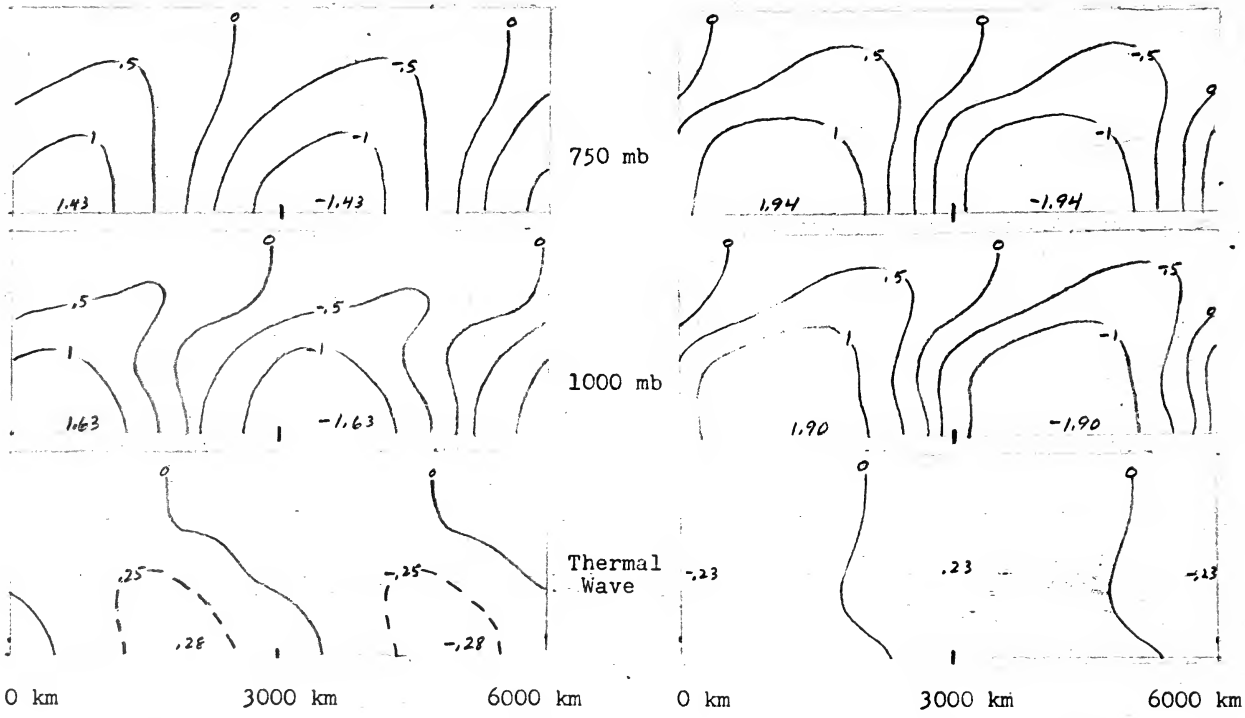

Figure 1.2. Case 1 (λ = 6000 km), Perturbation Stream Function. (Ψ').

t = 48 hr

t = 60 hr

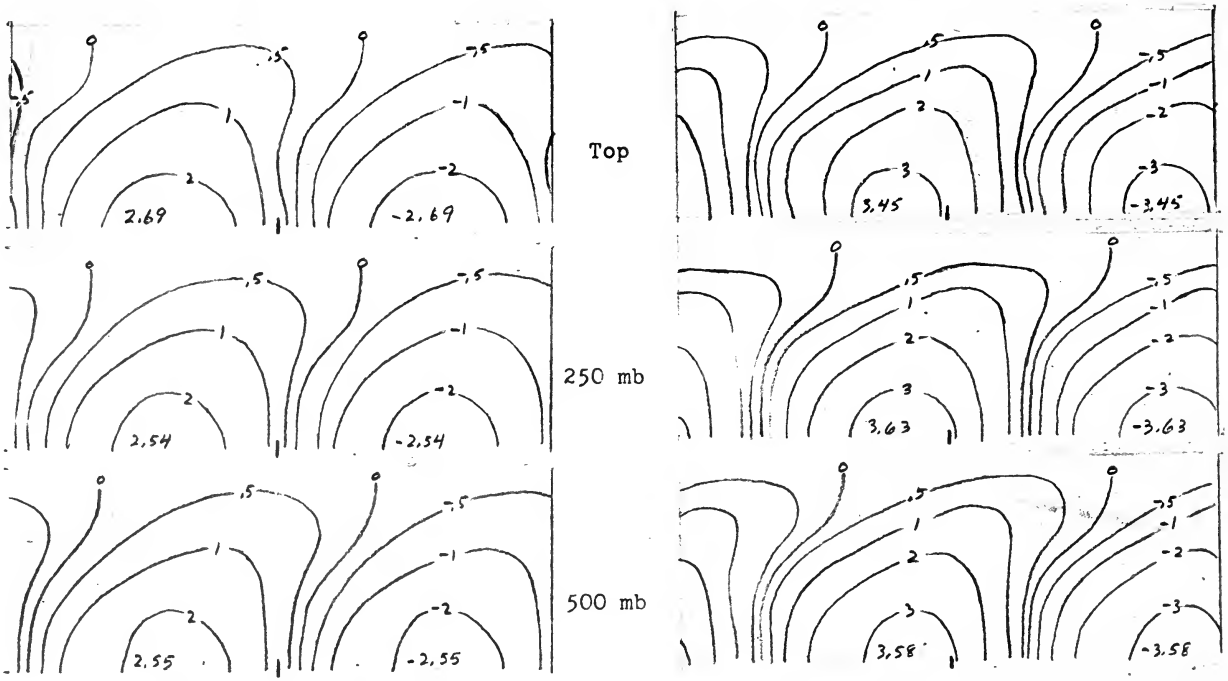

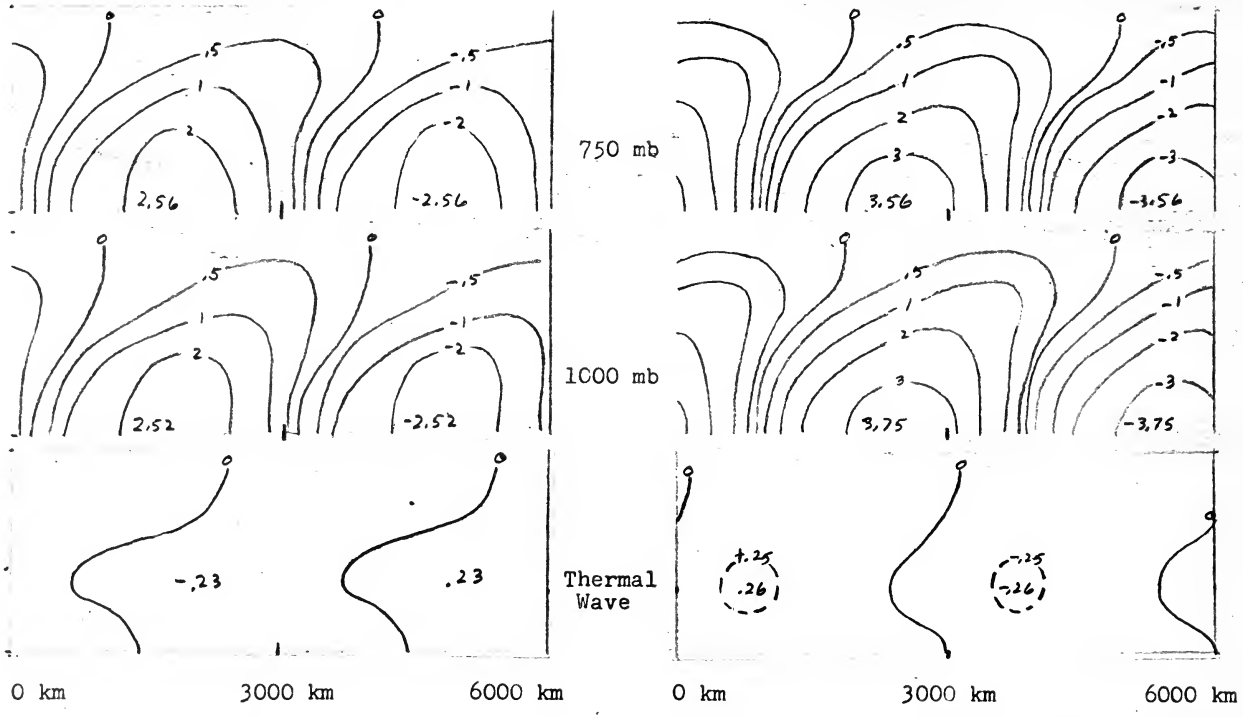

Figure 1.3. Case 1. (λ = 6000 km), Perturbation Stream Function (Ψ').

t = 72 hr

Top

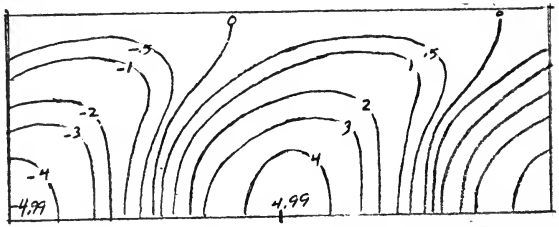

250 mb

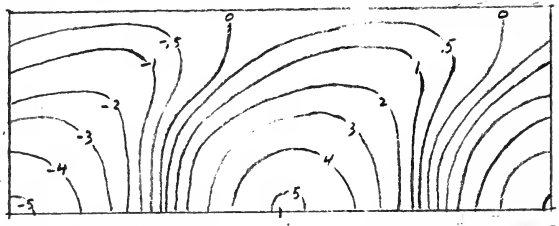

500 mb

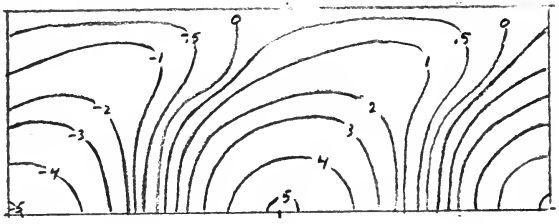

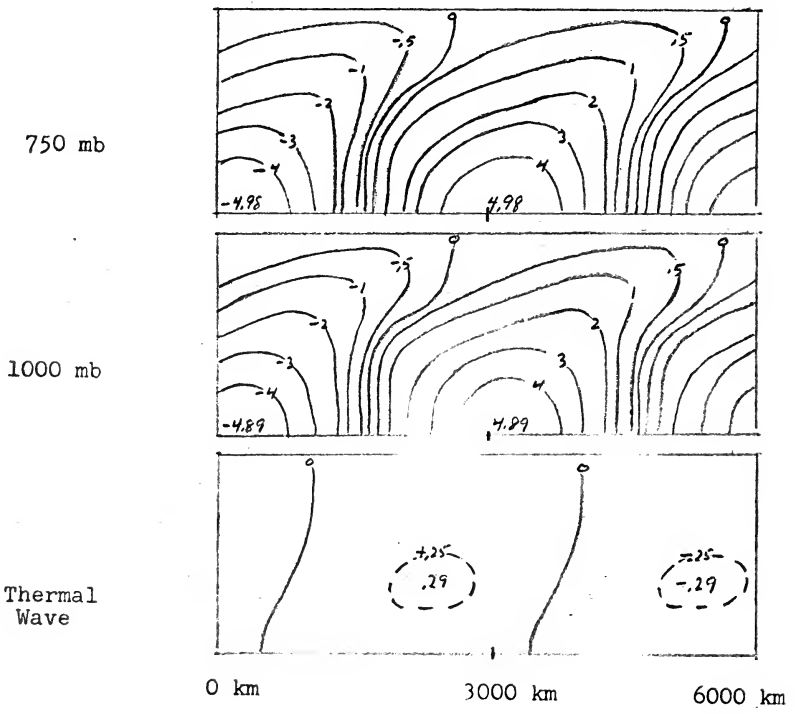

Figure 1.4. Case 1 (λ = 6000 km), Perturbation Stream Function (Ψ').

t = 0 hr

t = 12 hr

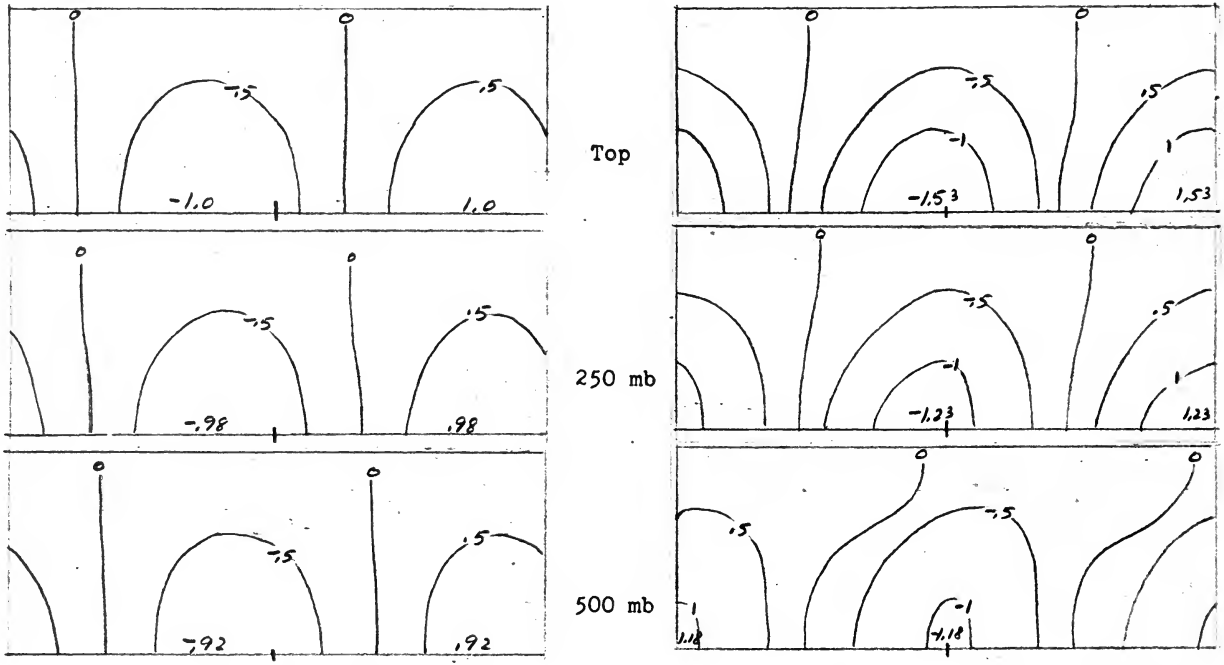

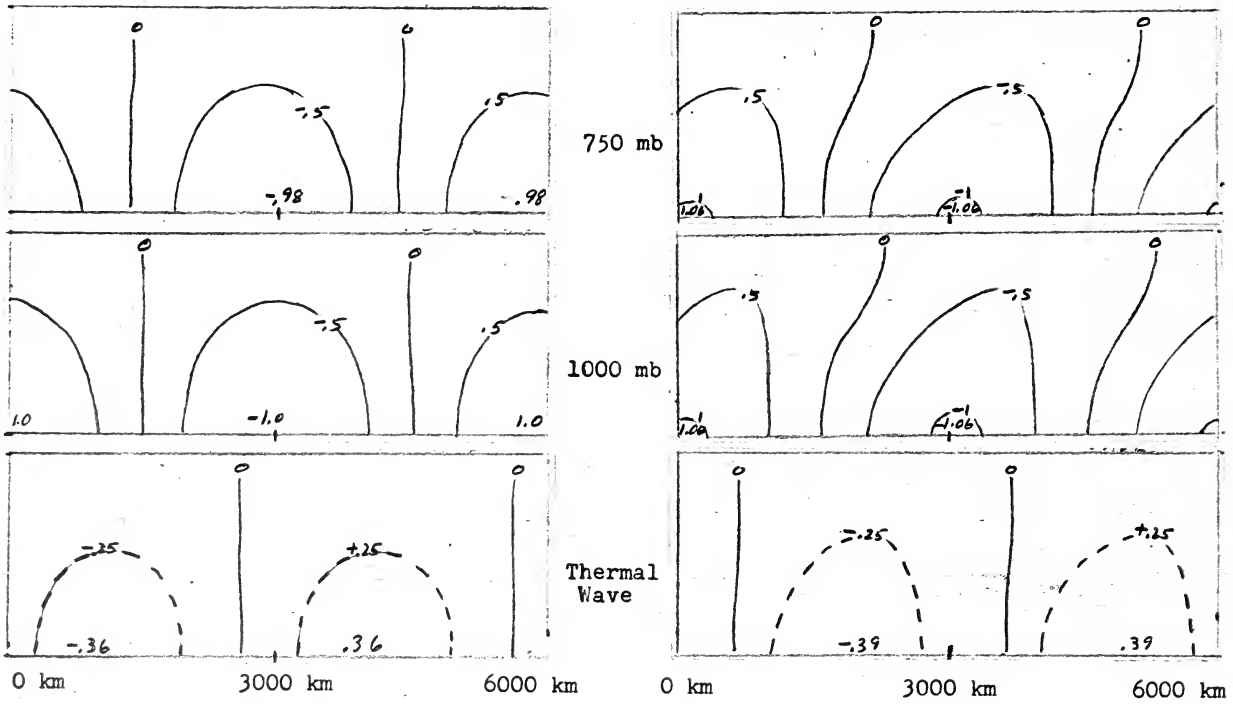

Figure 2.1. Case 2 (λ = 6000 km), Perturbation Stream Function (Ψ').

t = 24 hr

t = 36 hr

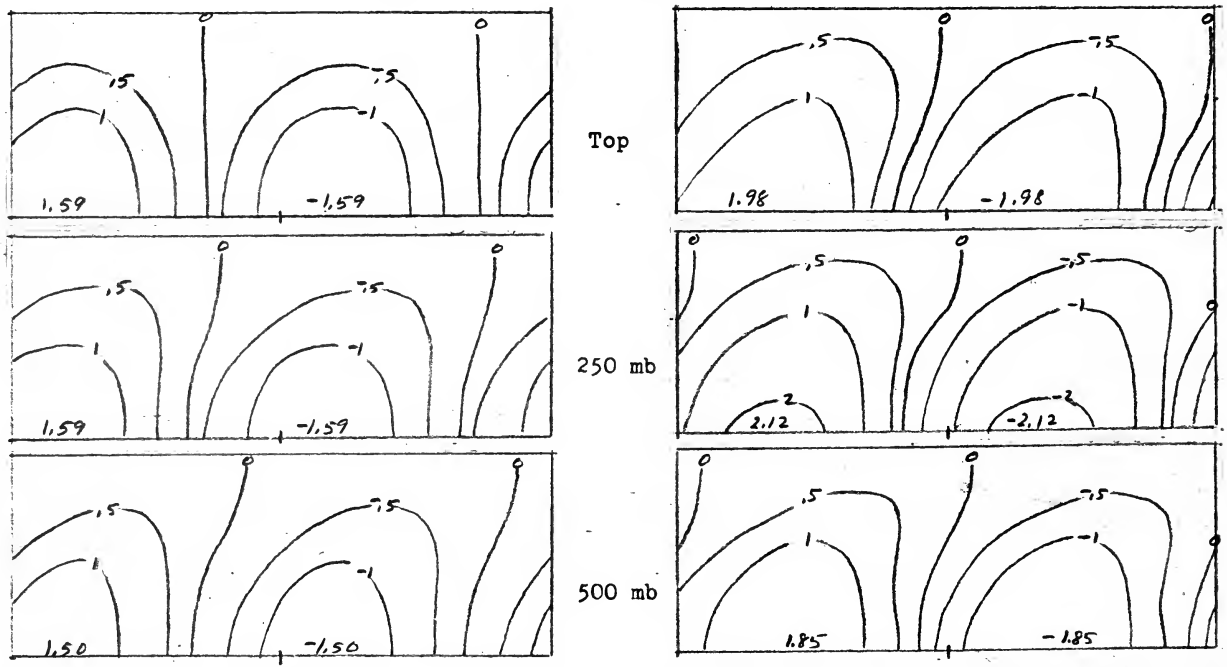

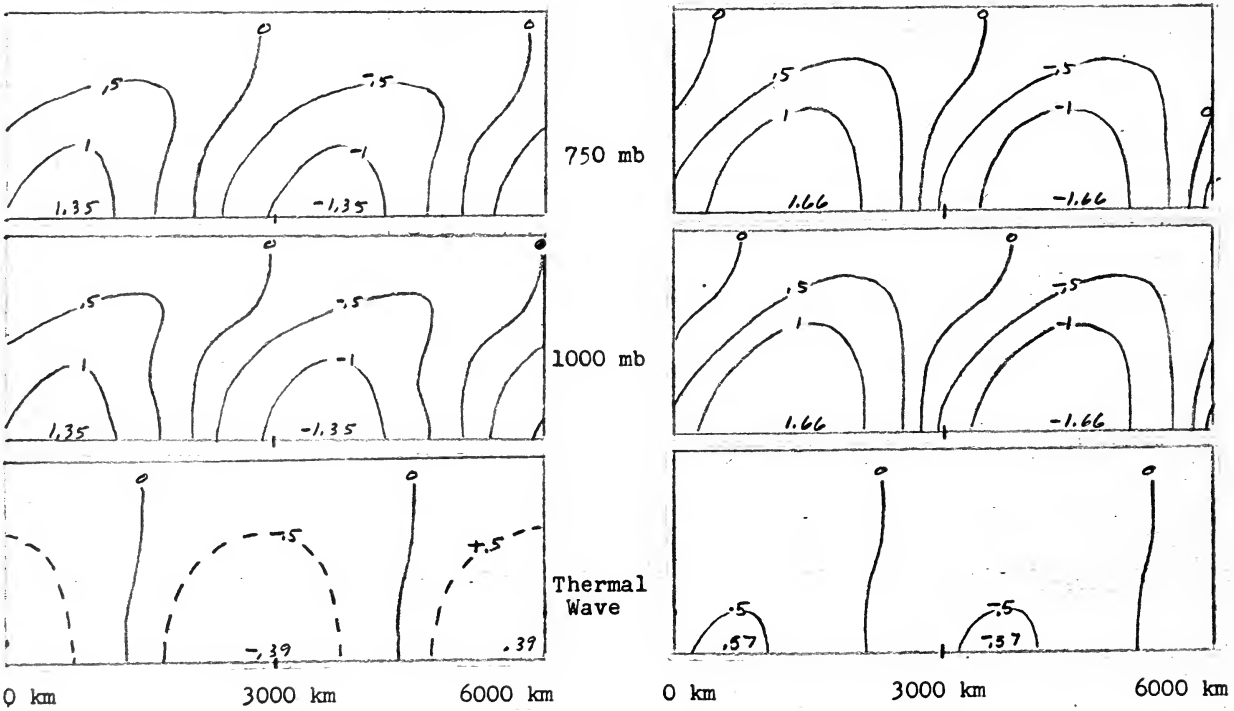

Figure 2.2. Case 2 (λ = 6000 km), Perturbation Stream Function (Ψ').

t = 48 hr

t = 60 hr

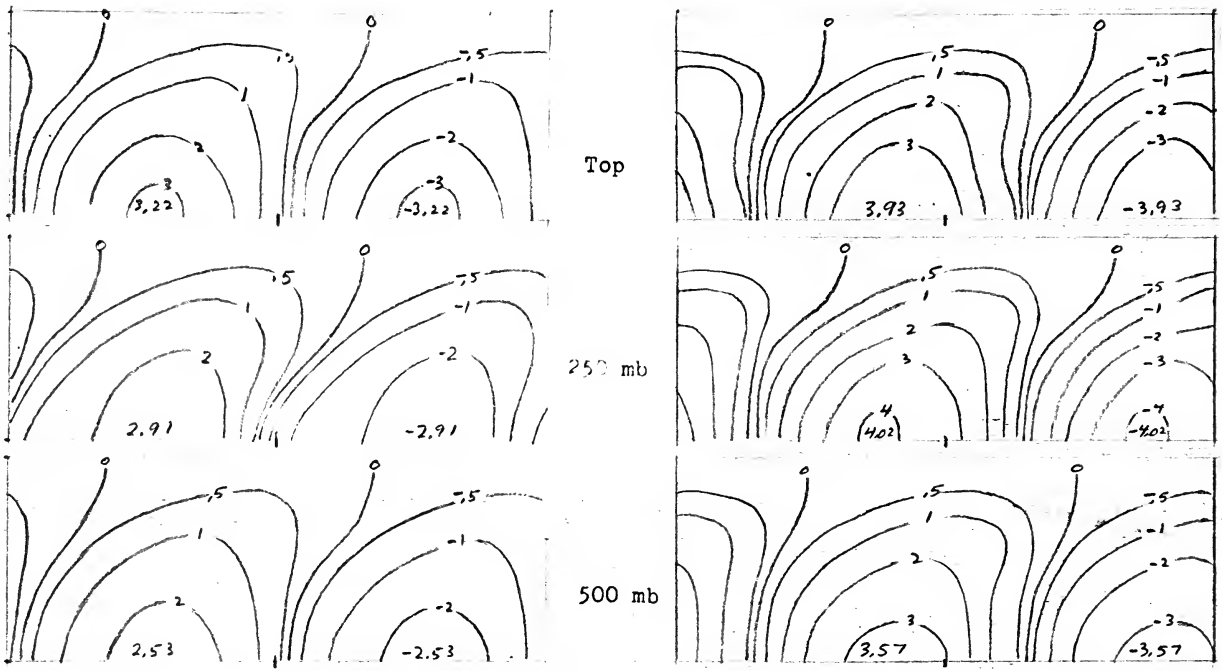

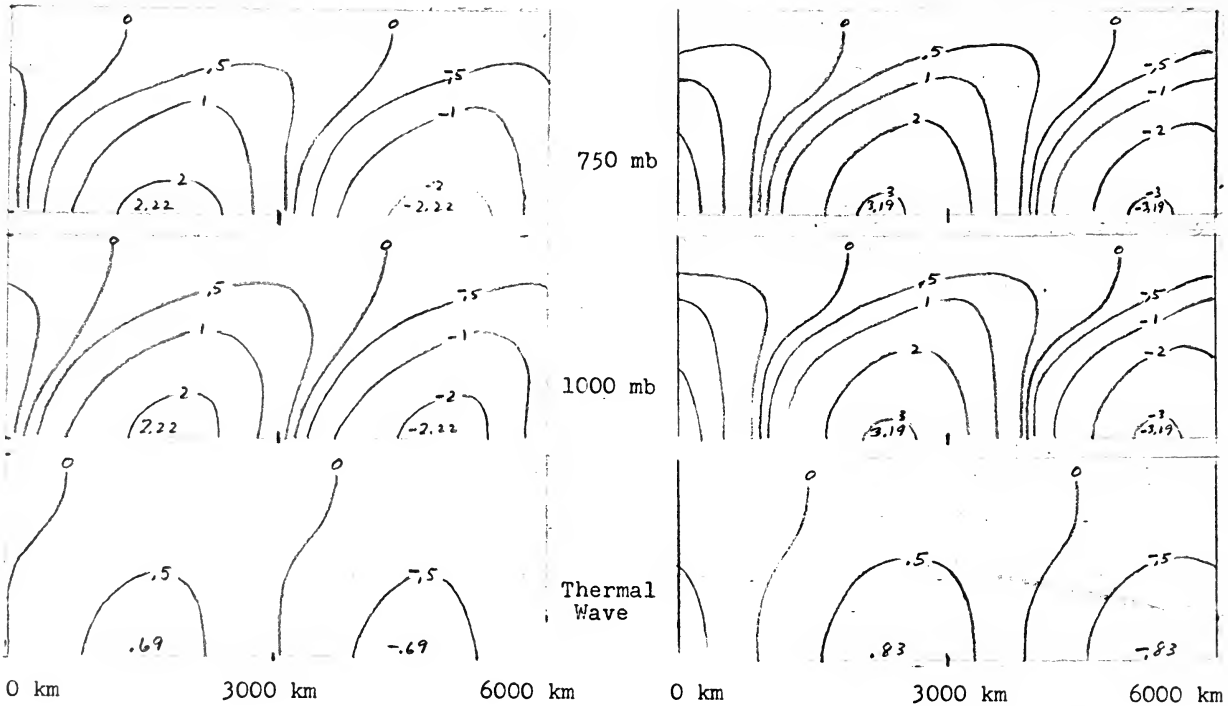

Figure 2.3. Case 2 (λ = 6000 km), Perturbation Stream Function (Ψ').

t = 72 hr

Top

250 mb

500 mb

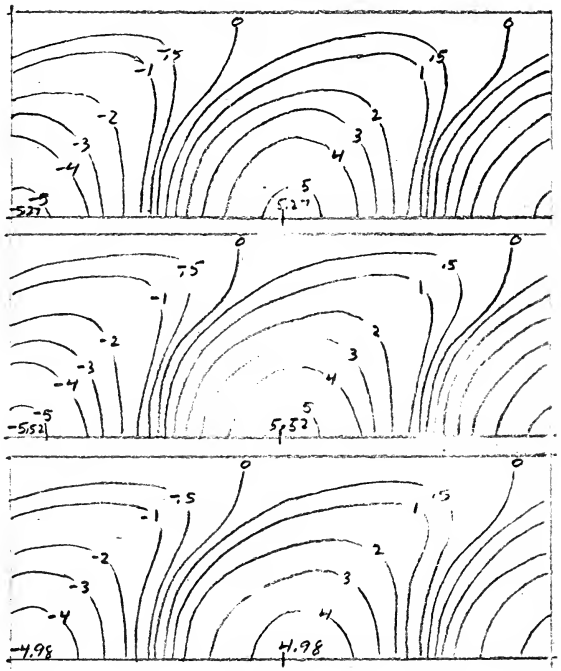

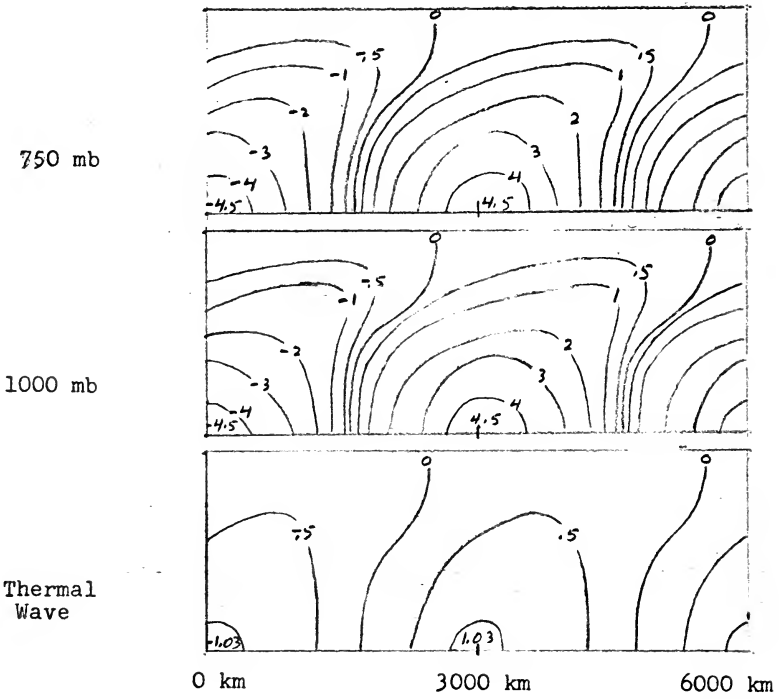

Figure 2.4. Case 2 (λ = 6000 km), Perturbation Stream Function (Ψ').

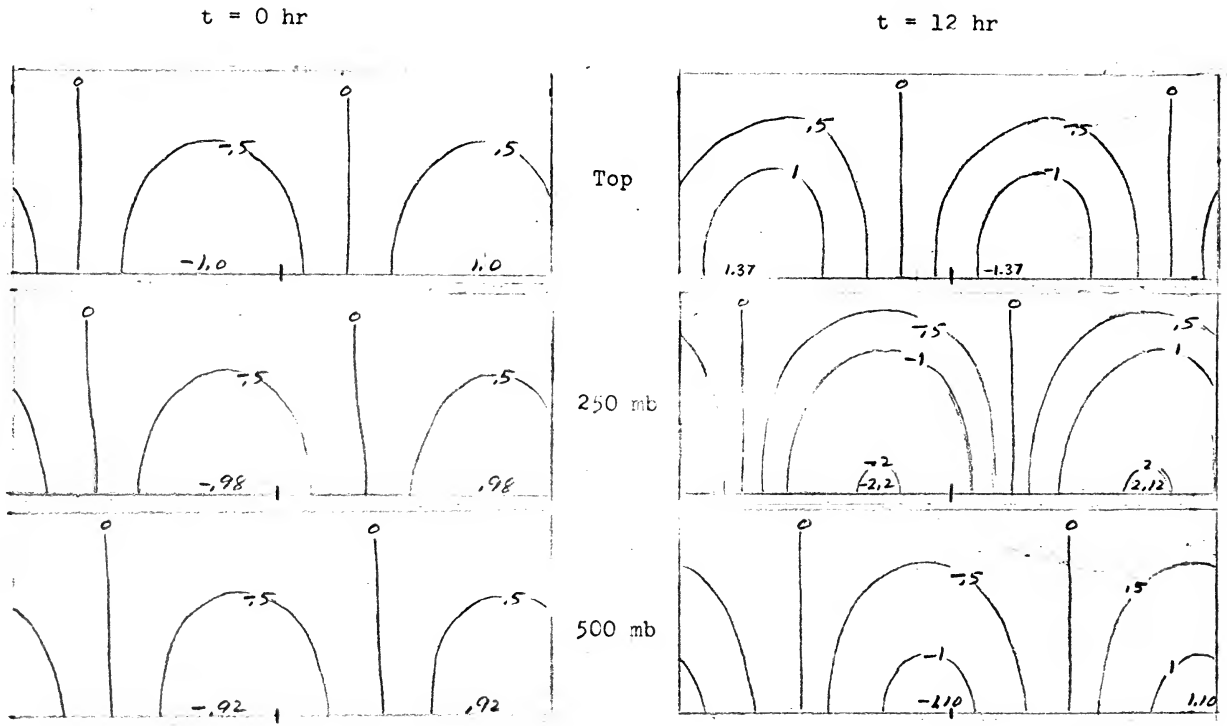
t = 0 hr
t = 12 hr
Top
250 mb
500 mb
0
.5
-.5
1.0
-1.0
.98
-.98
.92
-.92
1
-1
1.37
-1.37
2
(2,12)
-2
(-2,2)
1.10
-1.10

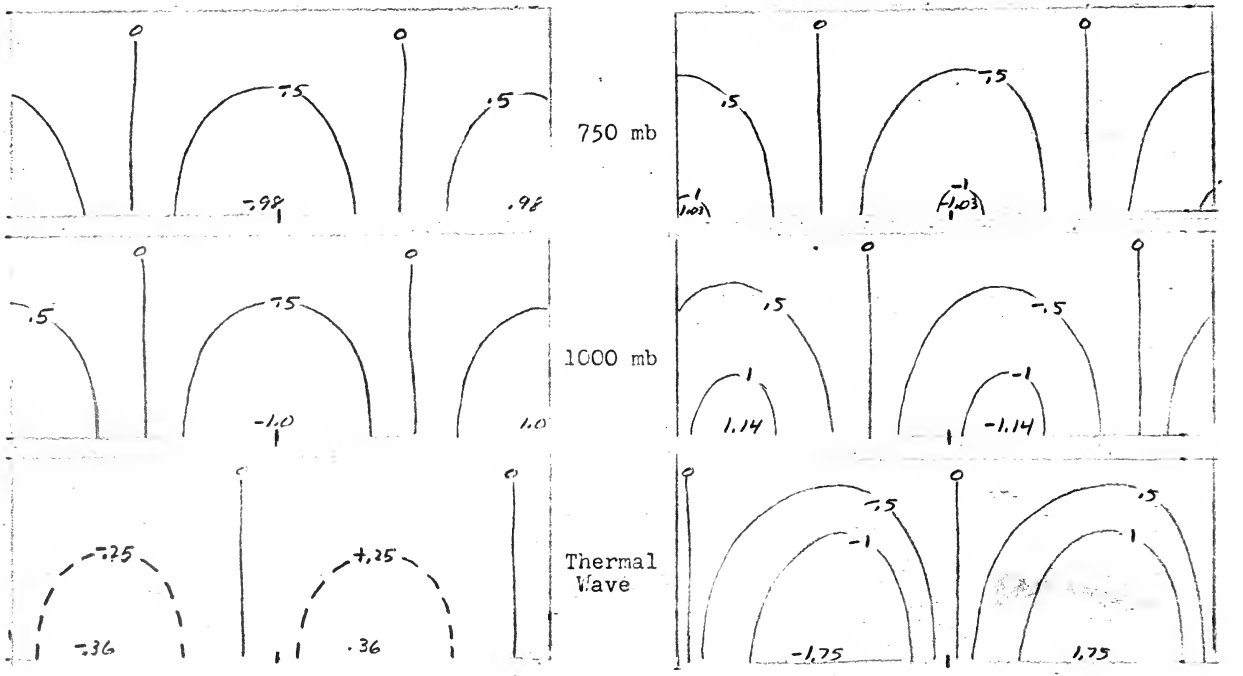

Figure 3.1. Case 3 (λ = 6000 km), Perturbation Stream Function (Ψ').

t = 24 hr

t = 36 hr

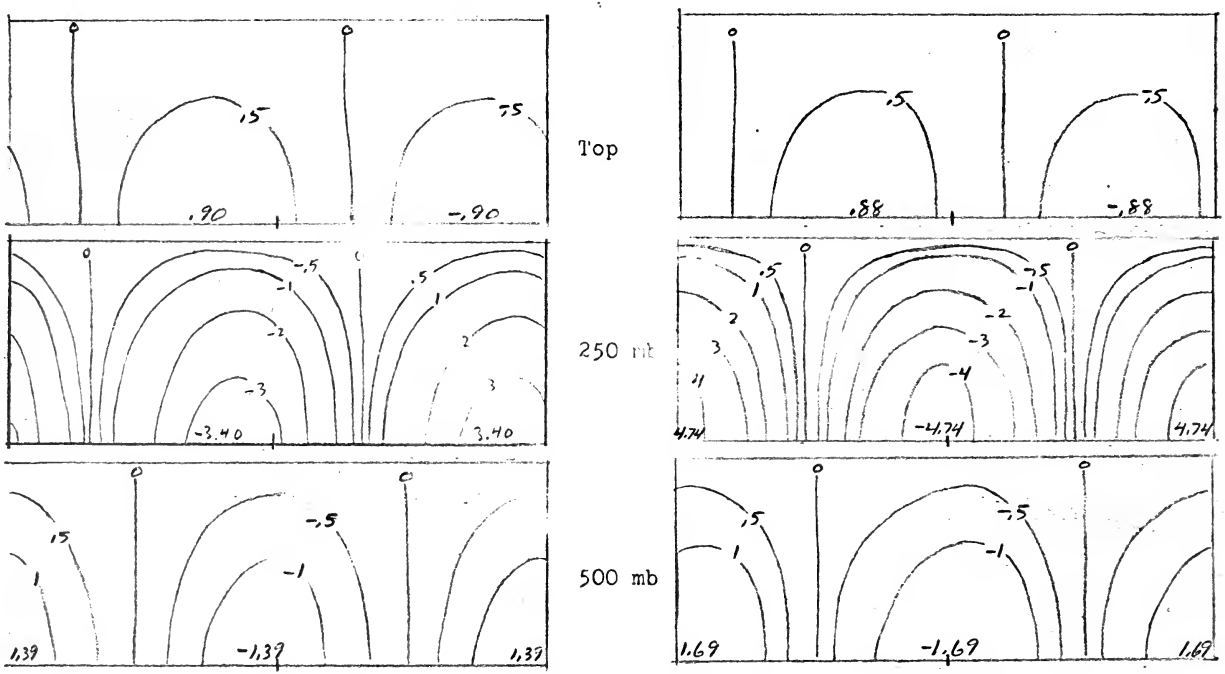

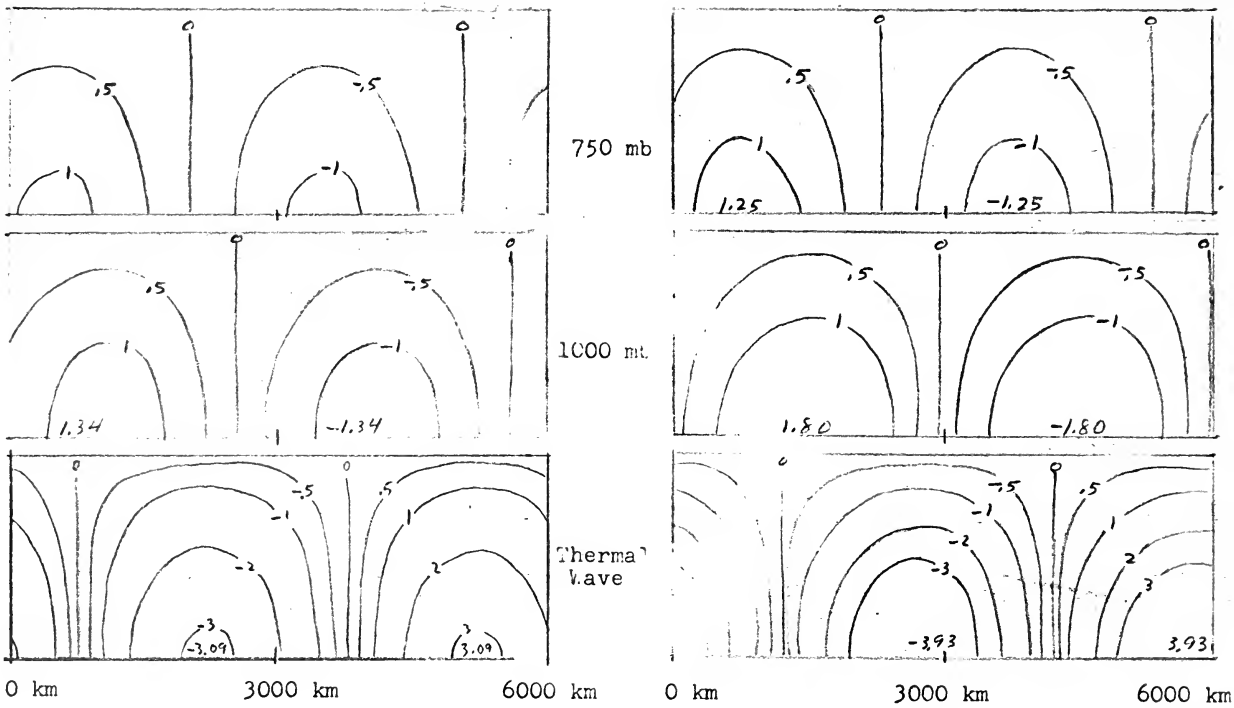

Figure 3.2. Case 3 (λ = 6000 km), Perturbation Stream Function (Ψ').

t = 48 hr

t = 60 hr

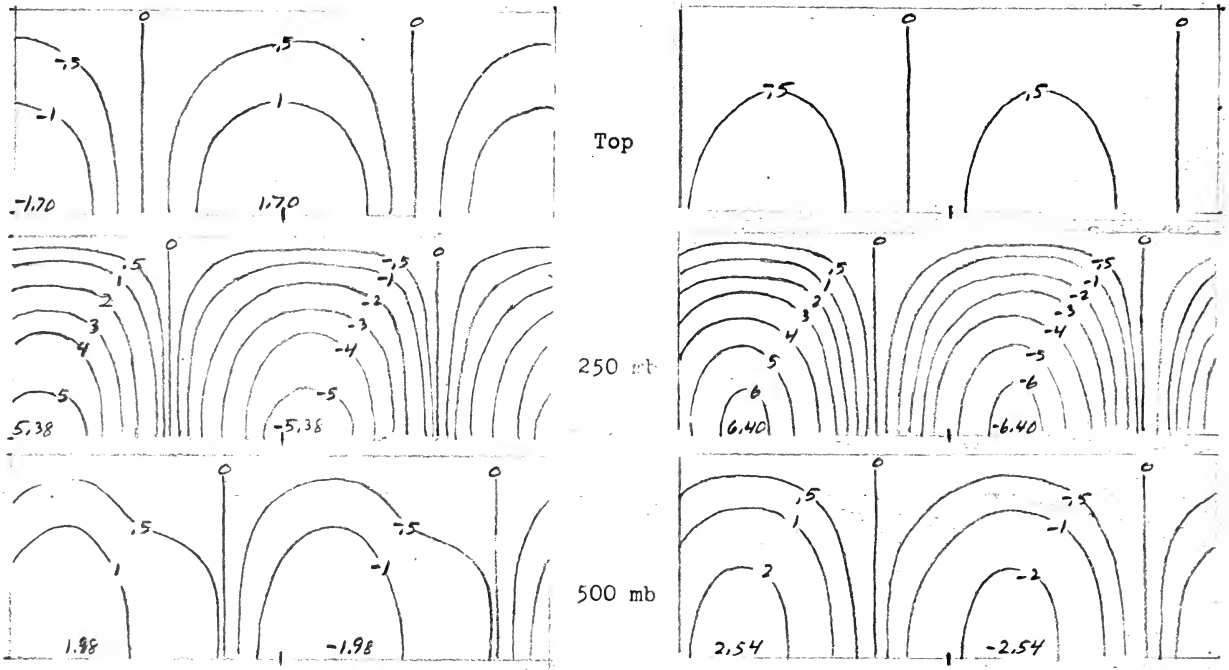

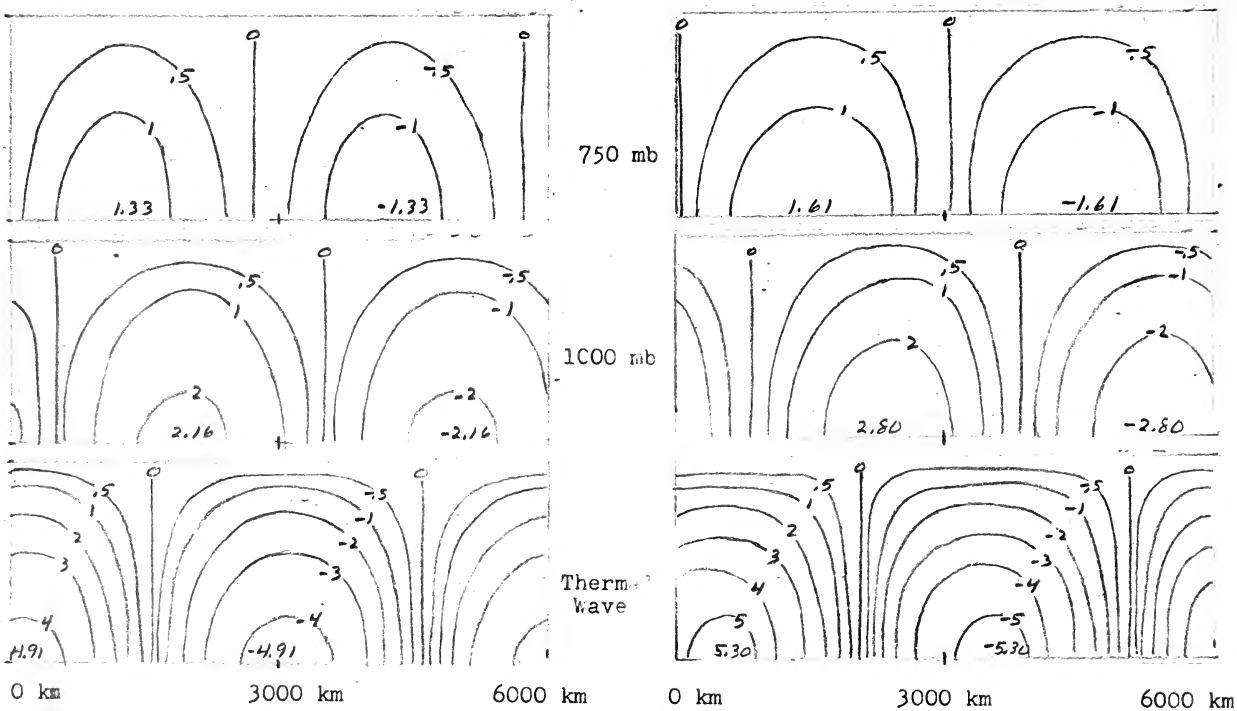

Figure 3.3. Case 3 (λ = 6000 km), Perturbation Stream Function (Ψ').

t = 72 hr

Top

250 mb

500 mb

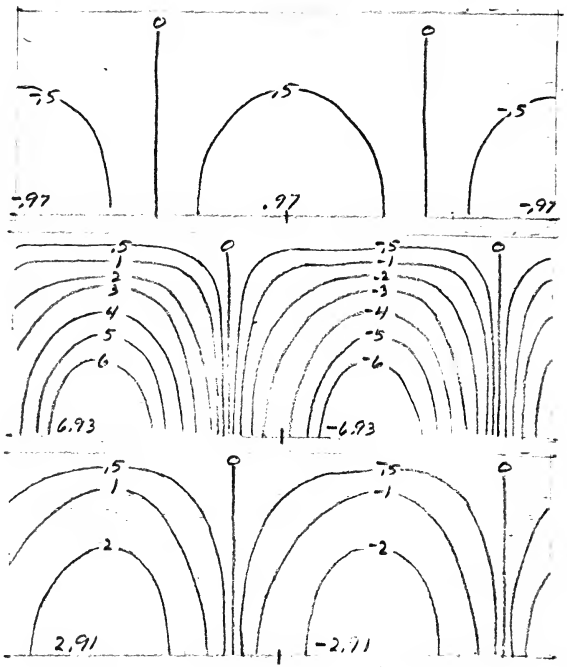

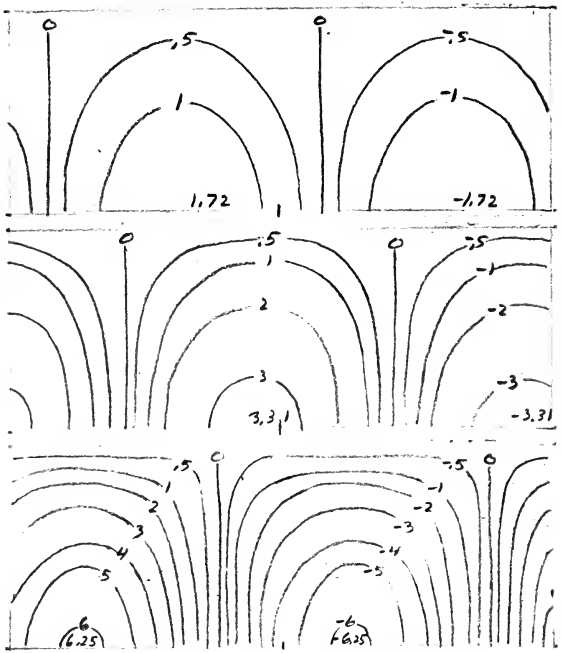

Figure 3.4. Case 3 (λ = 6000 km), Perturbation Stream Function (Ψ').

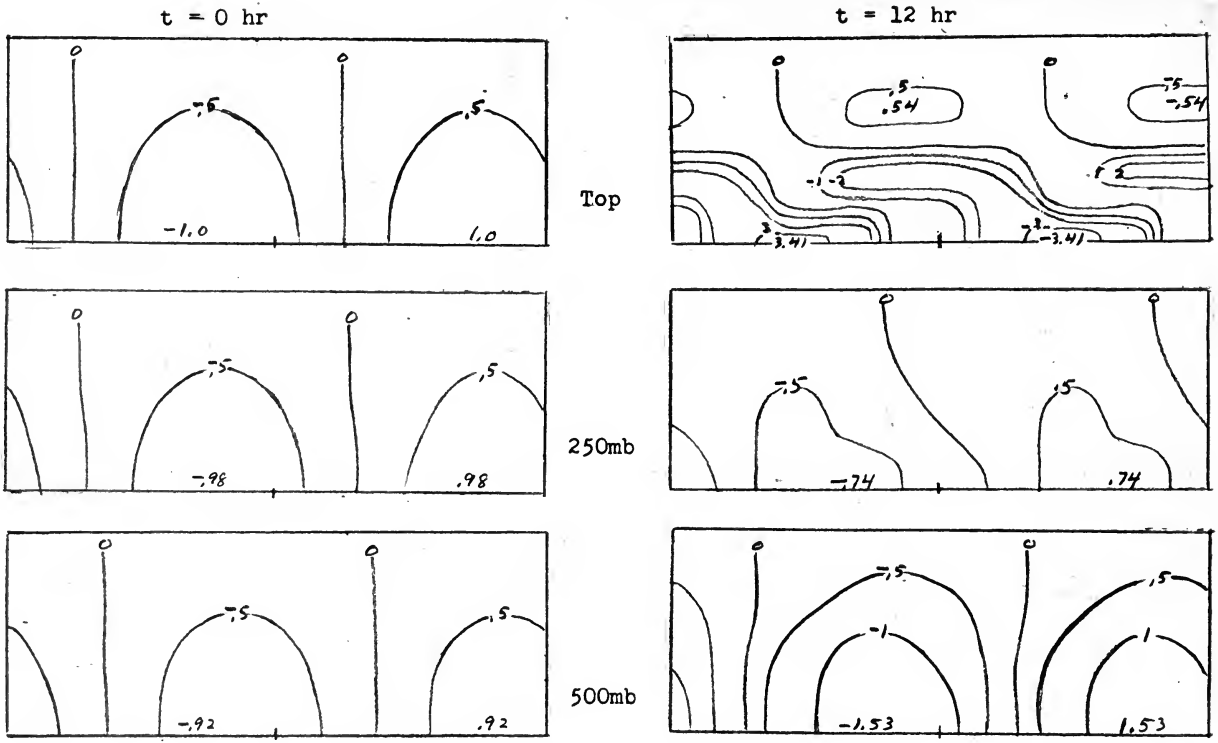
t = 0 hr
t = 12 hr
Top
250mb
500mb
0
-.5
.5
-1.0
1.0
-.54
-3.41
-.98
.98
-.74
.74
-1
1
-1.53
1.53

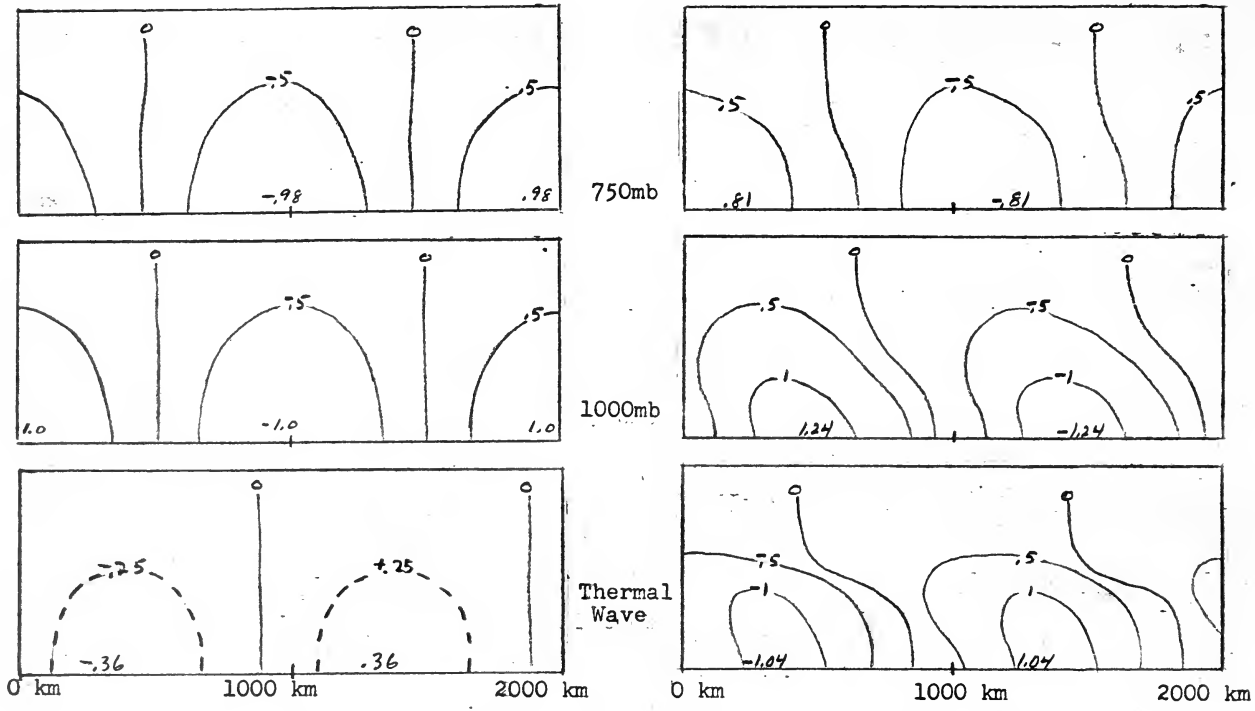

Figure 4.1. Case 4 (λ = 2000 km), Perturbation Stream Function (Ψ').

t = 24 hr

t = 36 hr

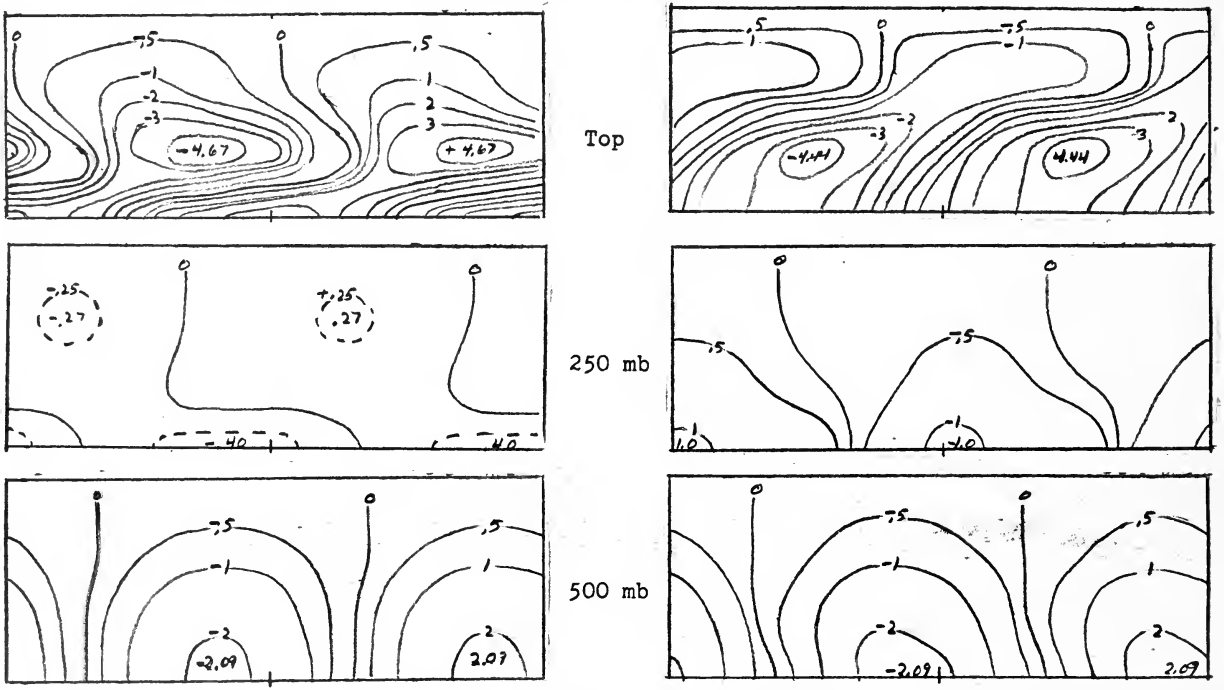

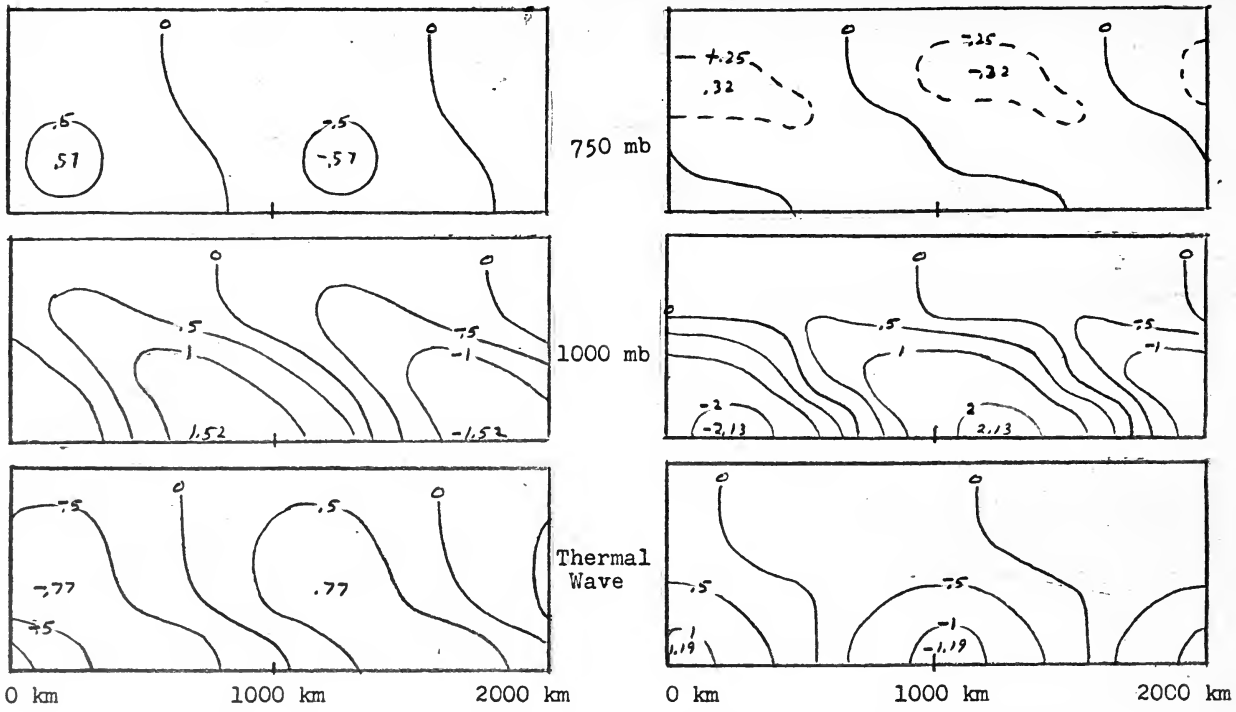

Figure 4.2. Case 4 (λ = 2000 km), Perturbation Stream Function (Ψ').

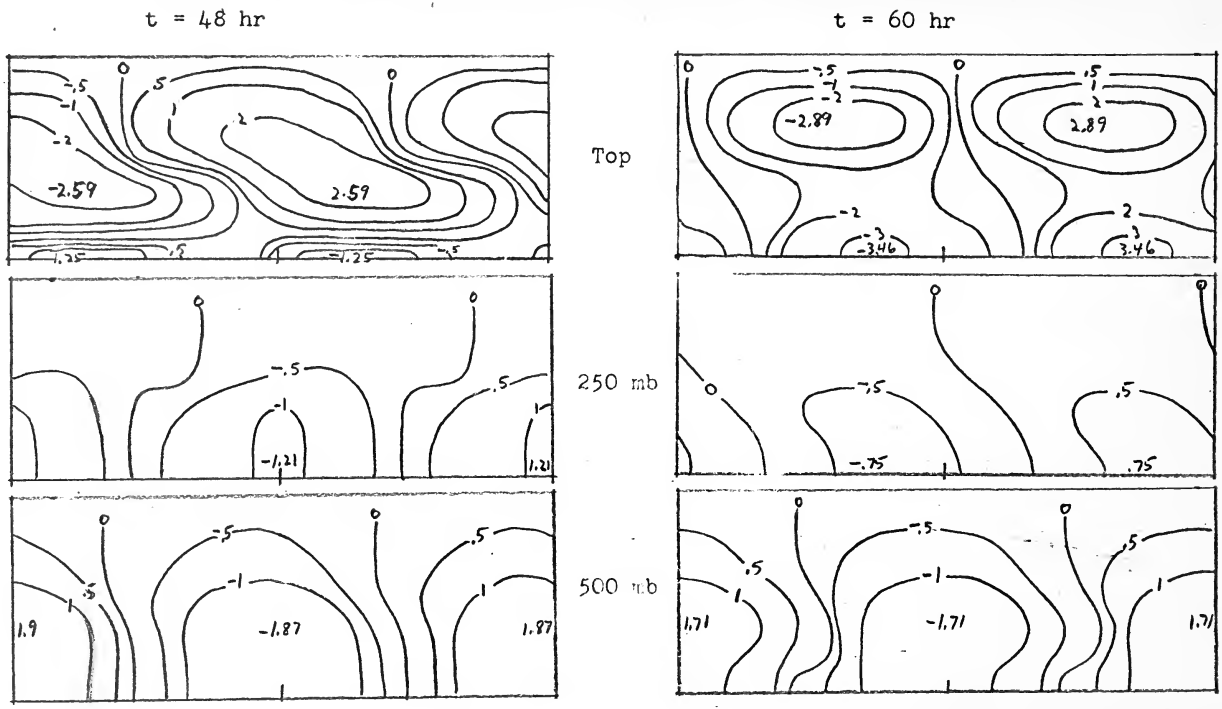
t = 48 hr
t = 60 hr
Top
250 mb
500 mb
-2.59
2.59
-1.25
-2.89
2.89
-3.46
3.46
-1.21
1.21
-.75
.75
1.9
-1.87
1.87
1.71
-1.71

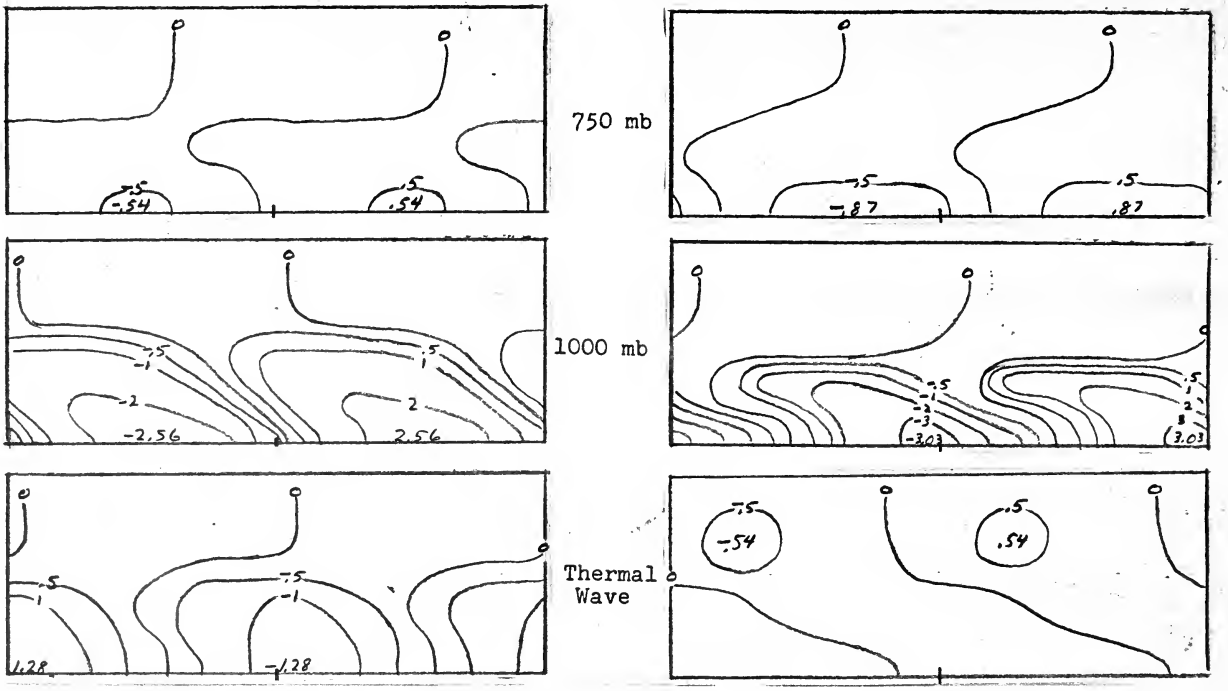

Figure 4.3. Case 4 (λ = 2000 km), Perturbation Stream Function (Ψ').

t = 72 hr

Top

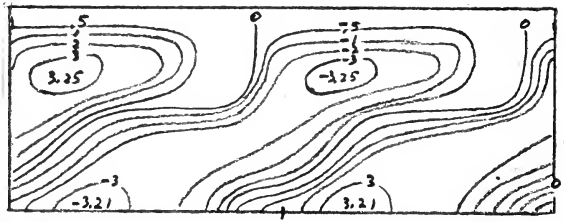

250 mb

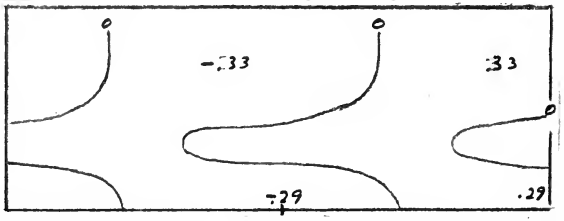

500 mb

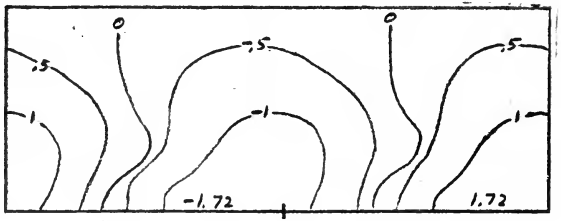

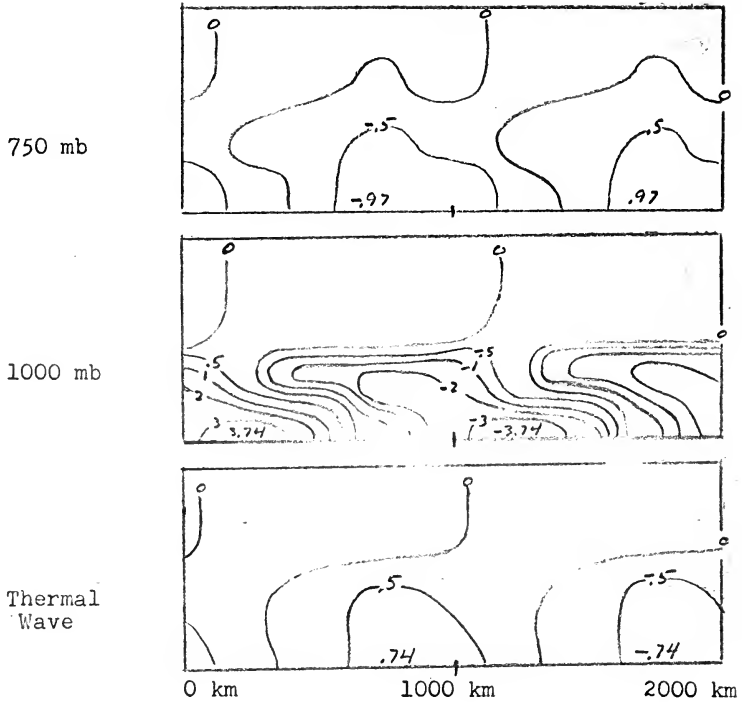

Figure 4.4. Case 4 (λ = 2000 km), Perturbation Stream Function (Ψ').

t = 0 hr

t = 12 hr

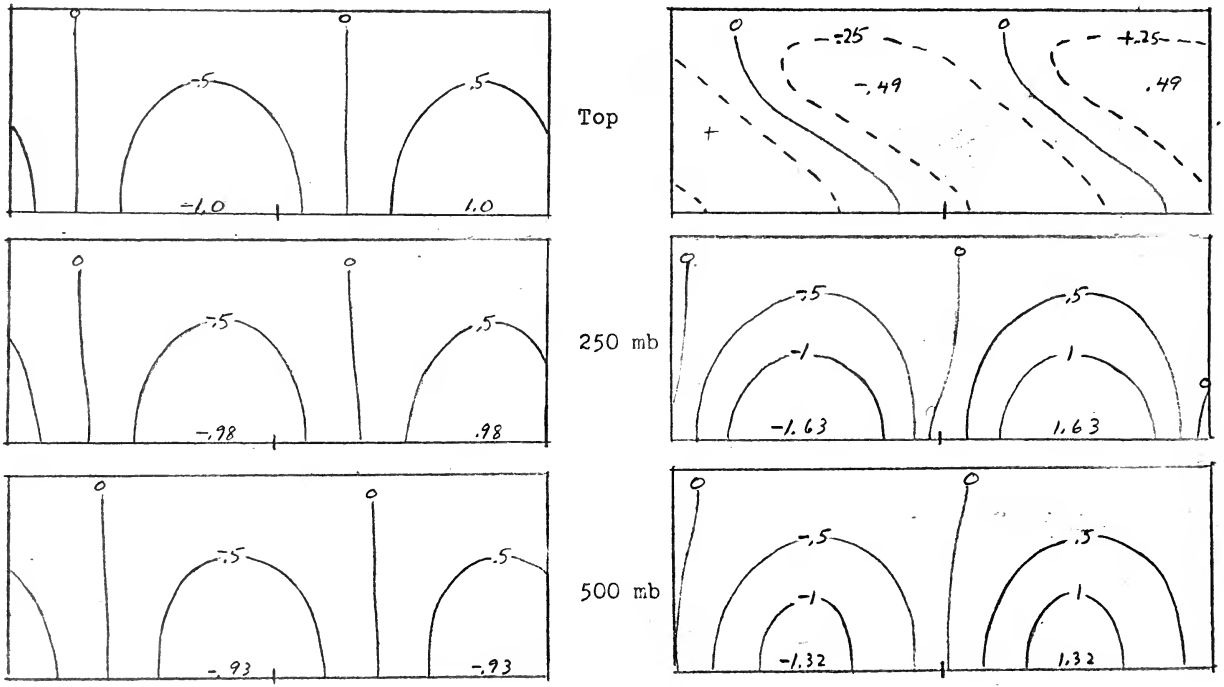

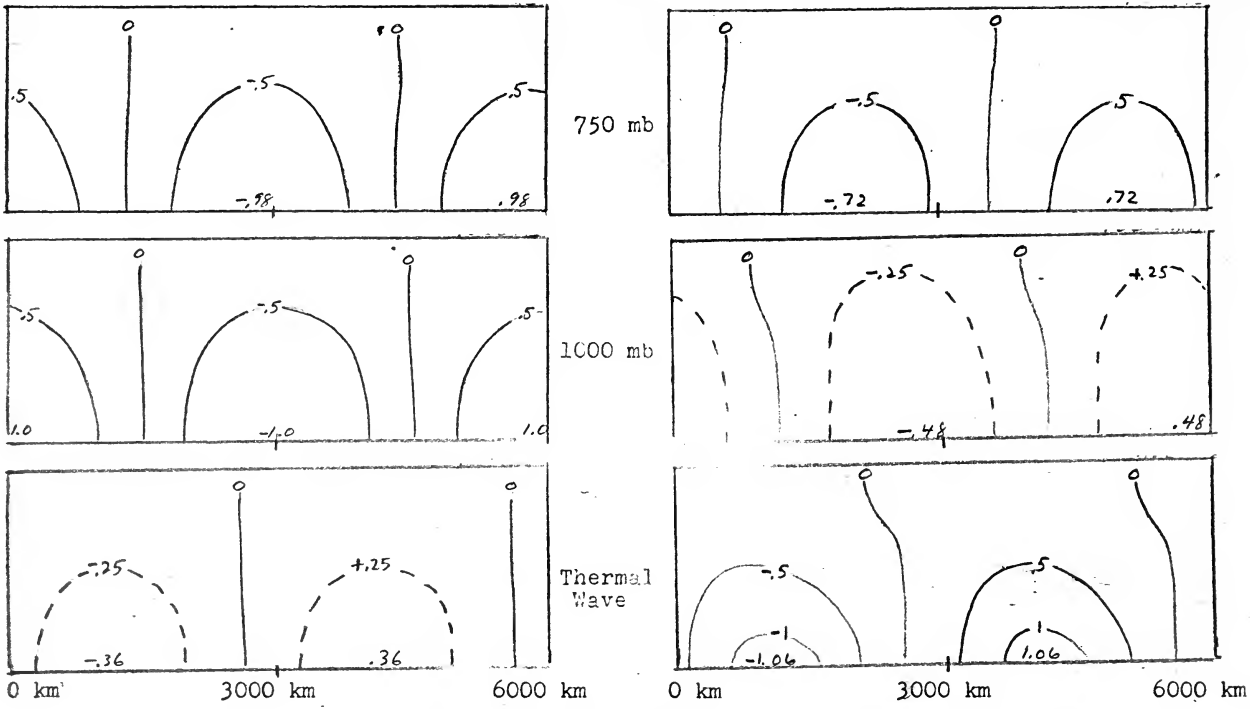

Figure 5.1. Case 5 (λ = 6000 km), Perturbation Stream Function (Ψ').

t = 24 hr

t = 36 hr

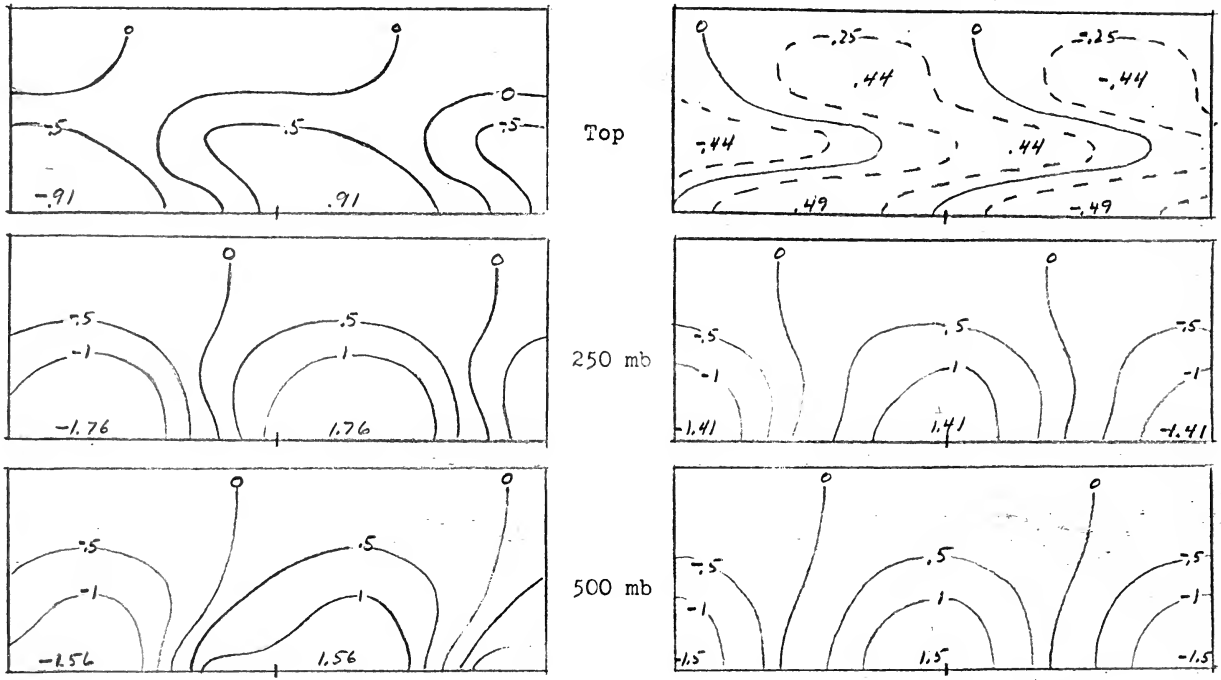
Top
250 mb
500 mb
-.91
.91
-.5
.5
0
-.25
.44
-.44
.49
-1.76
1.76
-1
1
-1.41
1.41
-1.56
1.56
-1.5
1.5

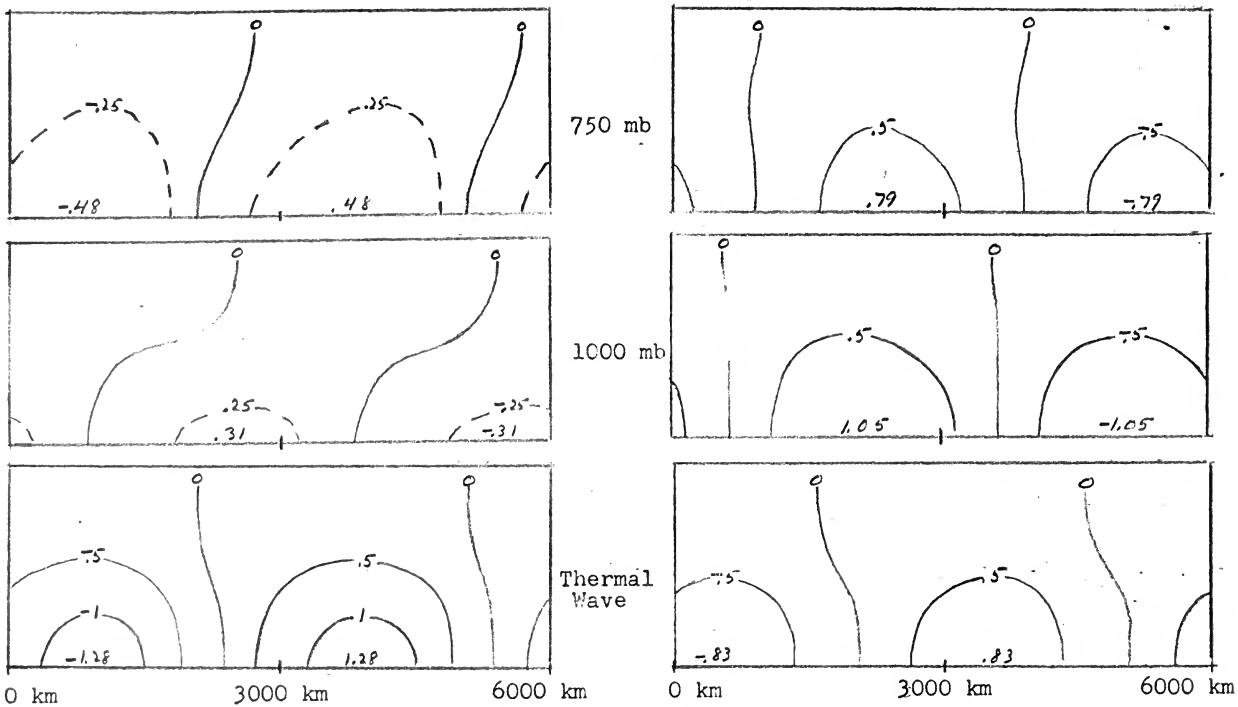

Figure 5.2. Case 5 (λ = 6000 km), Perturbation Stream Function (Ψ').

t = 48 hr

t = 60 hr

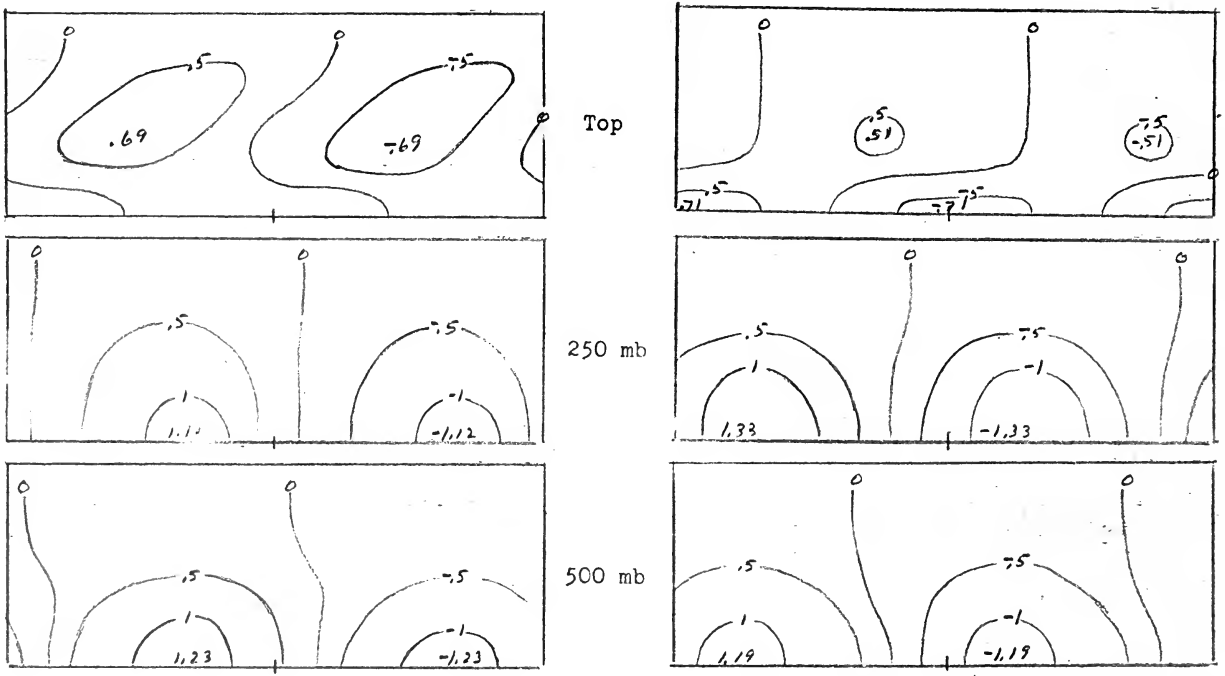

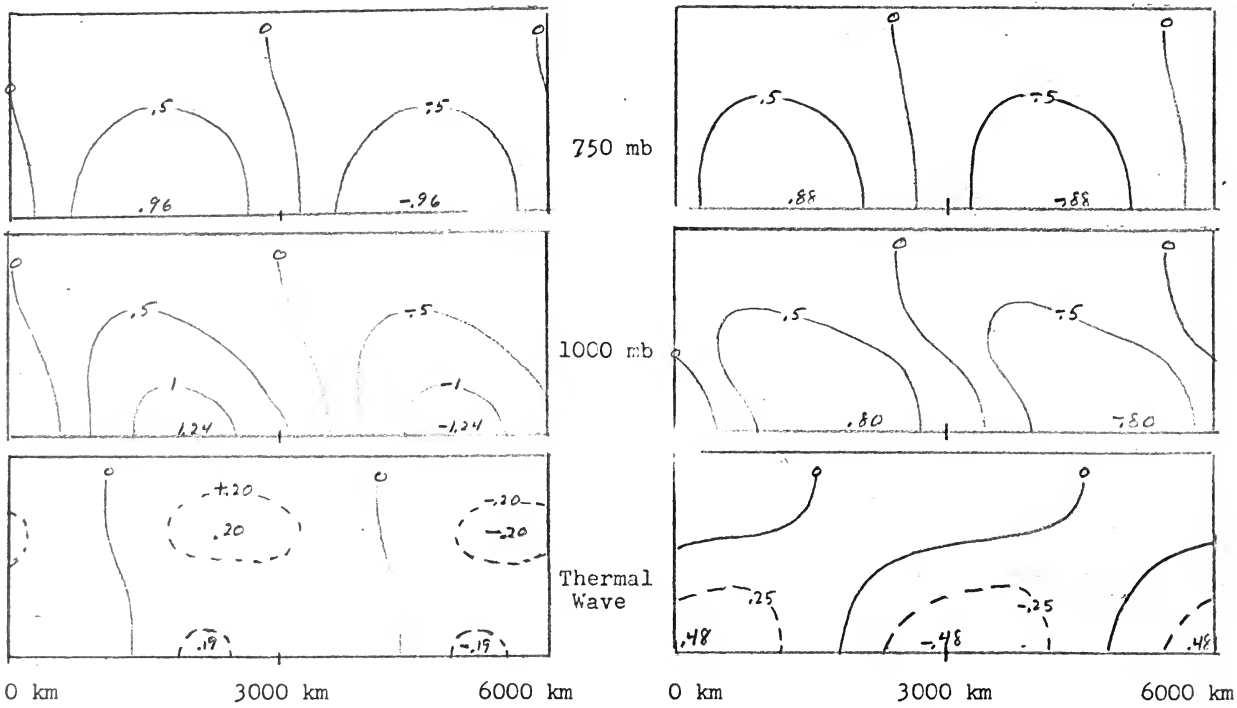

Figure 5.3. Case 5 (λ = 6000 km), Perturbation Stream Function (Ψ').

t = 72 hr

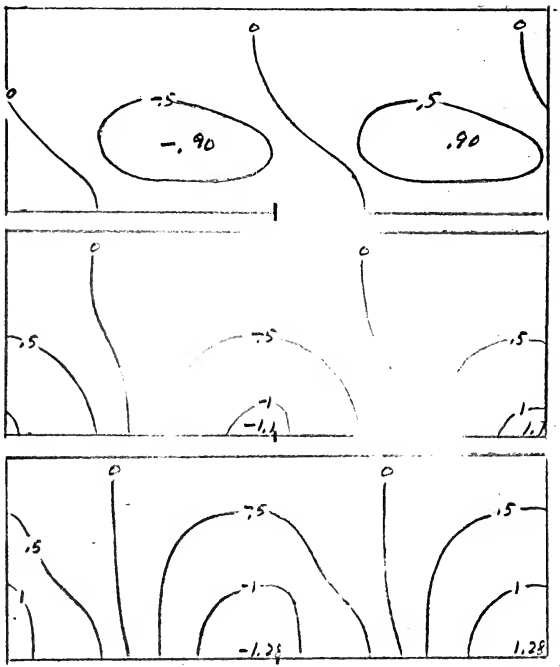

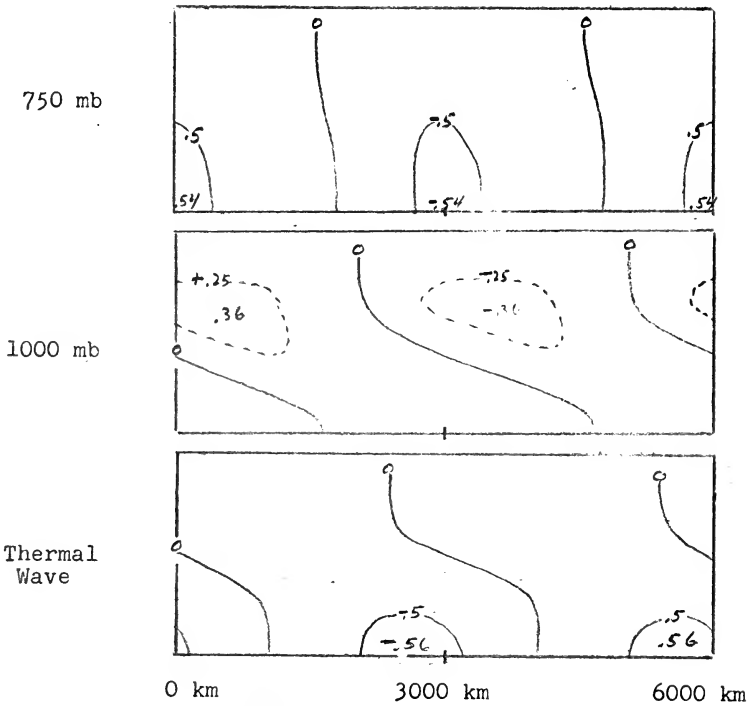

Figure 5.4. Case 5 (λ = 6000 km), Perturbation Stream Function (Ψ').

t = 0 hr

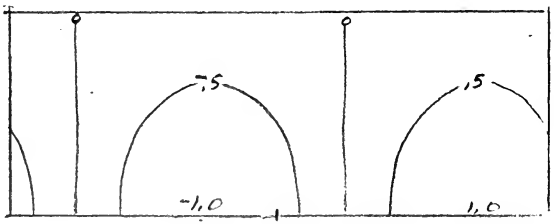

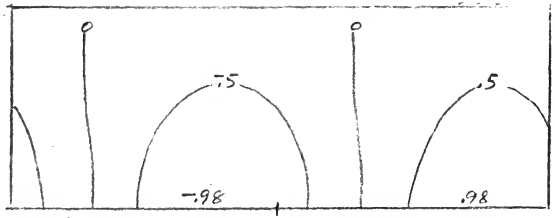

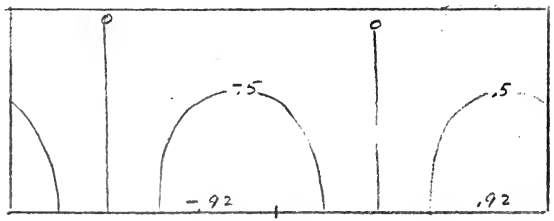

t = 0 hr

Top

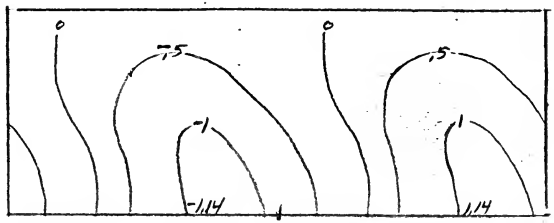

250 mb

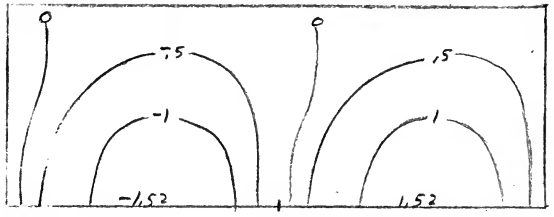

500 mb

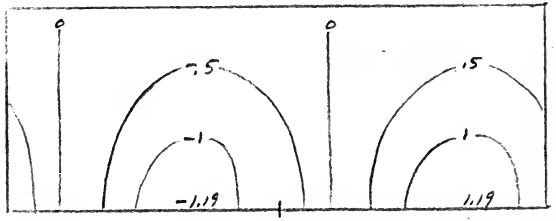

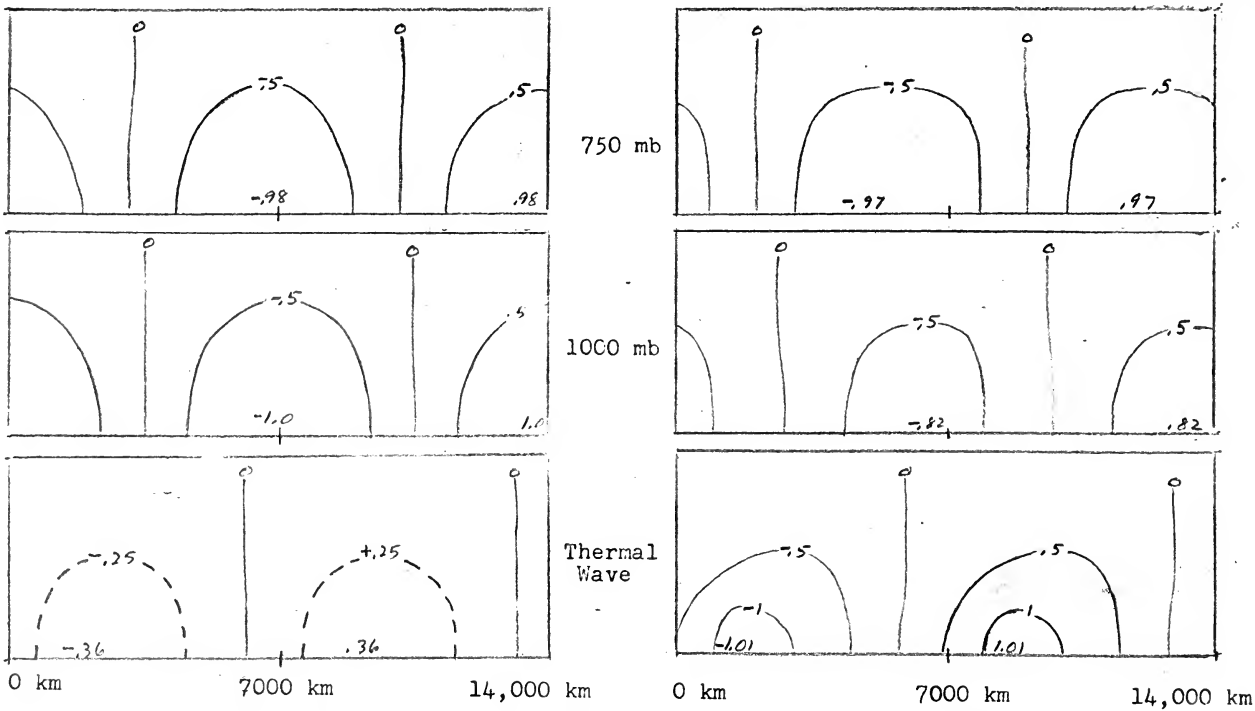

Figure 6.1 Case 6 (λ = 14,000 km), Perturbation Stream Function (Ψ').

t = 24 hr

t = 36 hr

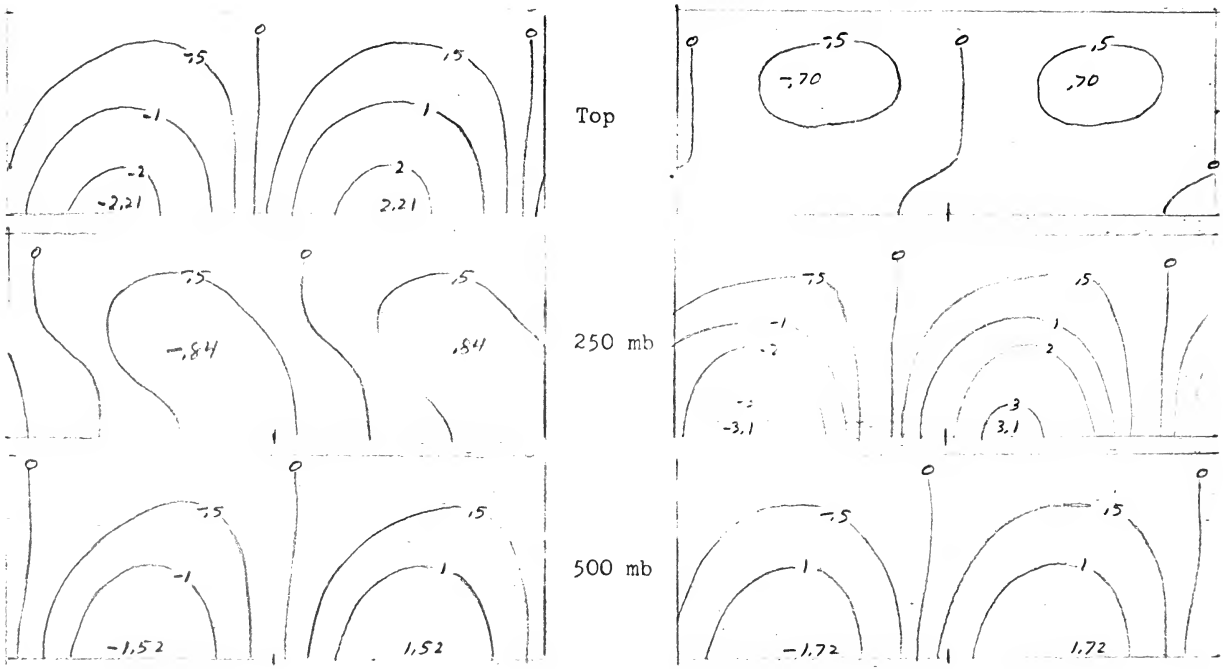
Top
250 mb
500 mb
-.5
0
.5
-1
1
-2
2
-2.21
2.21
-.84
.84
-1.52
1.52
-.70
.70
-3.1
3.1
-1.72
1.72

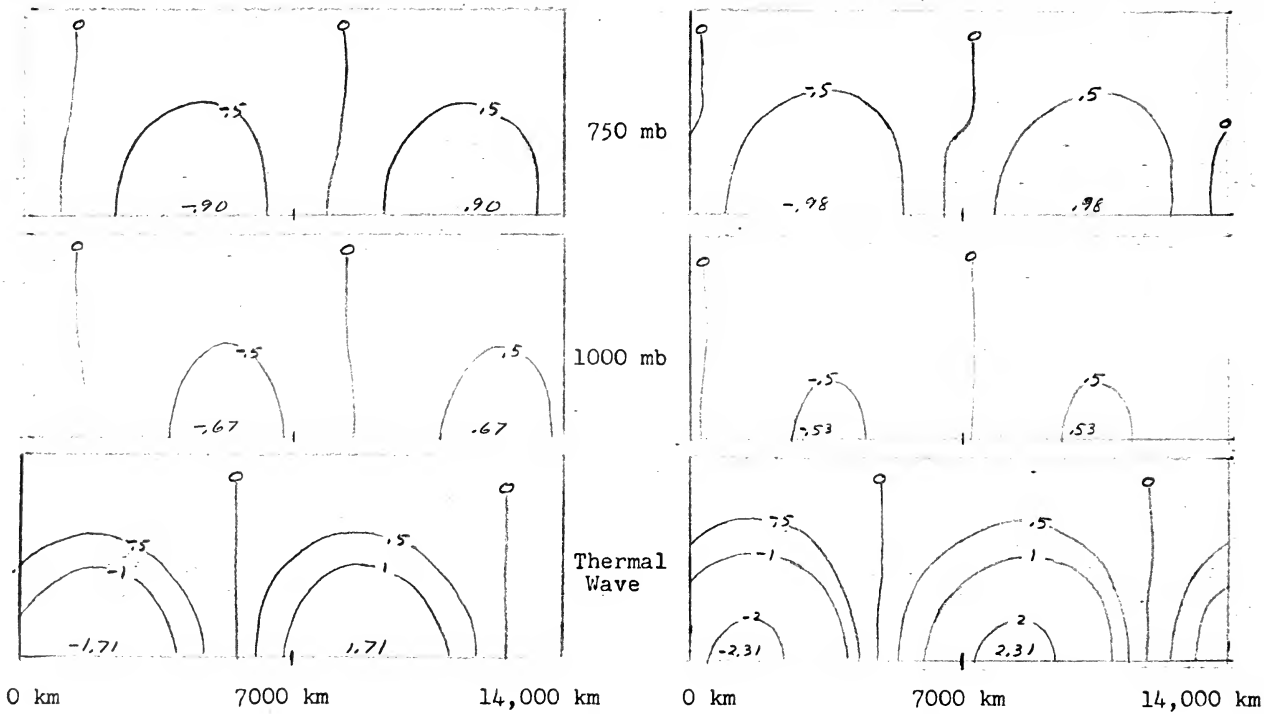

Figure 6.2. Case 6 (λ = 14,000 km), Perturbation Stream Function (Ψ').

t = 48 hr

t = 60 hr

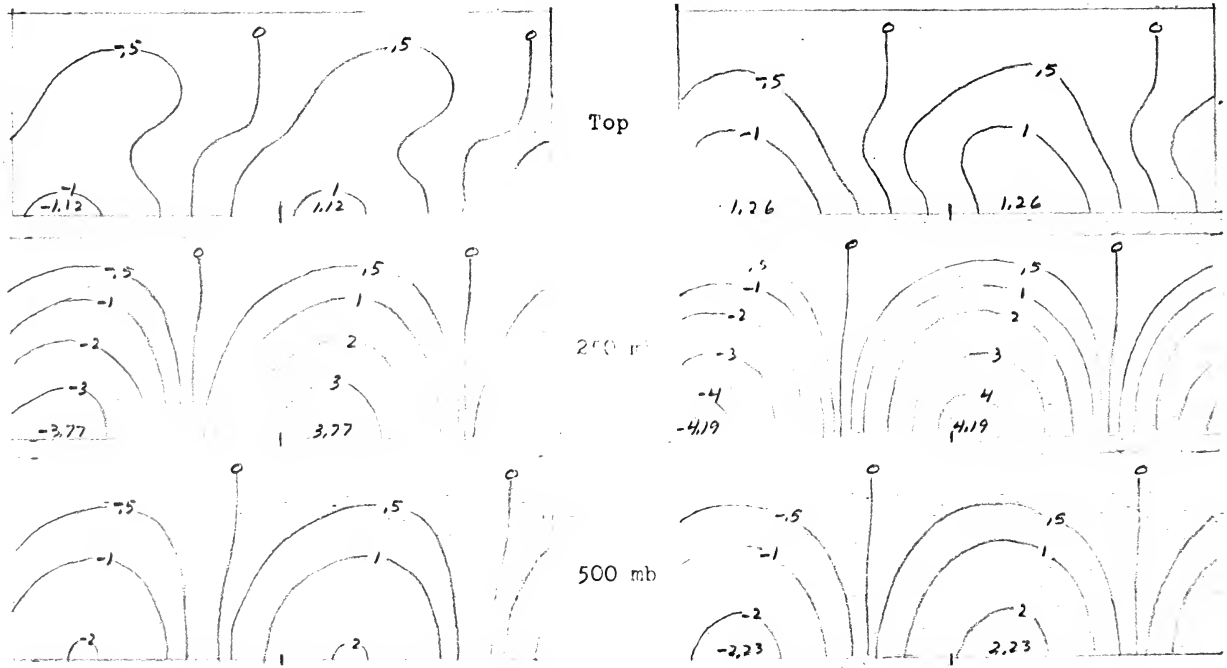
Top
200 mb
500 mb
-.5
0
.5
-1
1
-1.12
1.12
1.26
-2
2
-3
3
-3.77
3.77
-4
4
-4.19
4.19
-2.23
2.23

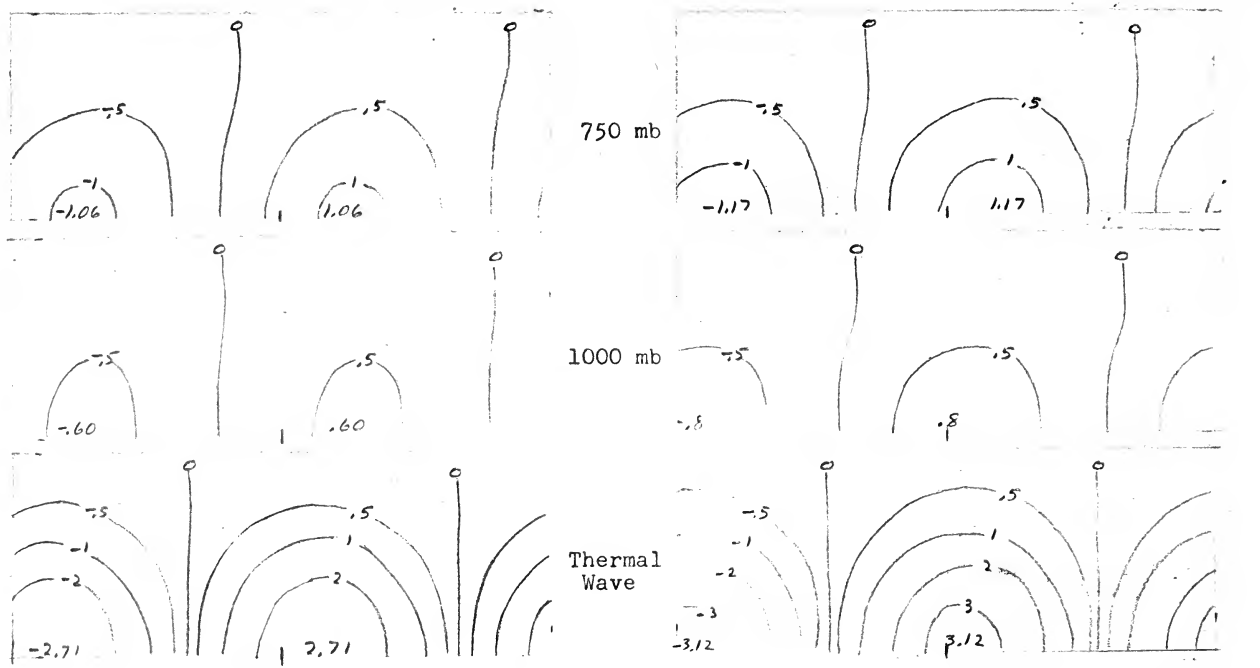

Figure 6.3. Case 6 (λ = 14,000 km), Perturbation Stream Function (Ψ').

t = 72 hr

Top

250 mb

500 mb

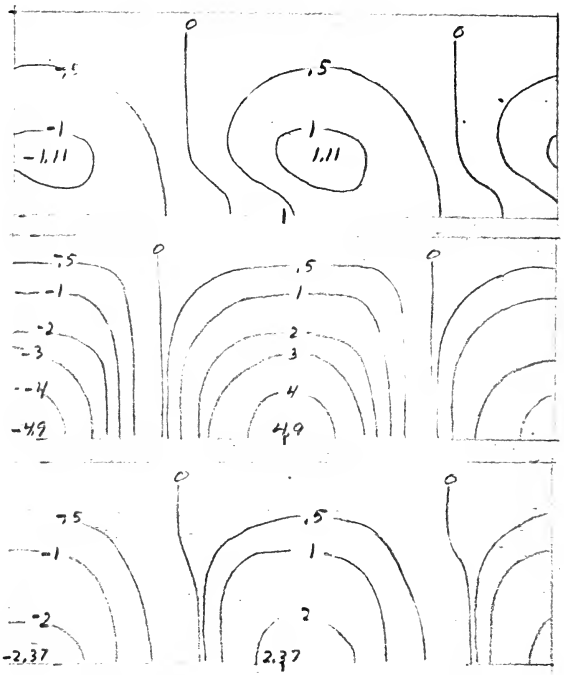

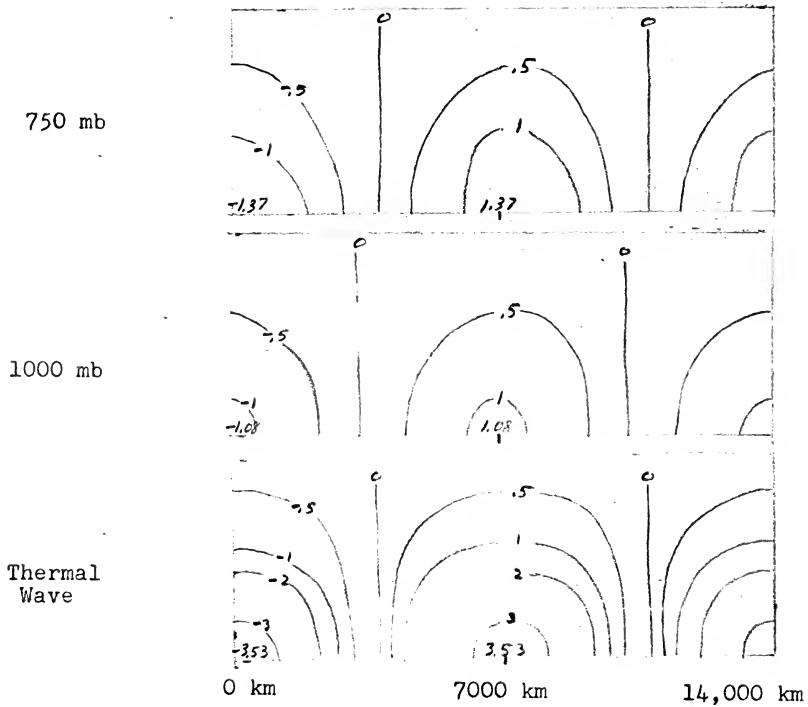

Figure 6.4. Case 6 (λ = 14,000 km), Perturbation Stream Function (Ψ').

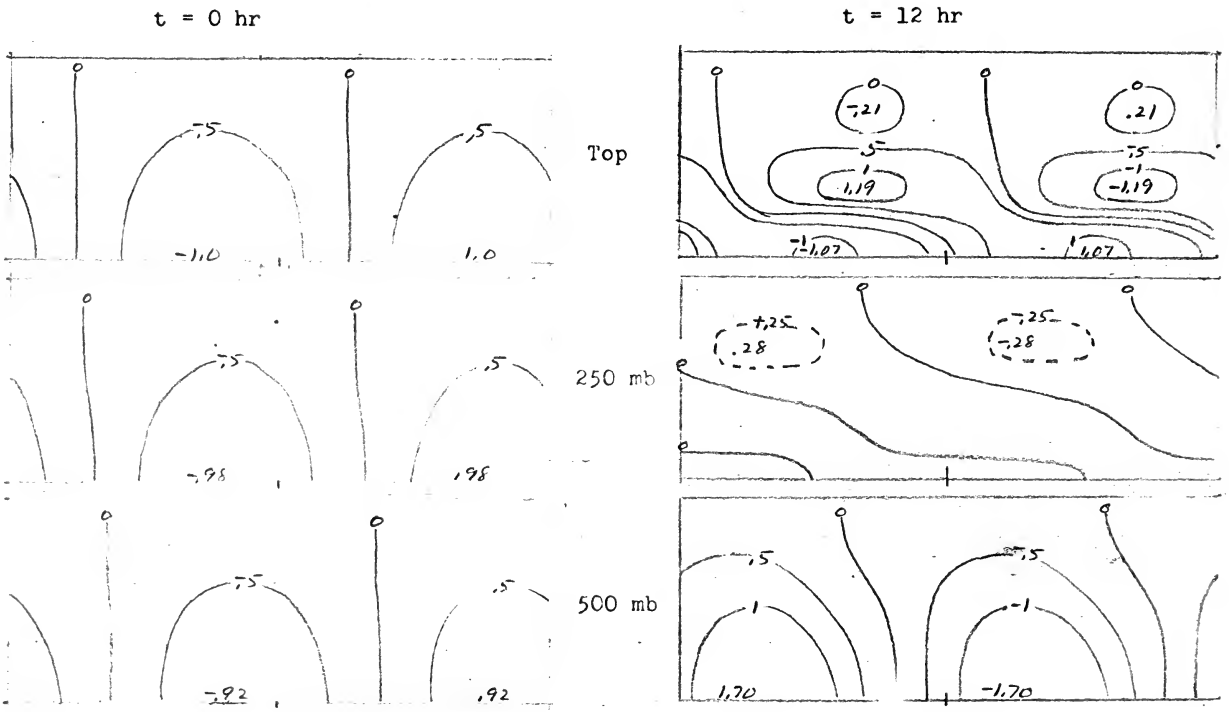
t = 0 hr
t = 12 hr
Top
250 mb
500 mb
-.5
.5
-1.0
1.0
-.98
.98
-.92
.92
-.21
.21
1.19
-1.19
-1.07
1.07
-.25
.28
-1.70
1.70

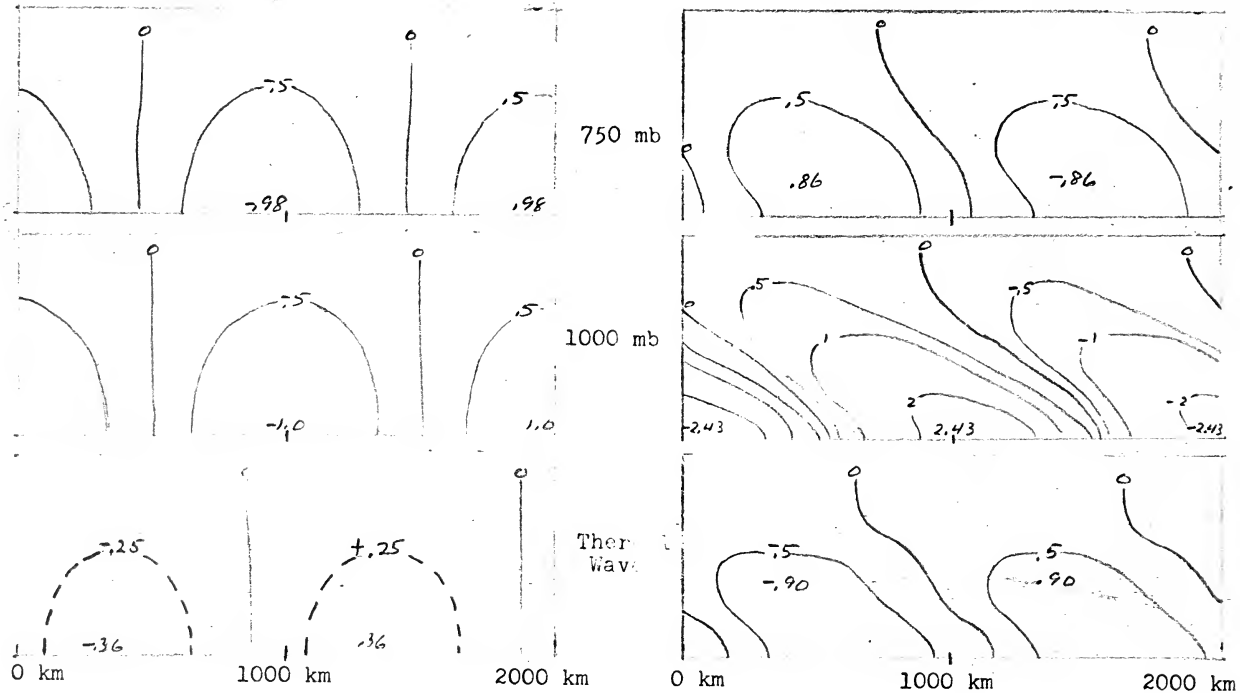

Figure 7.1. Case 7 (λ = 2000 km), Perturbation Stream Function (Ψ').

t = 24 hr

t = 36 hr

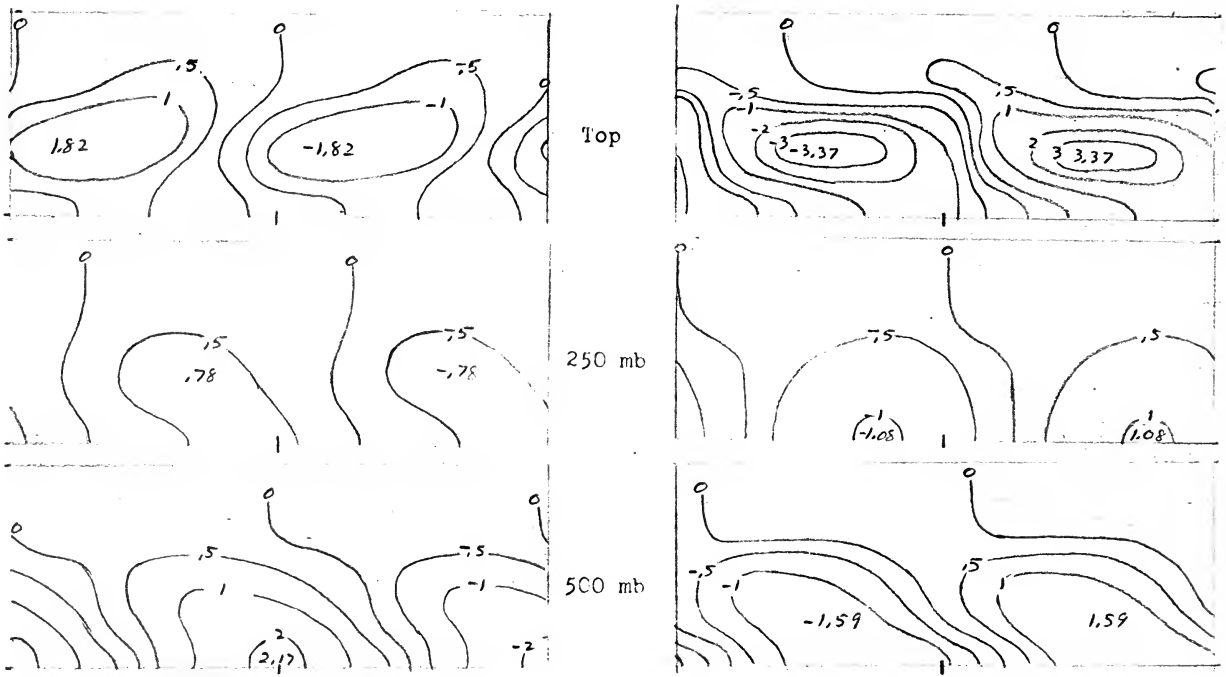

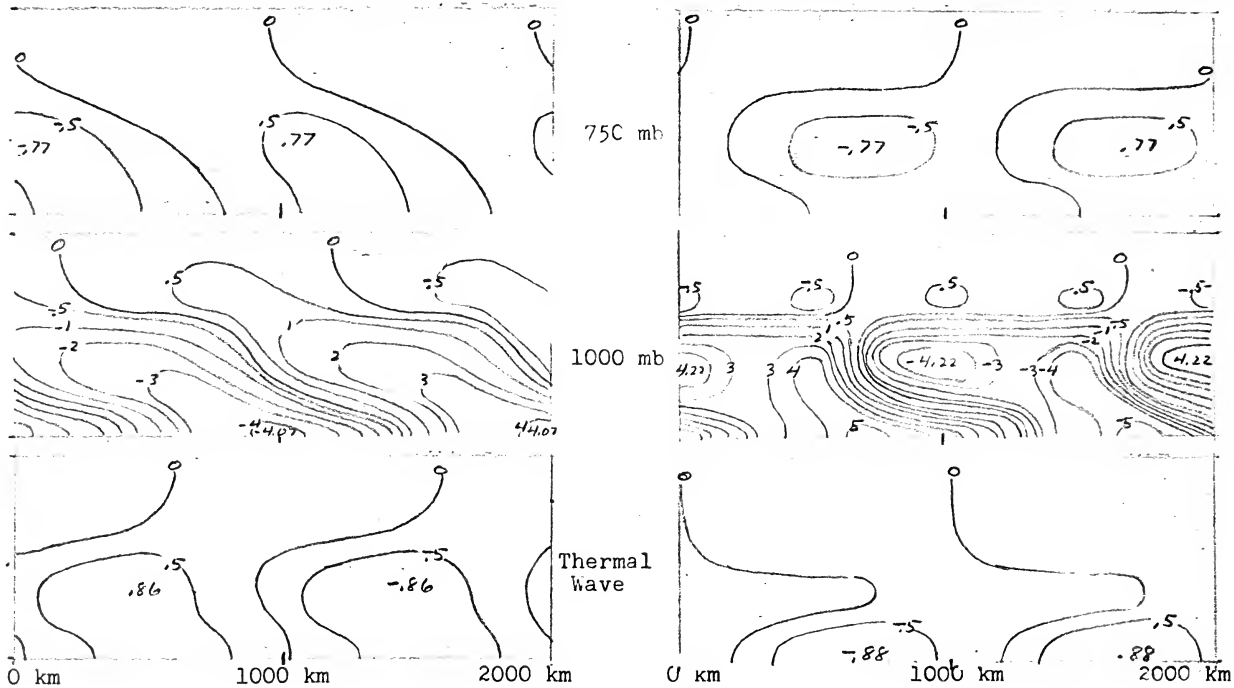

Figure 7.2. Case 7 (λ = 2000 km), Perturbation Stream Function (Ψ').

t = 48 hr

t = 60 hr

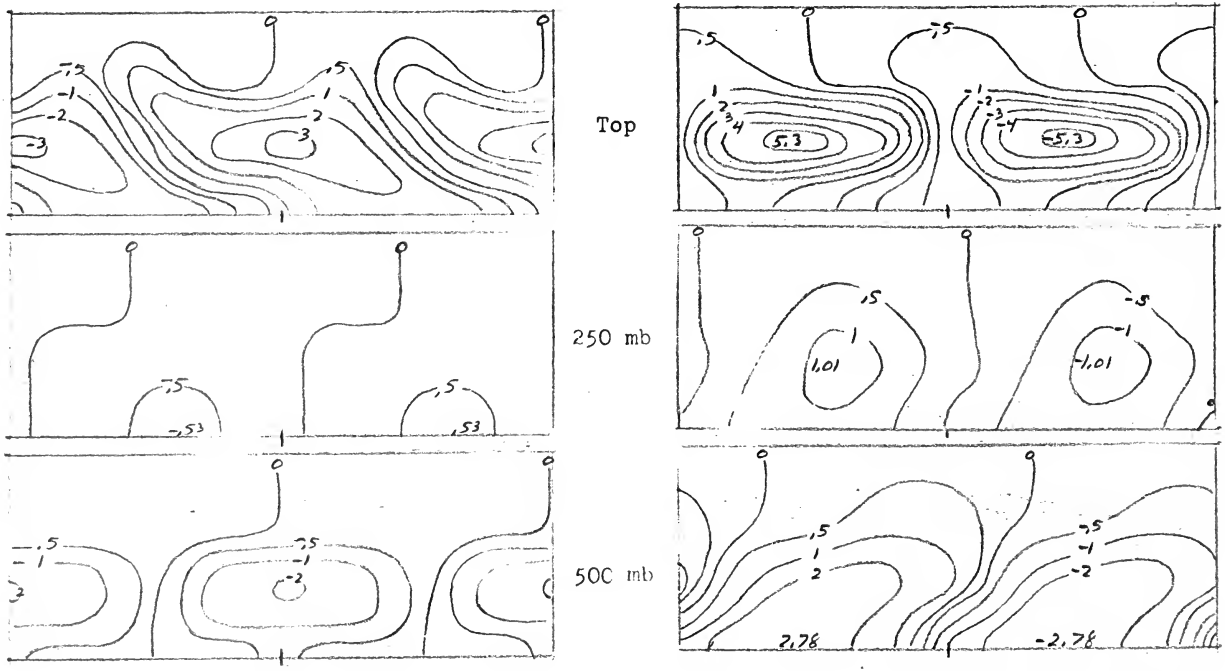

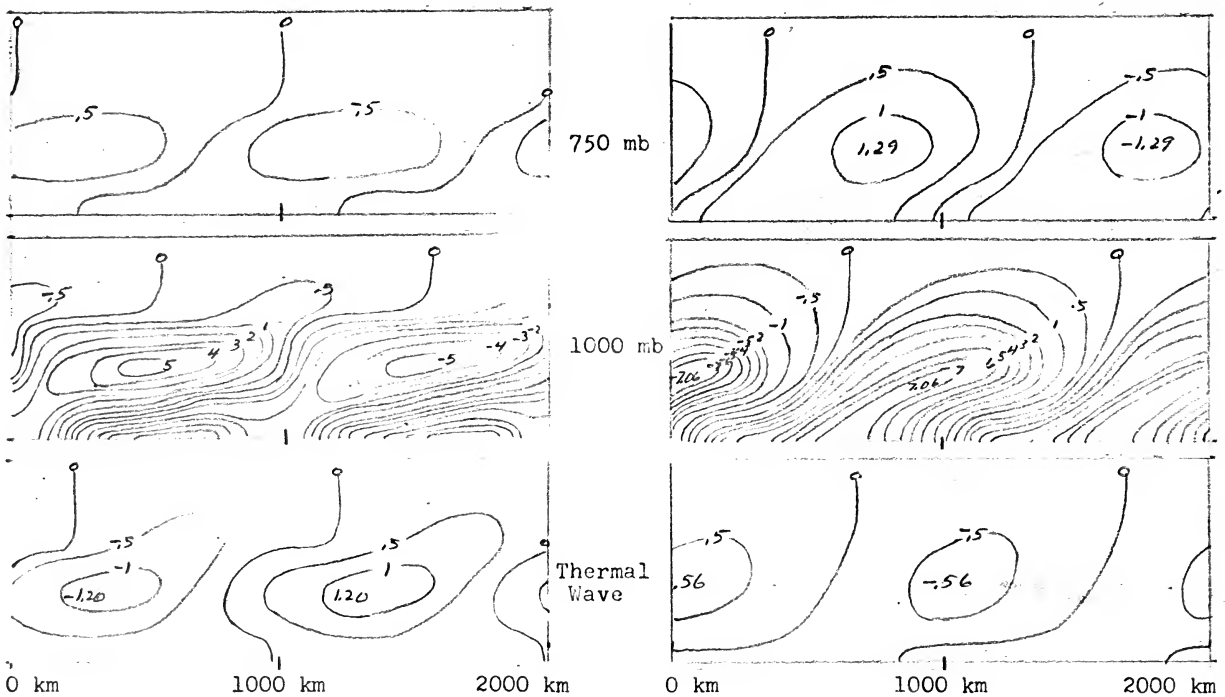

Figure 7.3. Case 7 (λ = 2000 km), Perturbation Stream Function (Ψ').

t = 72 hr

Top

250 mb

500 mb

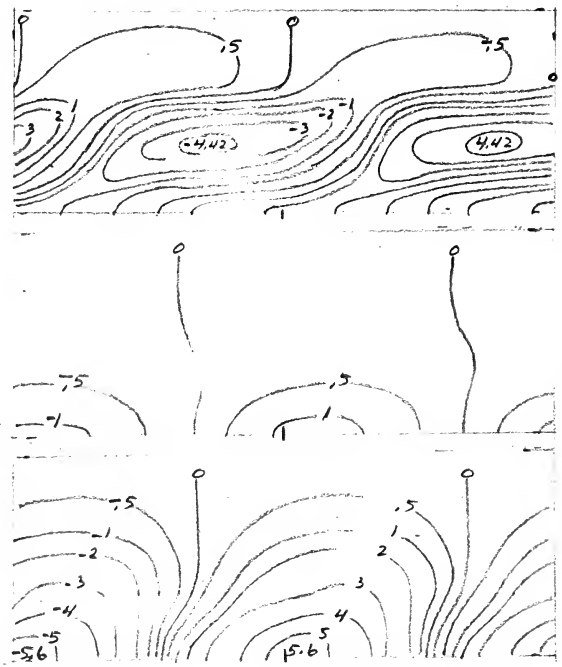

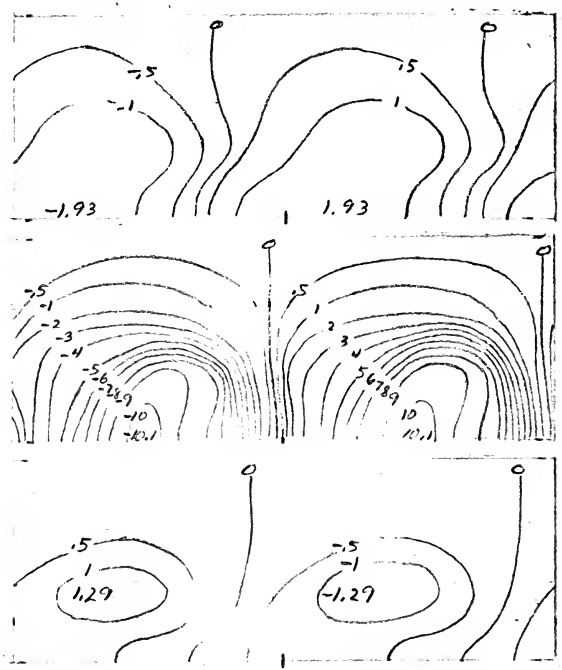

Figure 7.4. Case 7 (λ = 2000 km), Perturbation Stream Function (Ψ').

t = 0 hr

t = 12 hr

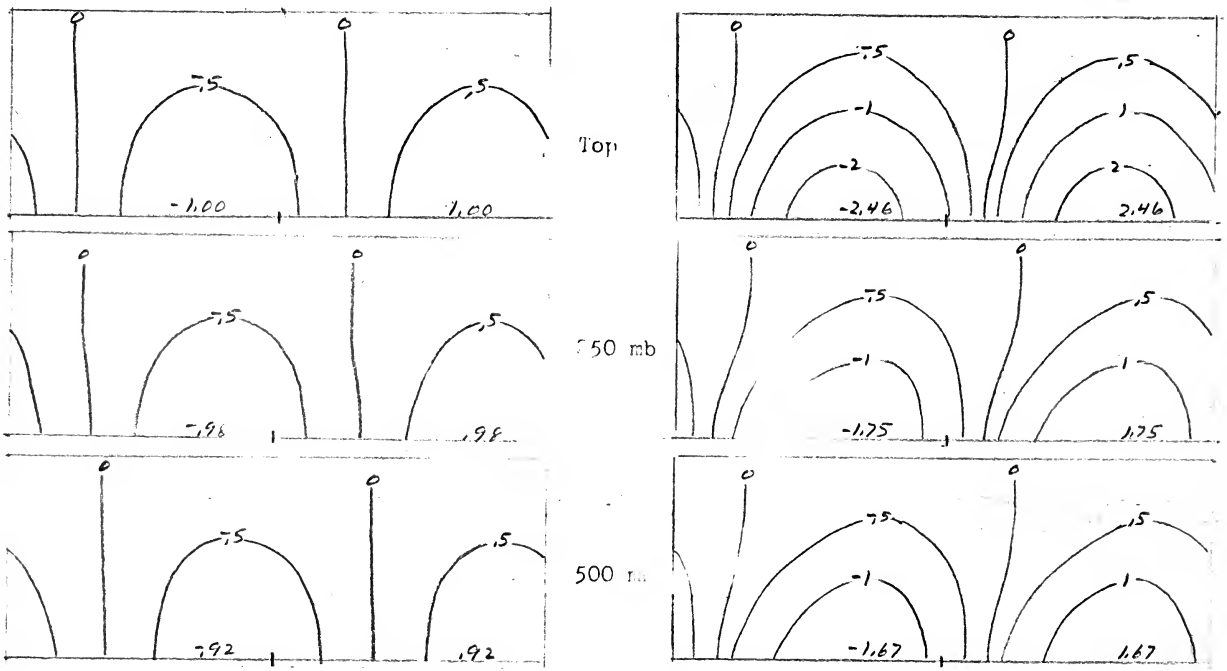

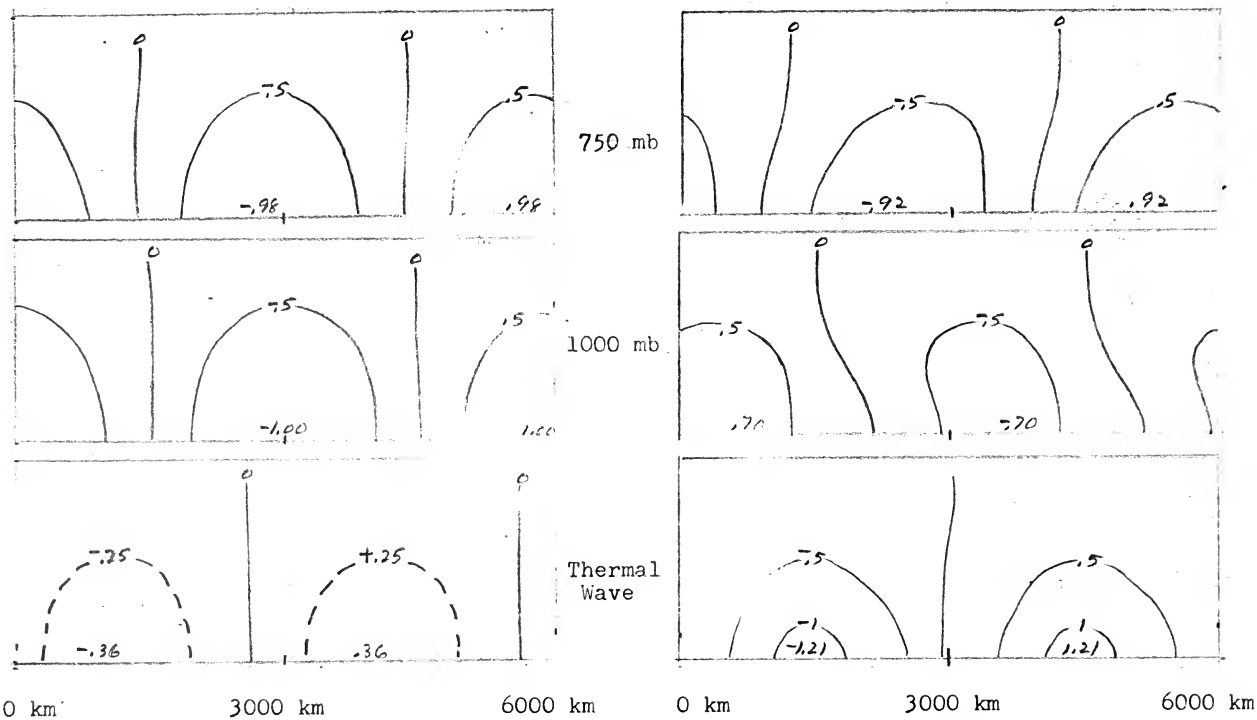

Figure 8.1. Case 8 (λ = 6000 km), Perturbation Stream Function (Ψ').

t = 24 hr

t = 36 hr

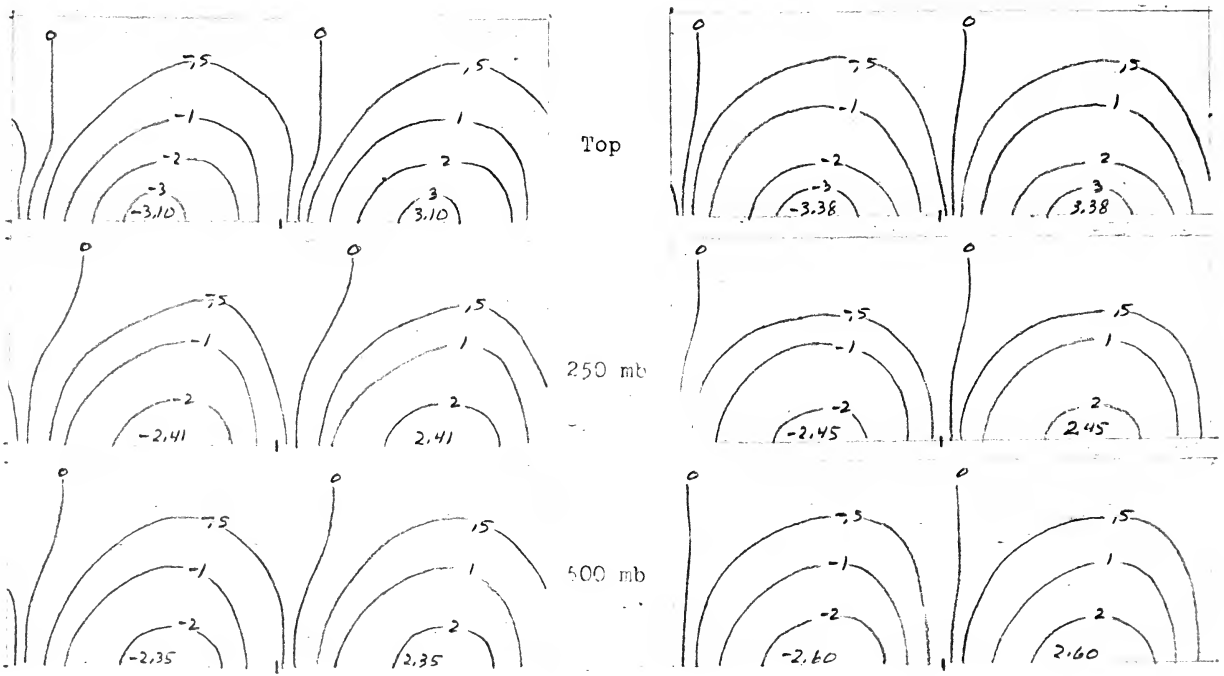

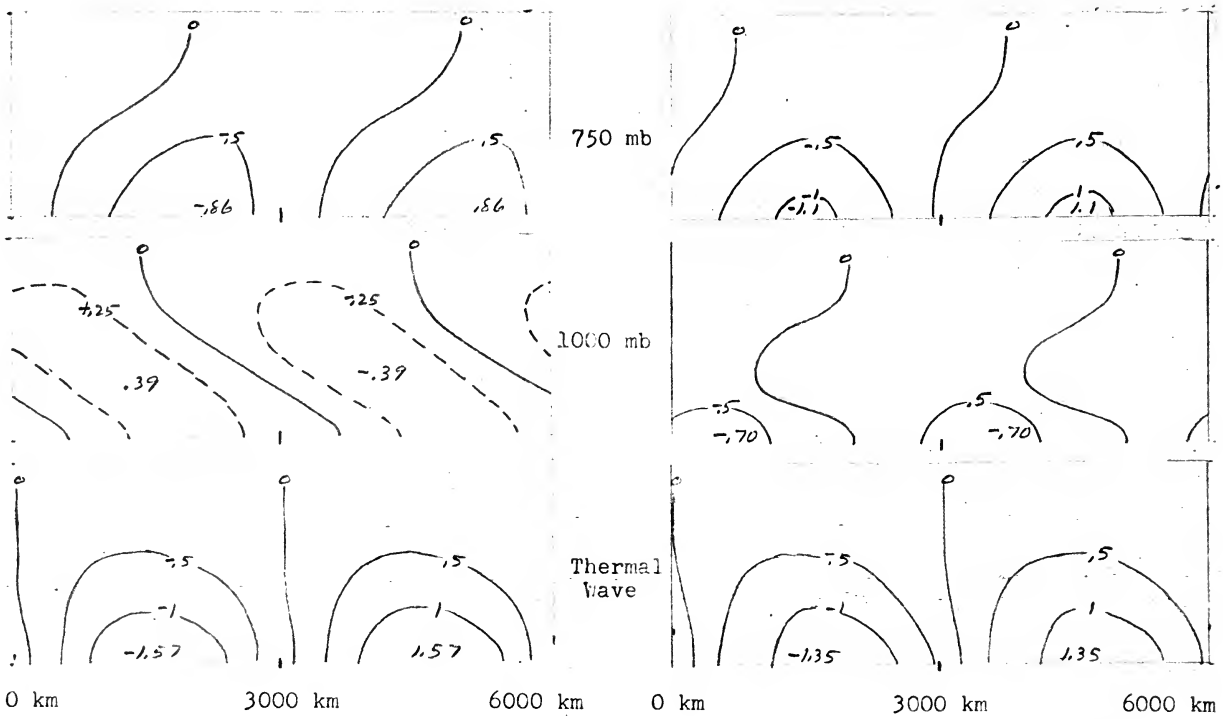

Figure 8.2. Case 8 (λ = 6000 km), Perturbation Stream Function (Ψ').

t = 48 hr

t = 60 km

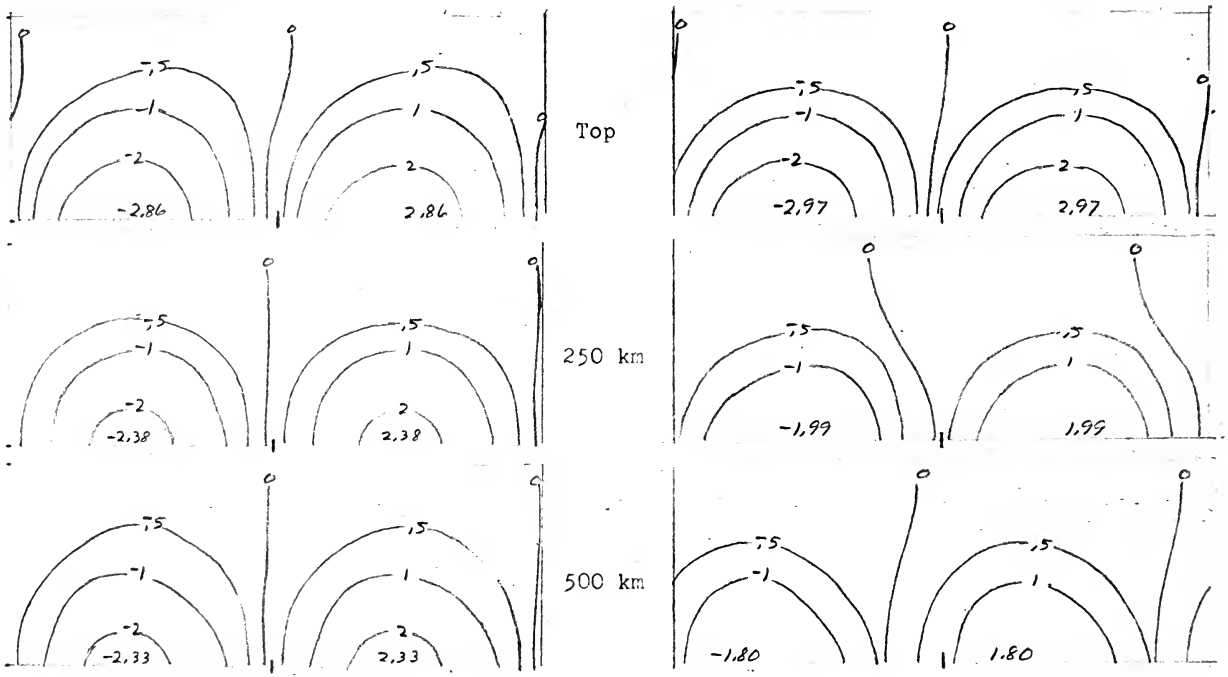
Top
250 km
500 km
-,5
-1
-2
-2,86
,5
1
2
2,86
-2,97
2,97
-2,38
2,38
-1,99
1,99
-2,33
2,33
-1,80
1,80

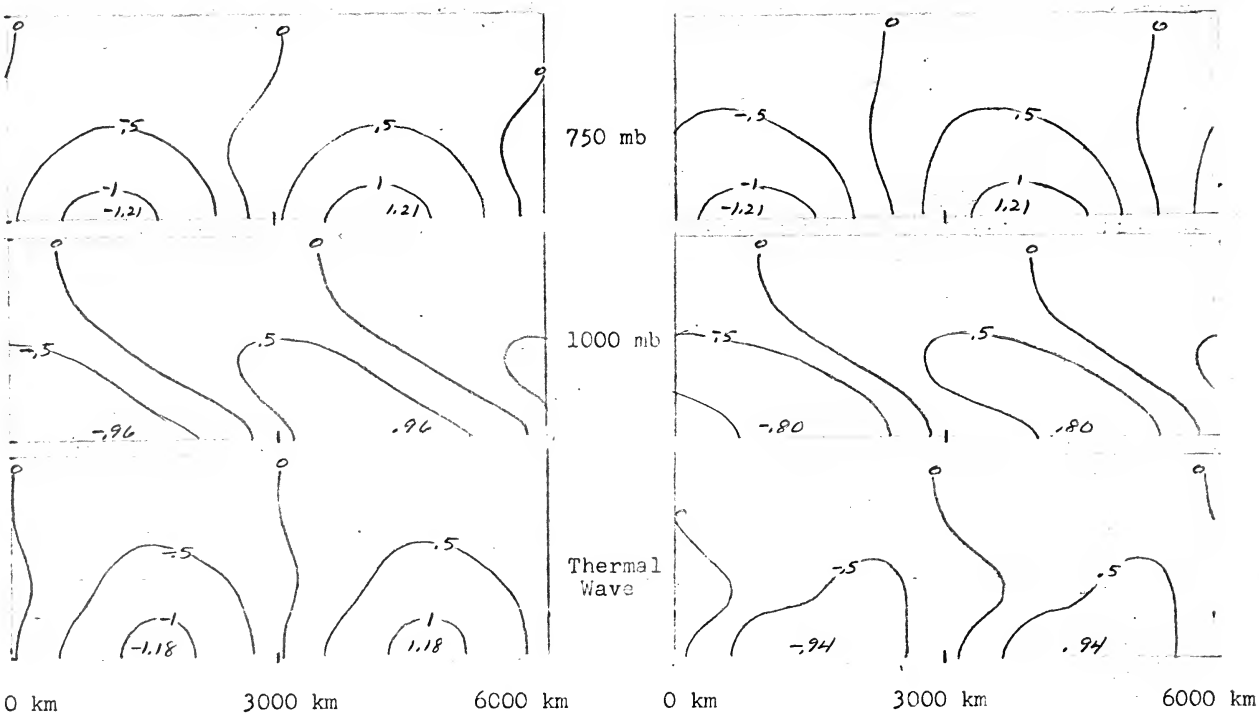

Figure 8.3. Case 8 (λ = 6000 km), Perturbation Stream Function (Ψ').

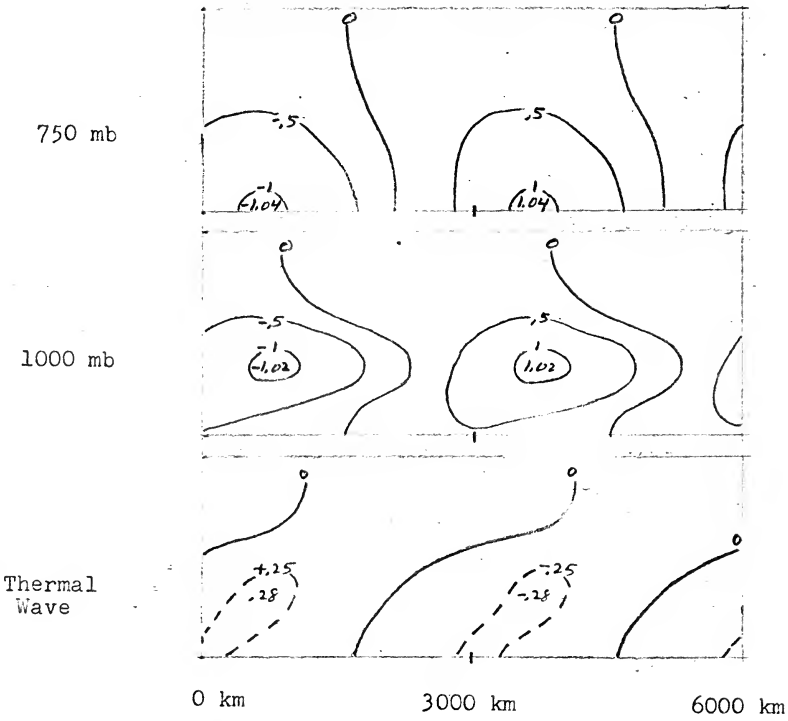

Figure 8.4. Case 8 (λ = 6000 km), Perturbation Stream Function (Ψ').

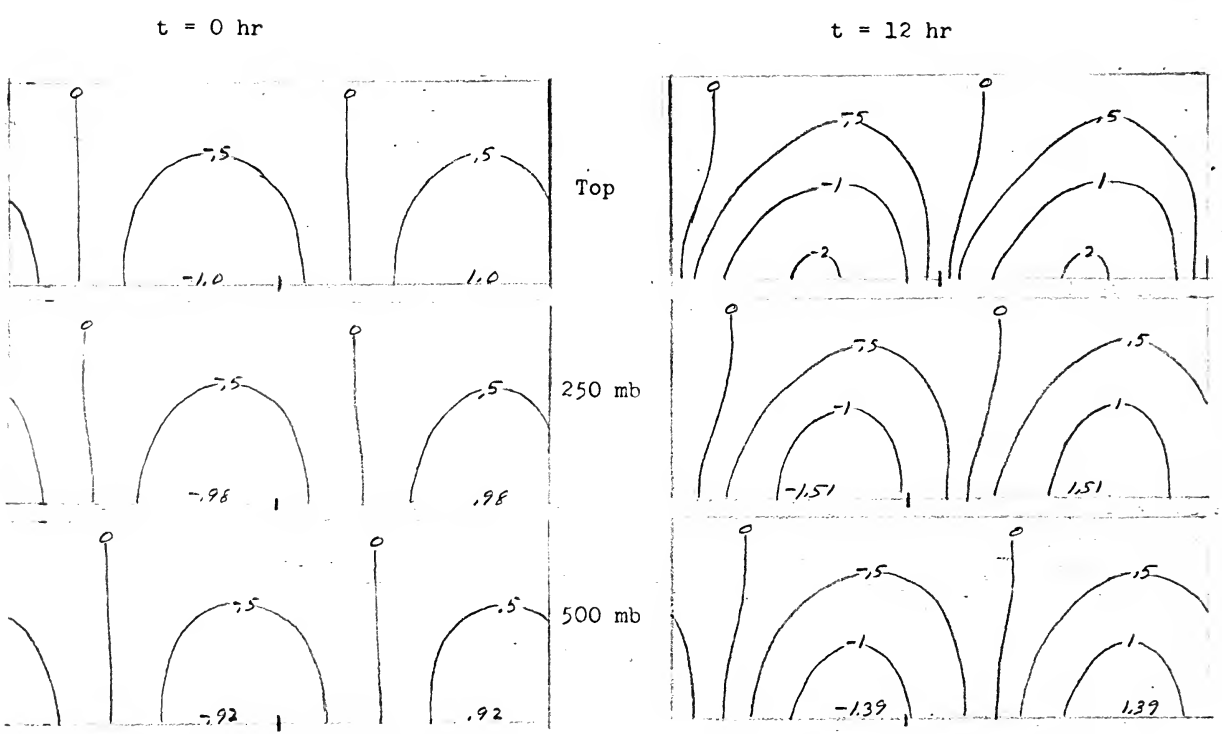
t = 0 hr
t = 12 hr
Top
250 mb
500 mb
0
.5
-.5
1.0
-1.0
.98
-.98
.92
-.92
1
-1
1.5
-1.5
1.51
-1.51
1.39
-1.39
2
-2

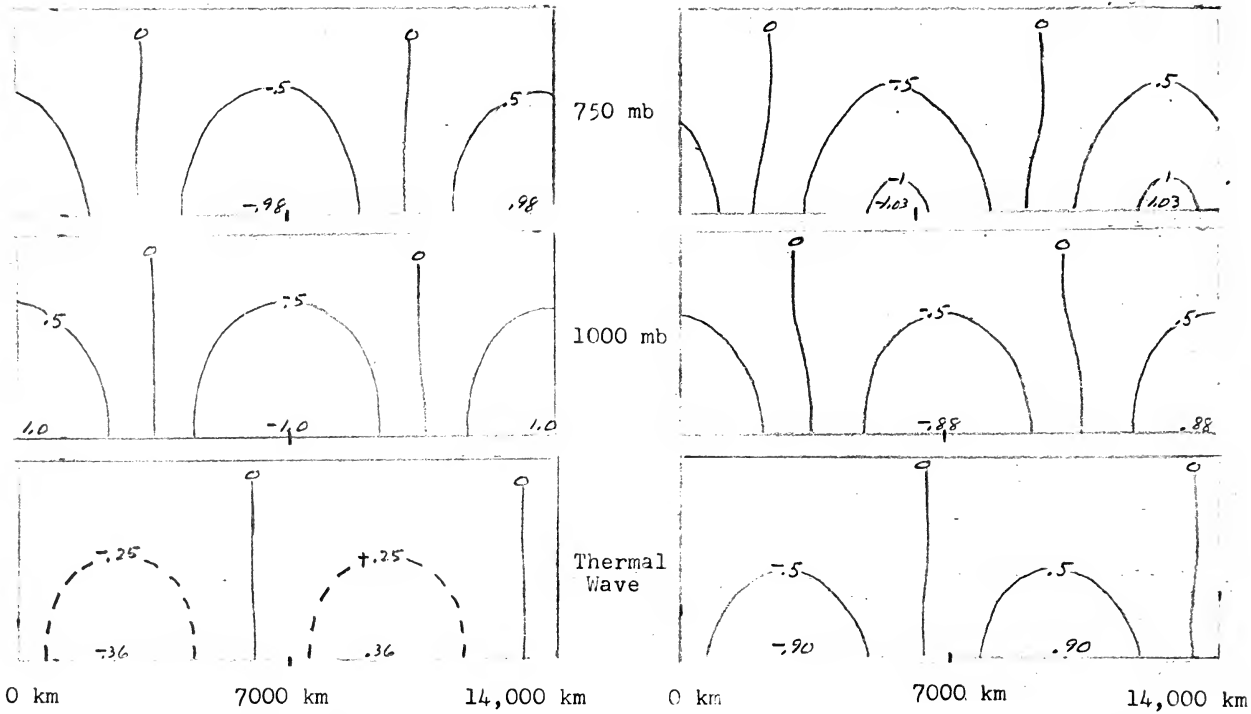

Figure 9.1. Case 9 (λ = 14,000 km), Perturbation Stream Function (Ψ').

t = 24 hr

t = 36 hr

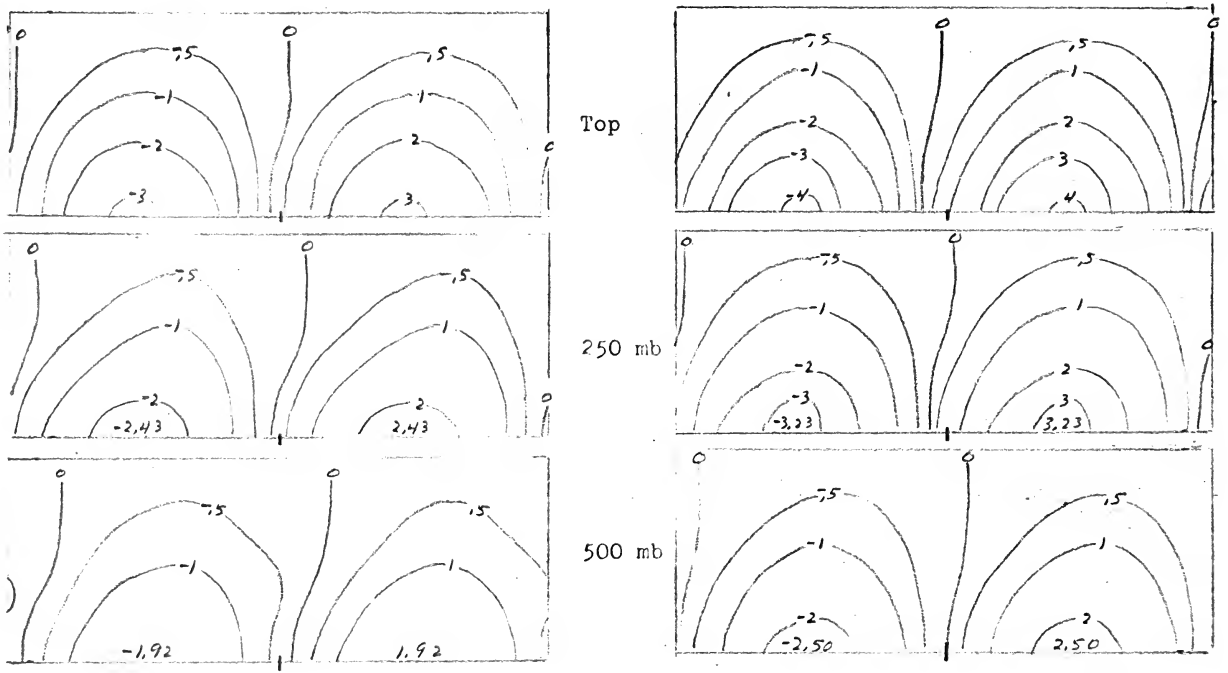

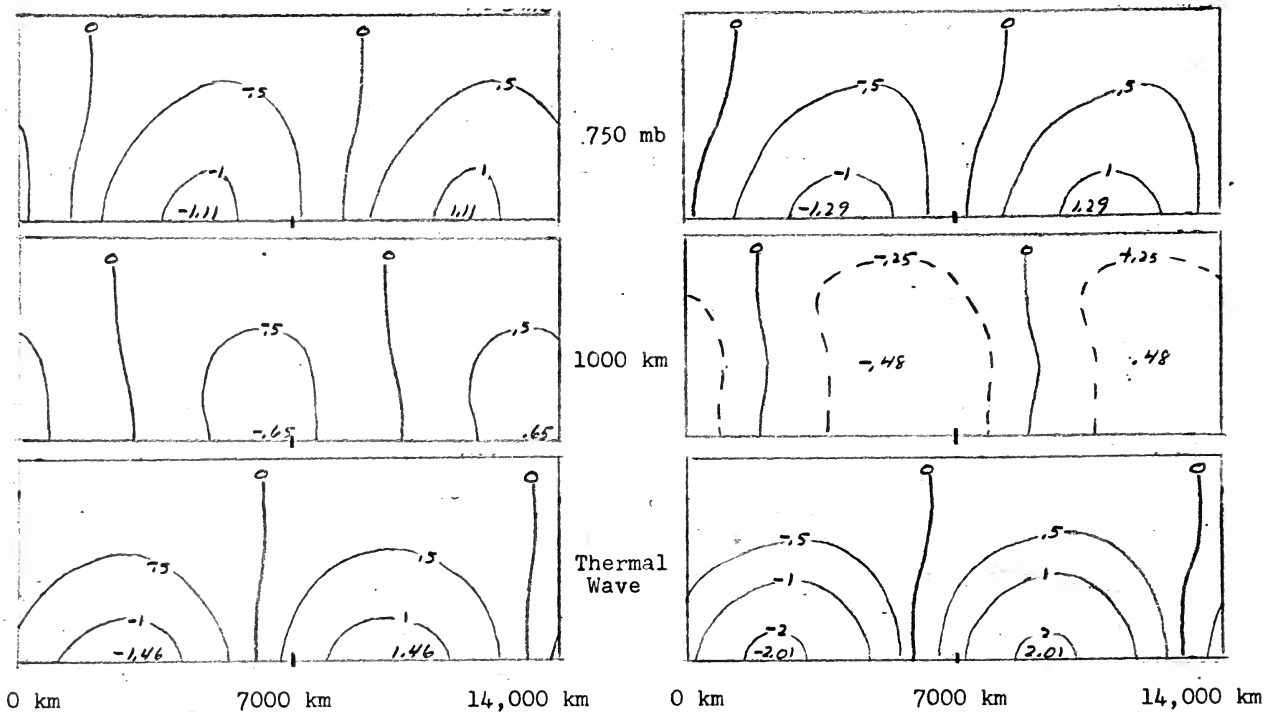

Figure 9.2. Case 9 (λ = 14,000 km), Perturbation Stream Function (Ψ').

t = 48 hr

t = 60 hr

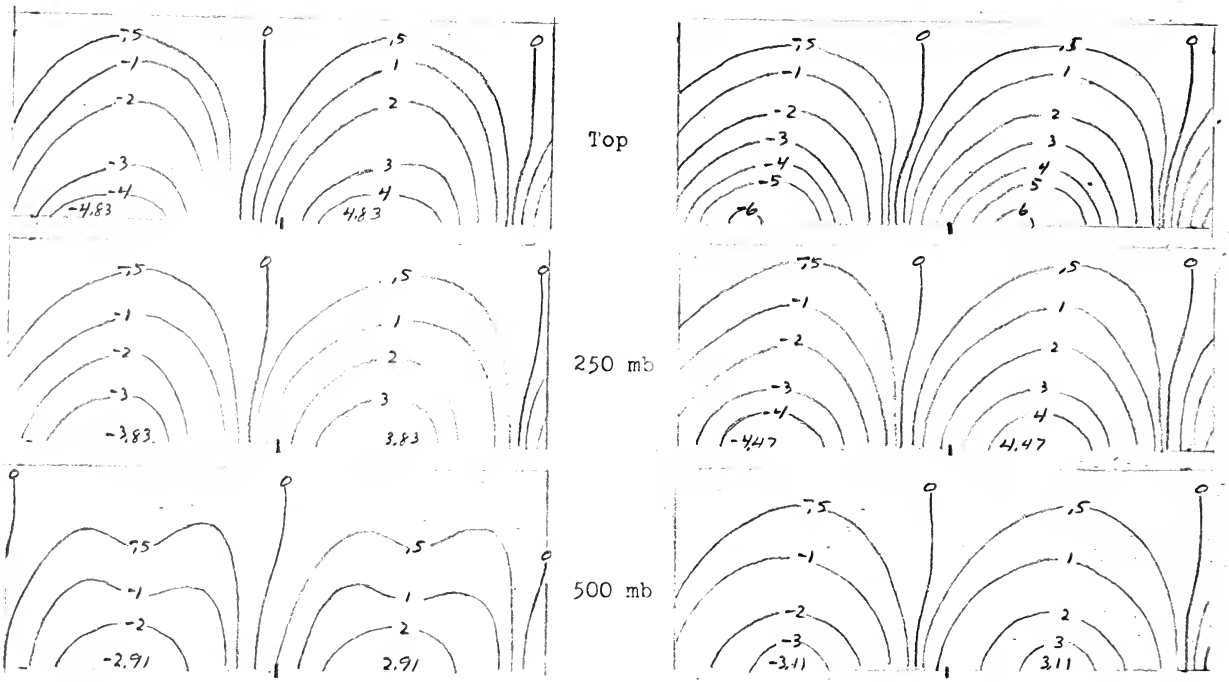

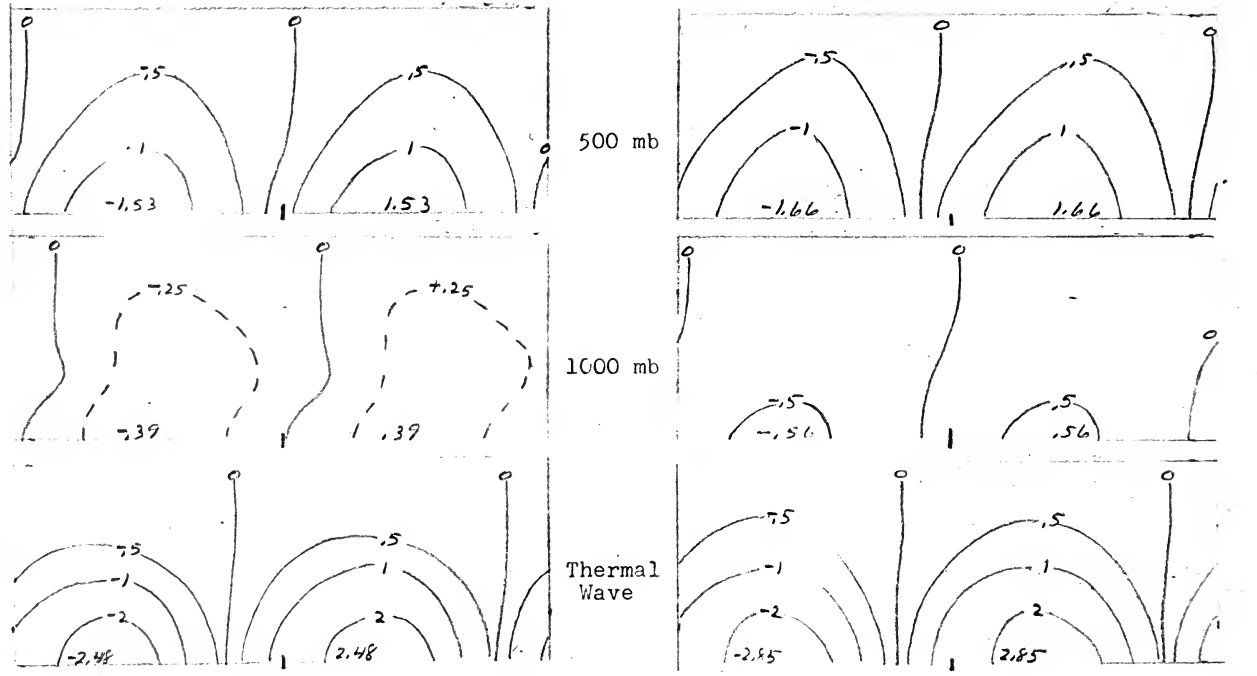

Figure 9.3. Case 9. (λ = 14,000 km), Perturbation Stream Function (Ψ').

t = 72 hr

Top

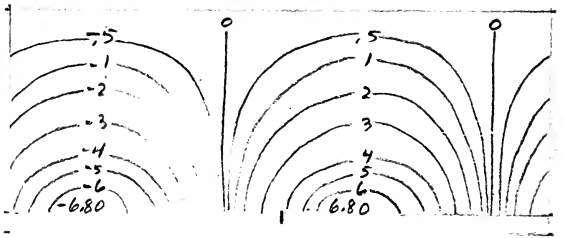

250 mb

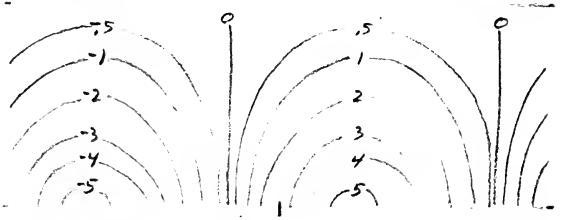

500 mb

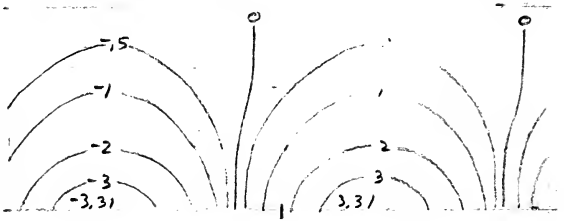

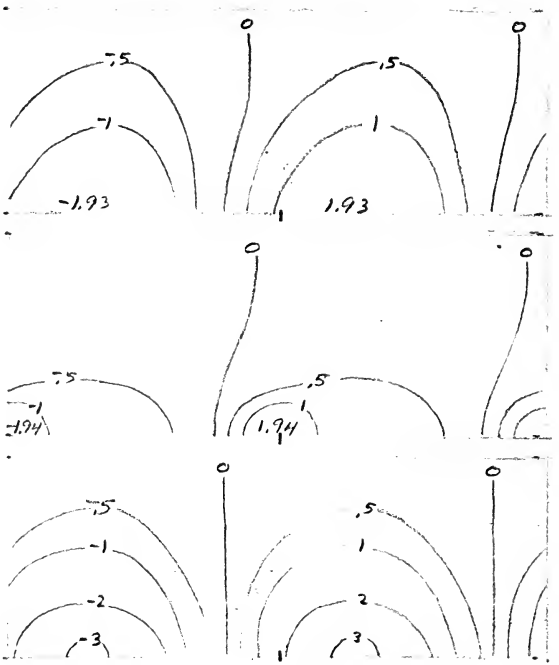

Figure 9.4. Case 9 (λ = 14,000 km), Perturbation Stream Function (Ψ').

t = 0 hr

t = 12 hr

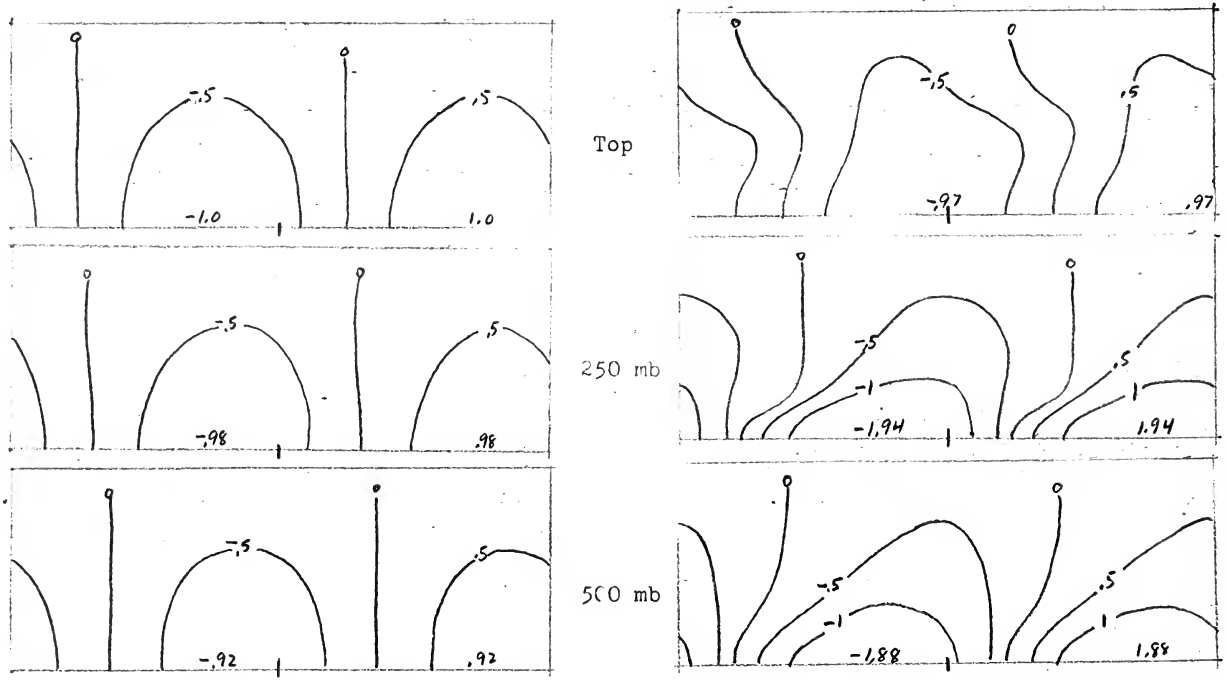

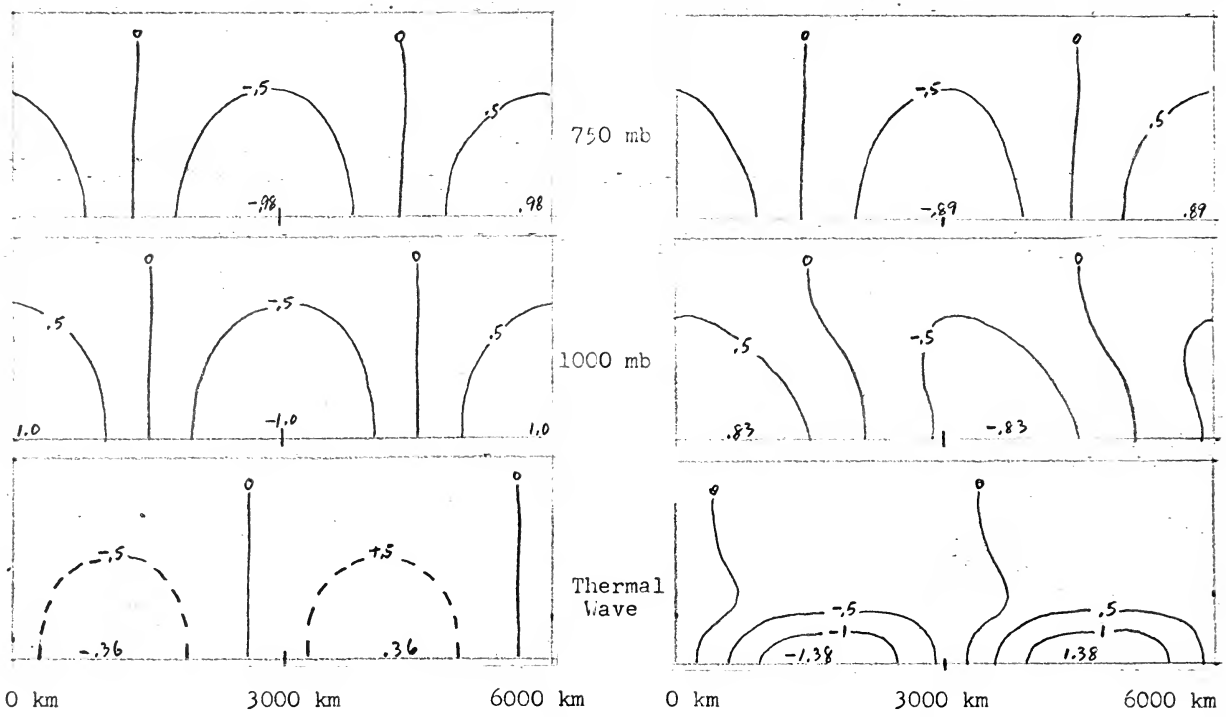

Figure 10.1. Case 10 (λ = 6000 km), Perturbation Stream Function (Ψ').

t = 24 hr

t = 36 hr

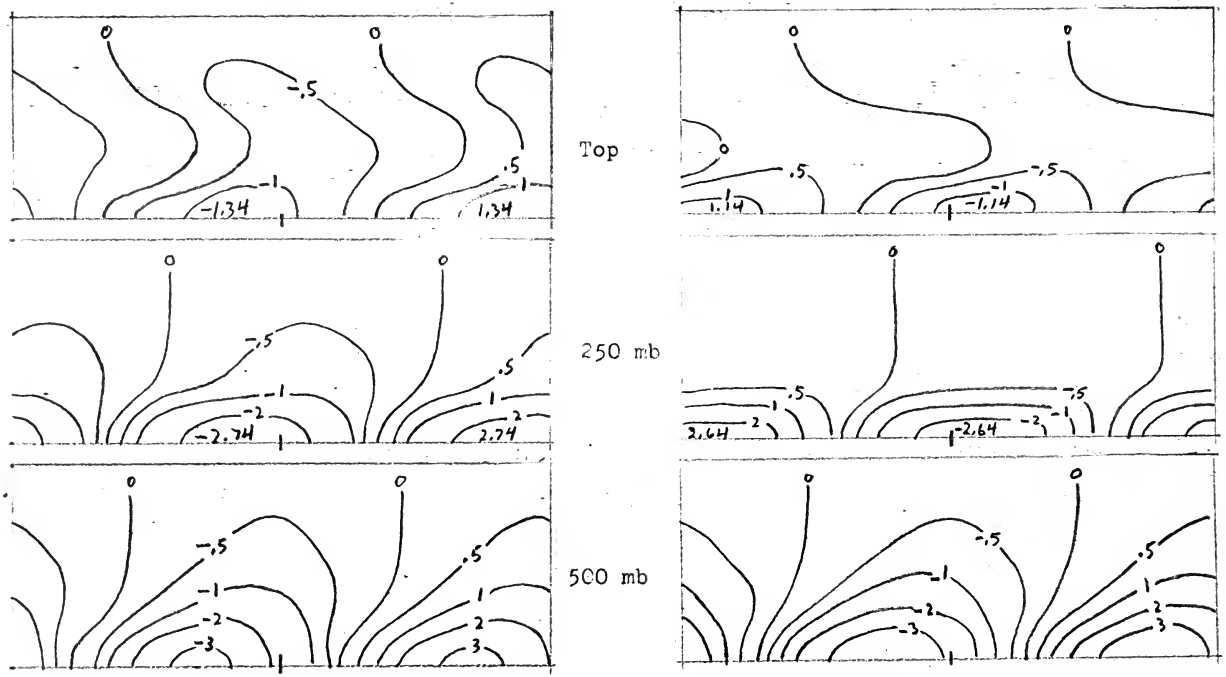

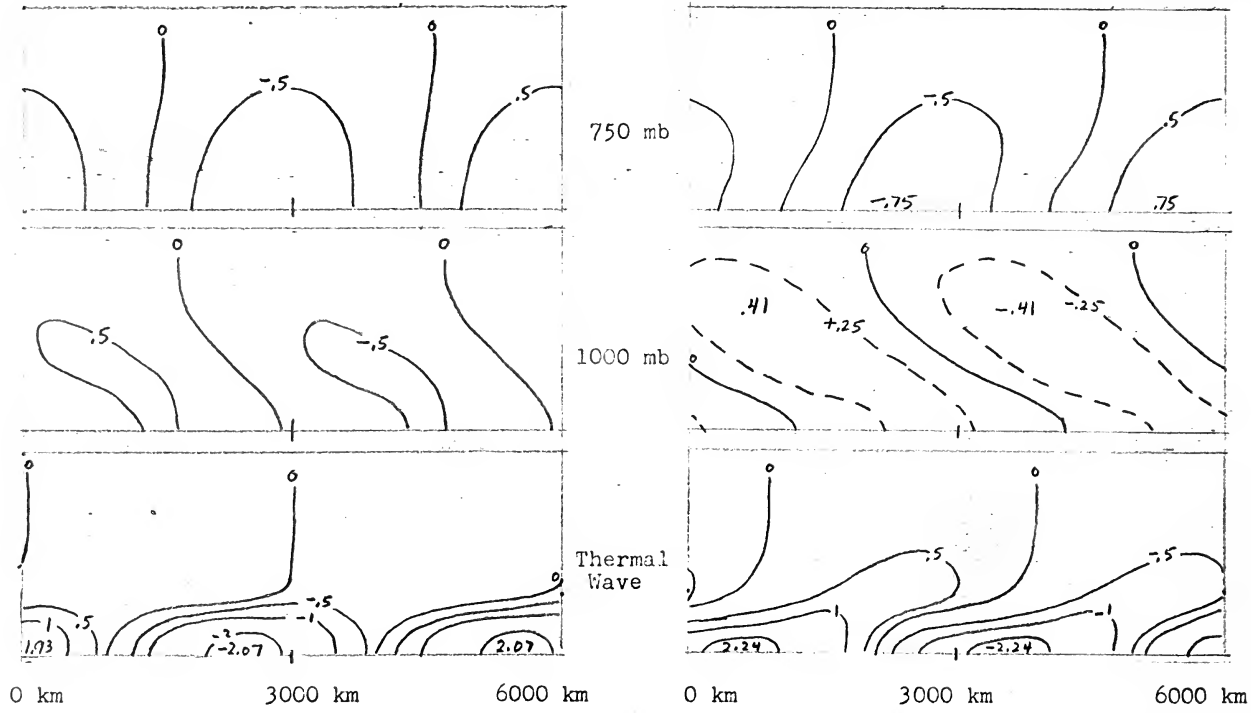

Figure 10.2. Case 10 (λ = 6000 km), Perturbation Stream Function (Ψ').

t = 48 hr

t = 60 hr

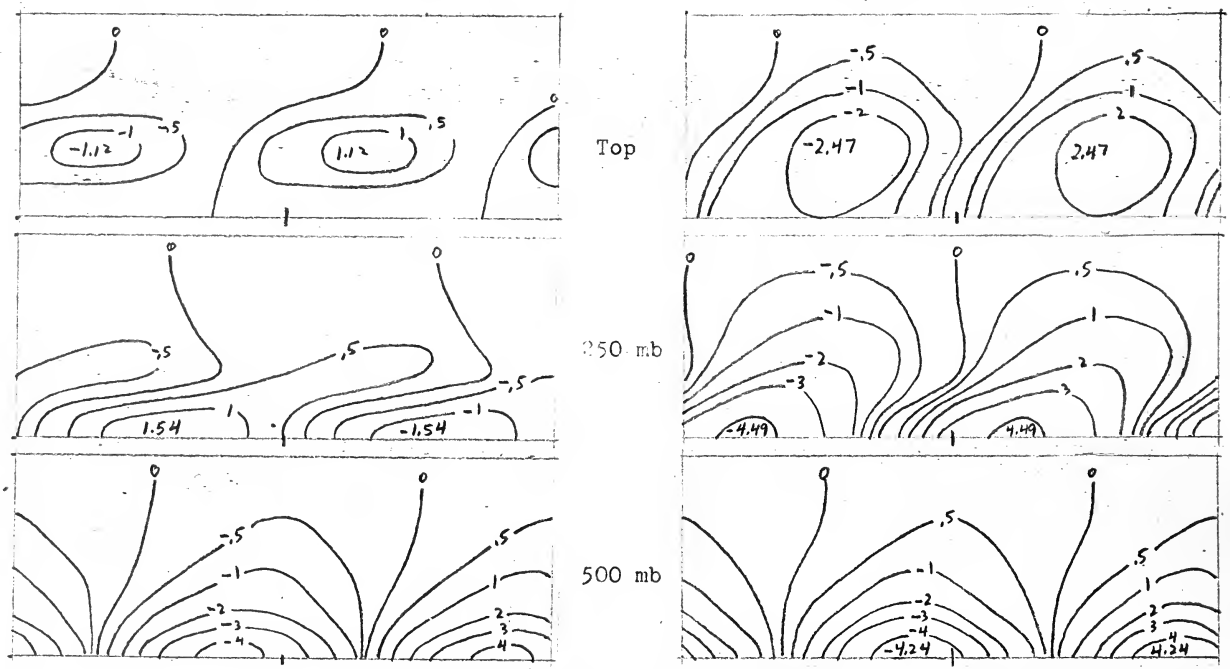

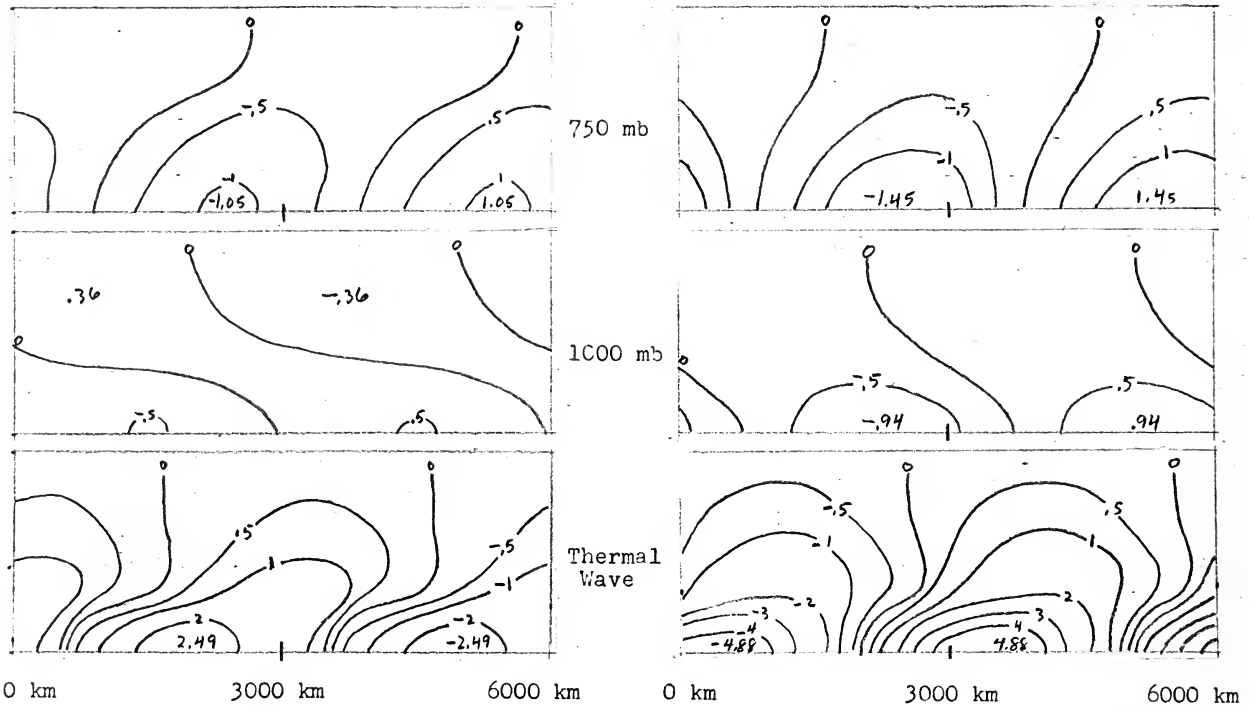

Figure 10.3. Case 10. (λ = 6000 km), Perturbation Stream Function (Ψ').

t = 72 hr

Top

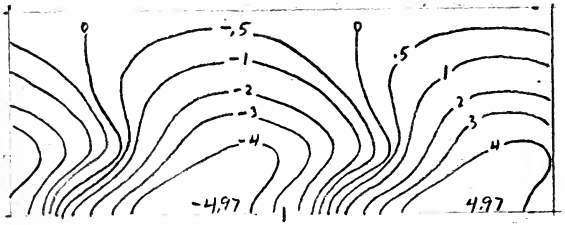

250 mb

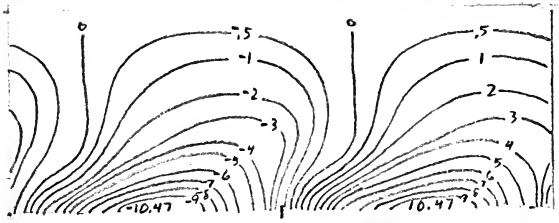

500 mb

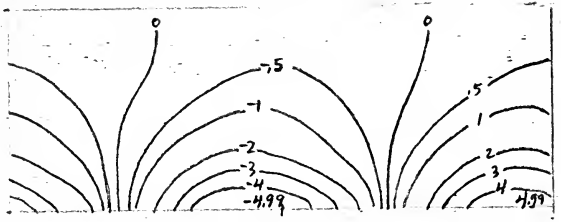

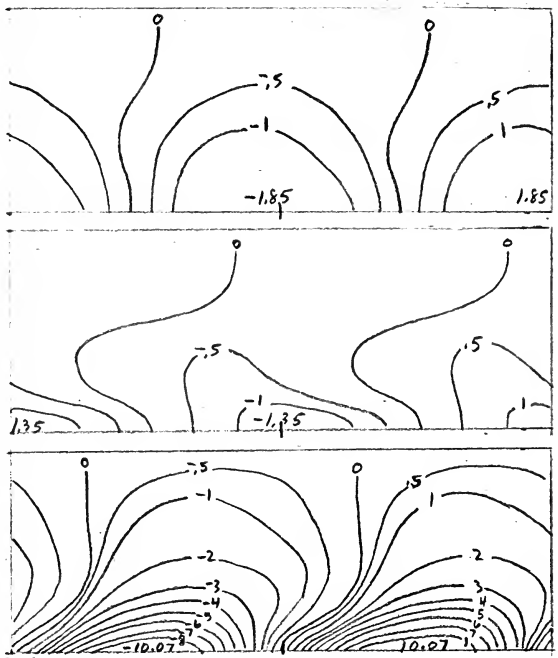

Figure 10.4. Case 10 (λ = 6000 km), Perturbation Stream Function (Ψ').

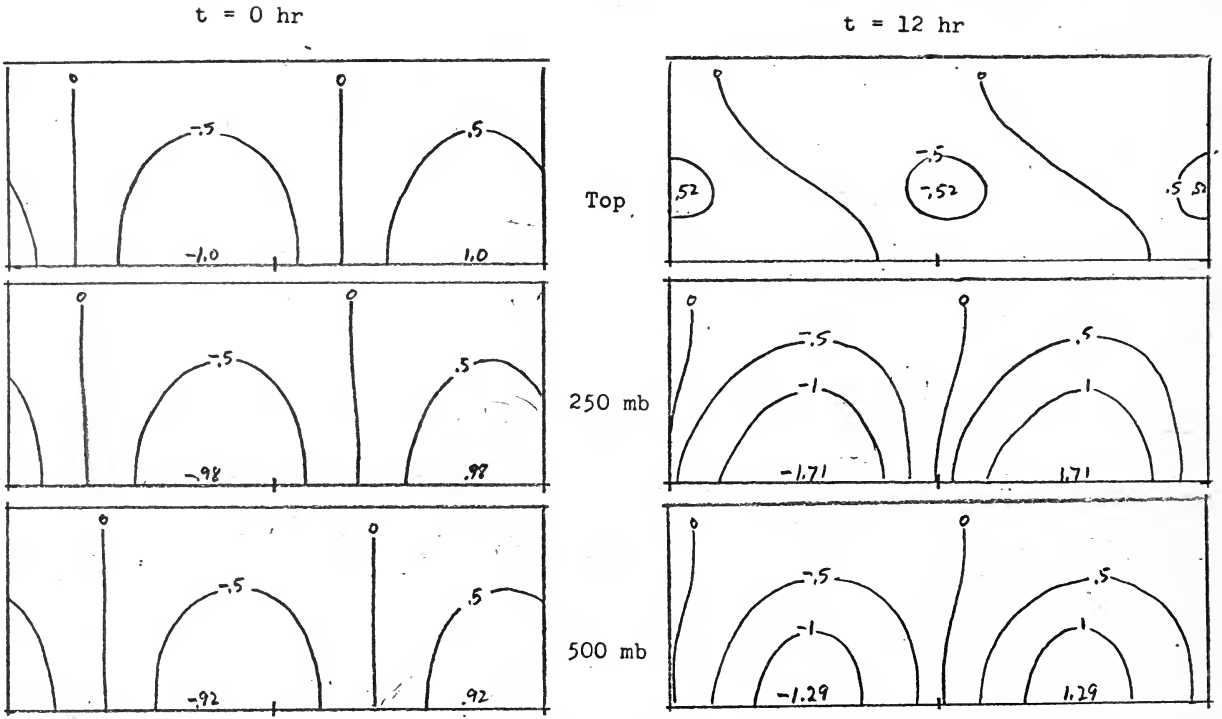
t = 0 hr
t = 12 hr
Top
250 mb
500 mb
0
-.5
.5
-1.0
1.0
-.98
.98
-.92
.92
-.52
-1
-1.71
1.71
-1.29
1.29

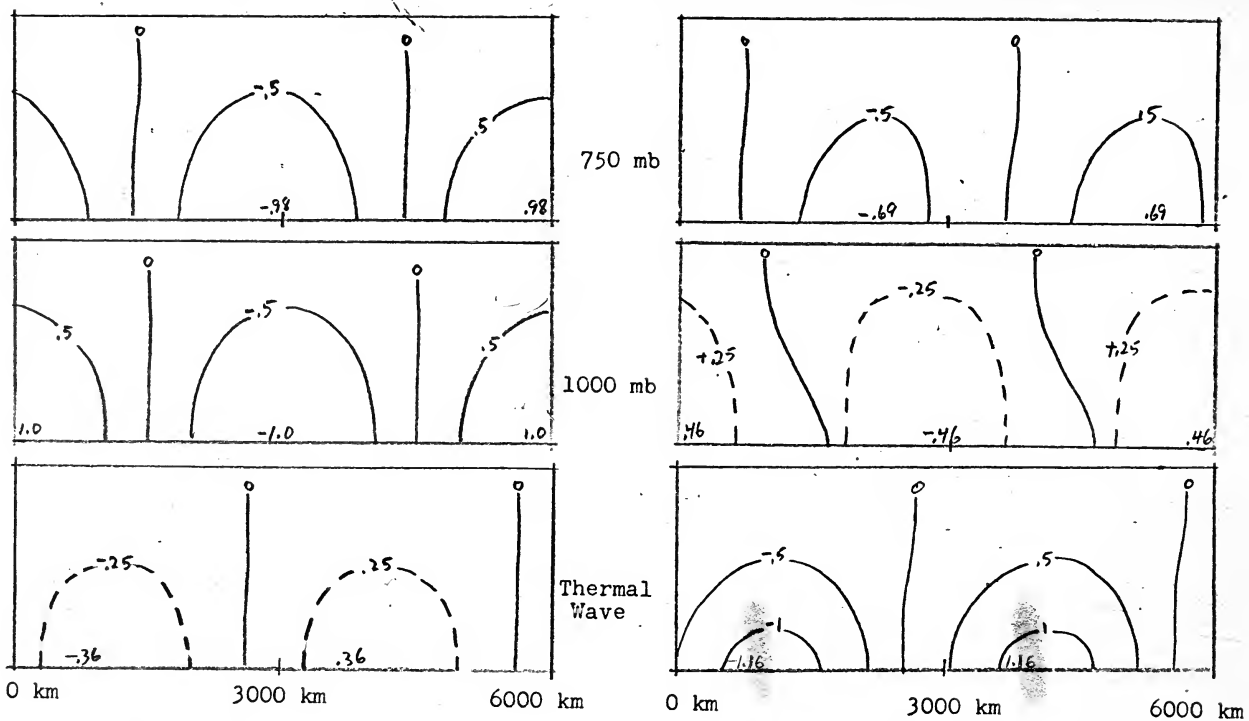

Figure 11.1. Case 11 (λ = 6000 km), Perturbation Stream Function (Ψ').

t = 24 hr

t = 36 hr

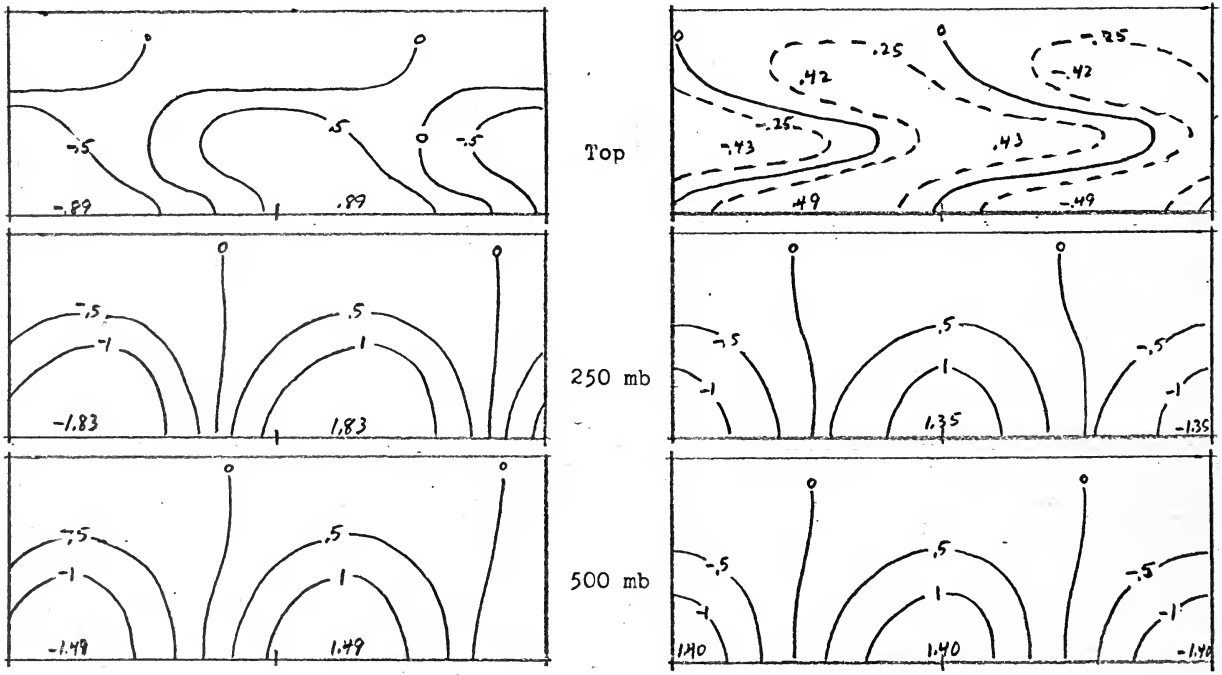
Top
250 mb
500 mb
-.5
.5
-.89
.89
-1
1
-1.83
1.83
-1.49
1.49
.25
.42
-.25
-.42
.43
-.43
.49
-.49
1.35
-1.35
1.40
-1.40

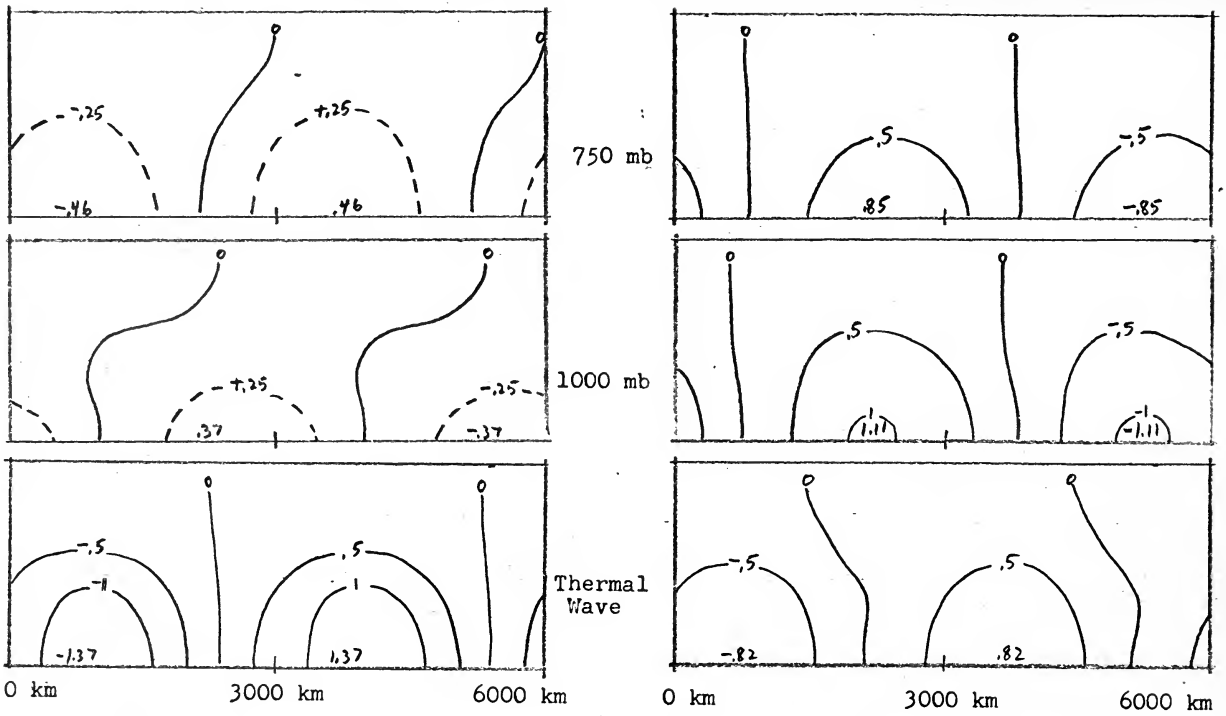

Figure 11.2. Case 11 (λ = 6000 km), Perturbation Stream Function (Ψ').

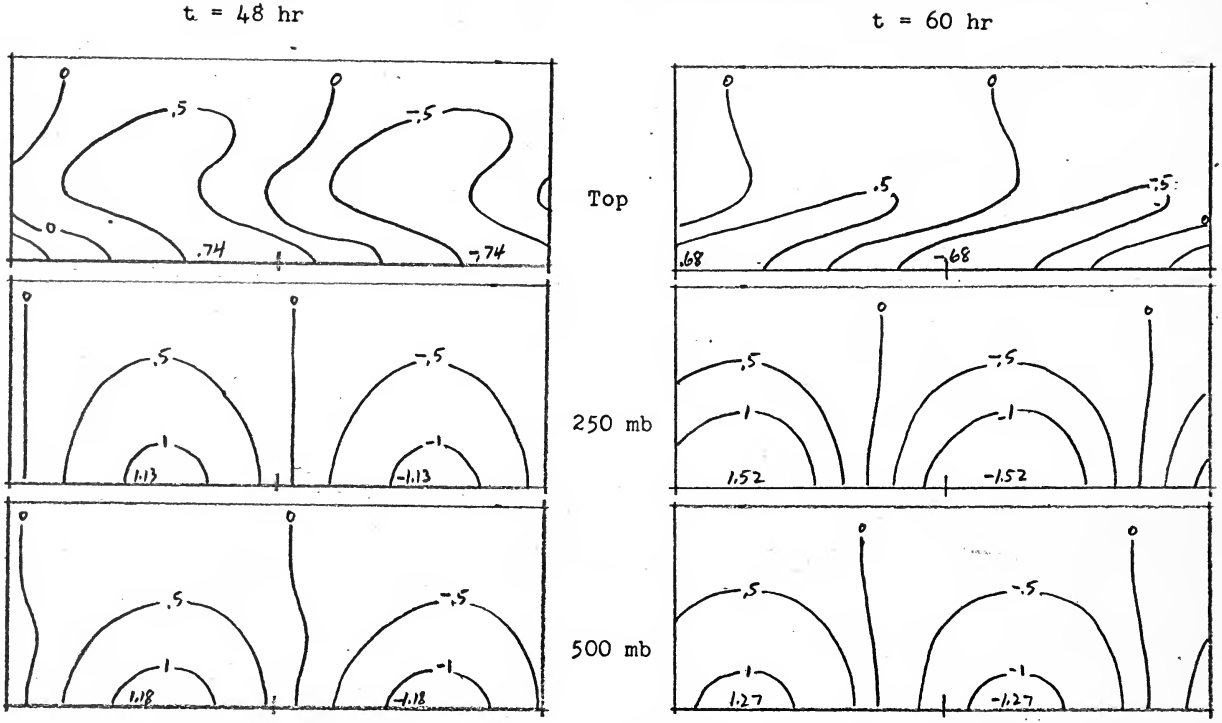
t = 48 hr
t = 60 hr
Top
250 mb
500 mb
0
.5
-.5
.74
-.74
1
-1
1.13
-1.13
1.18
-1.18
.68
-.68
1.52
-1.52
1.27
-1.27

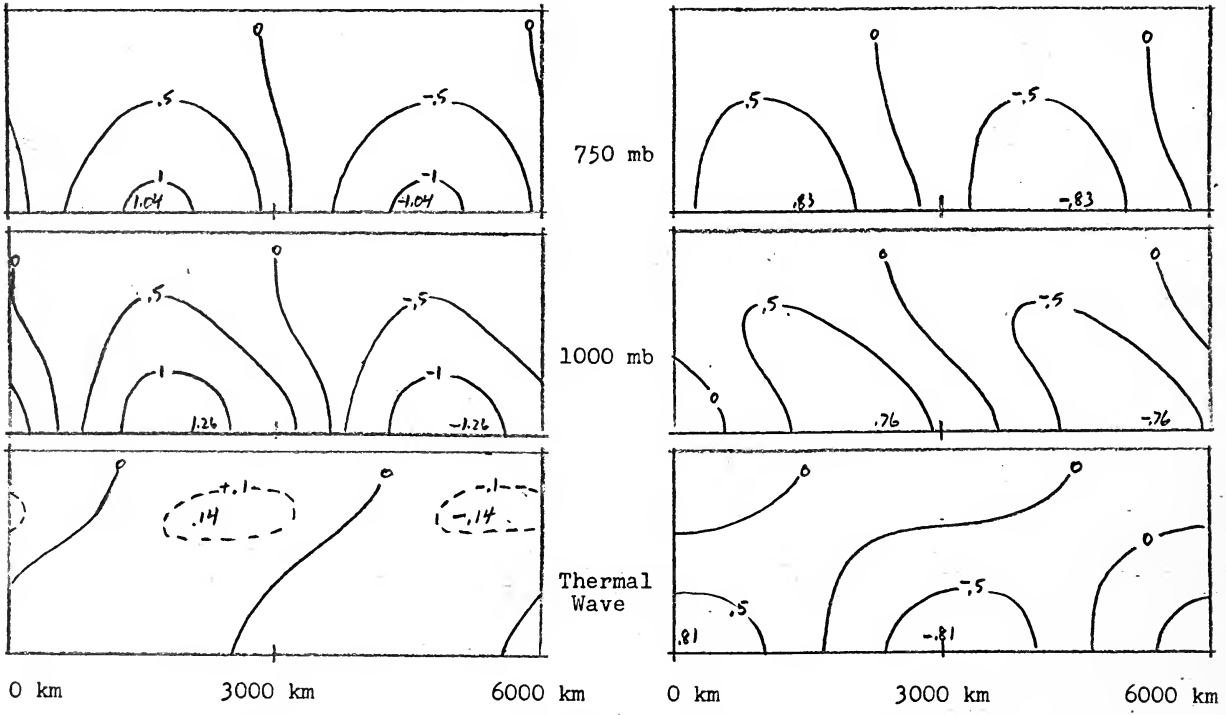

Figure 11.3. Case 11 (λ = 6000 km), Perturbation Stream Function (Ψ').

t = 72 hr

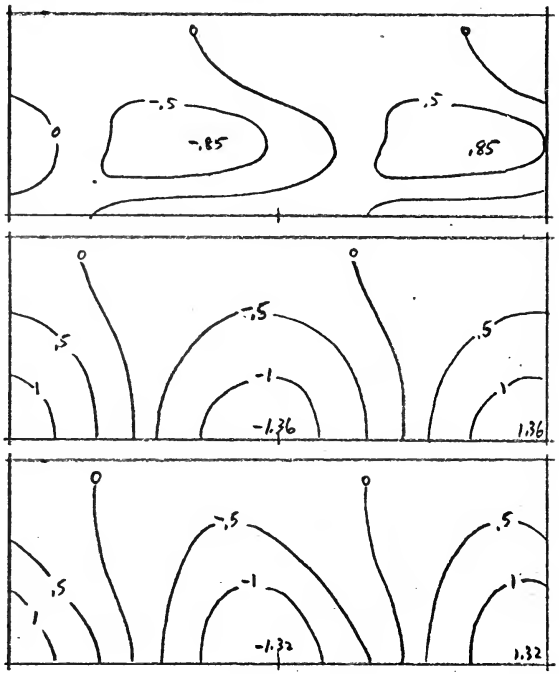

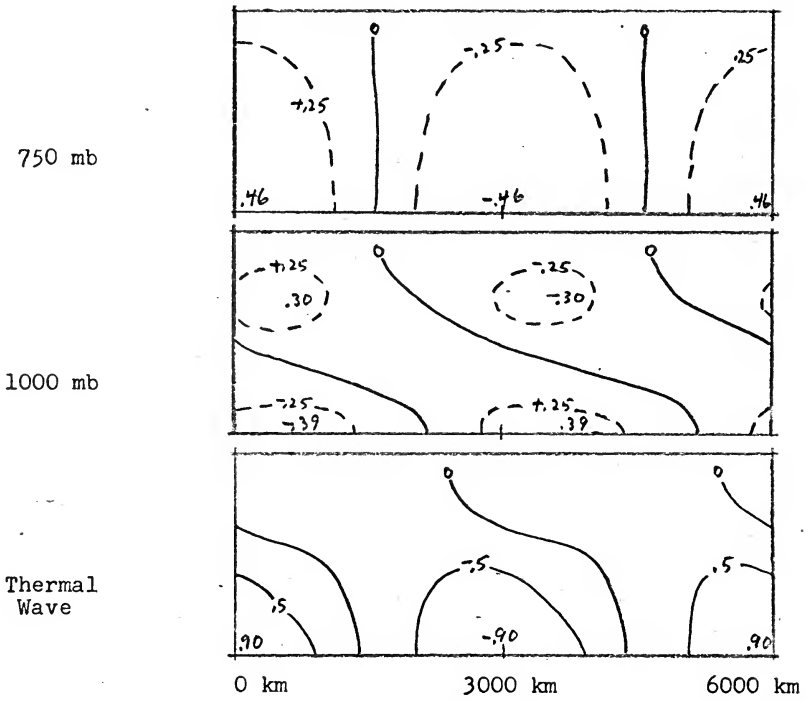

Figure 11.4. Case 11 (λ = 6000 km), Perturbation Stream Function (Ψ').

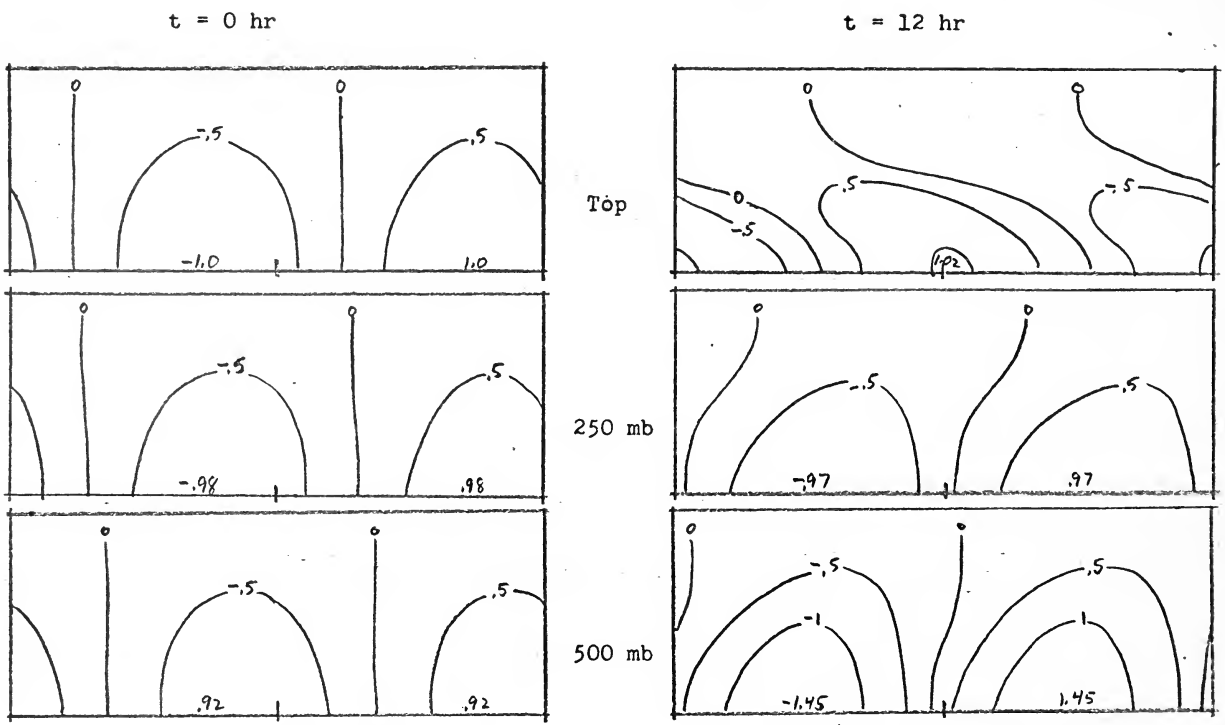
t = 0 hr
t = 12 hr
Top
250 mb
500 mb
0
-.5
.5
-1.0
1.0
-.98
.98
.92
-1
1
-1.45
1.45
-.97
.97

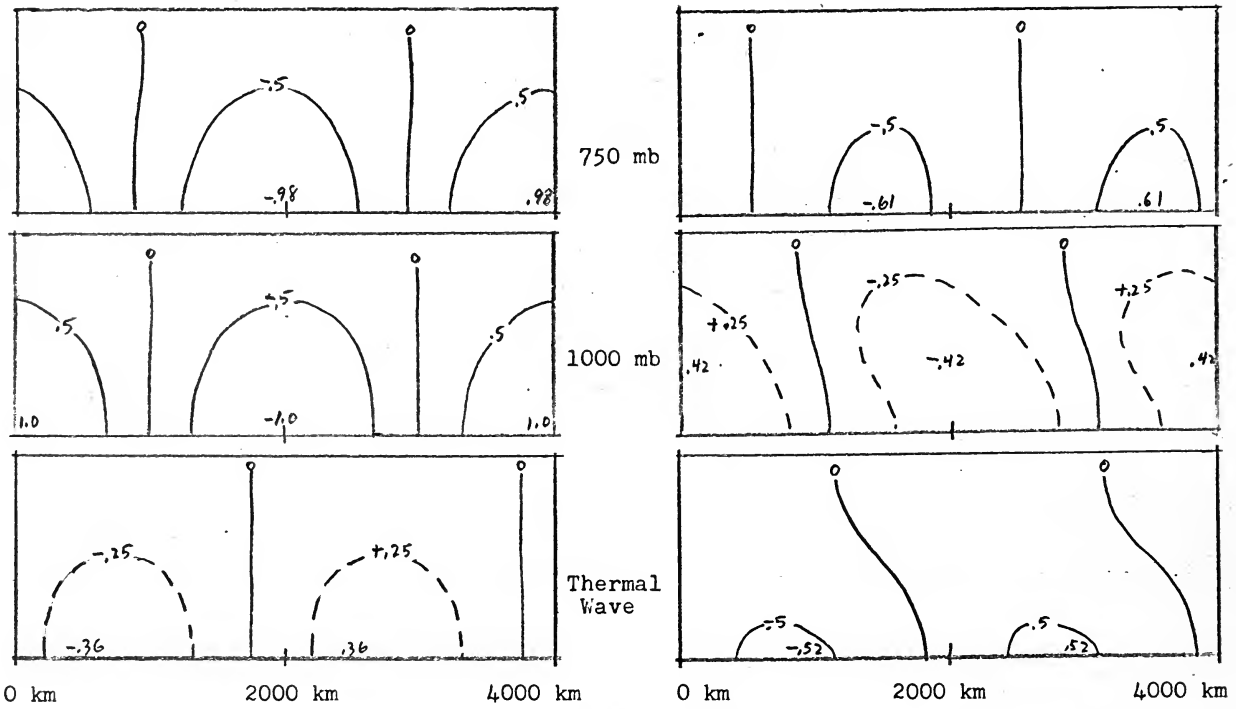

Figure 12.1. Case 12 (λ = 4000 km), Perturbation Stream Function (Ψ').

t = 24 hr

t = 36 hr

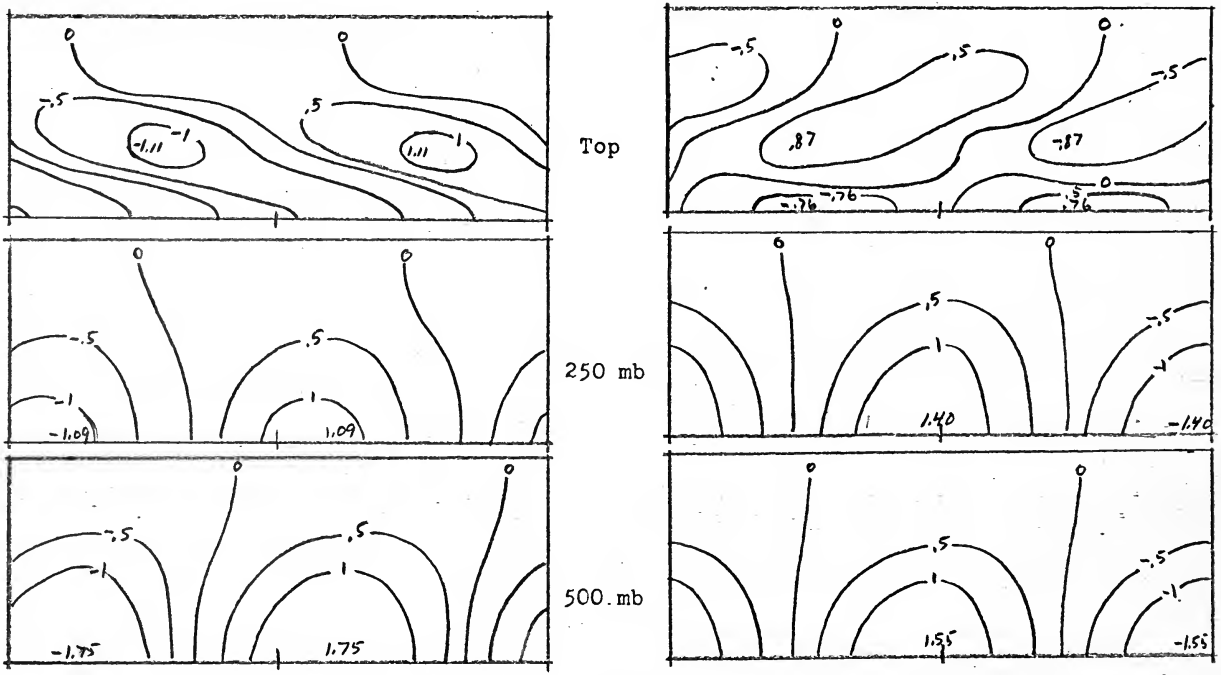
Top
250 mb
500 mb
0
-.5
.5
-1
1
-1.11
1.11
-1.09
1.09
-1.75
1.75
.87
-.87
-.76
.76
1.40
-1.40
1.55
-1.55

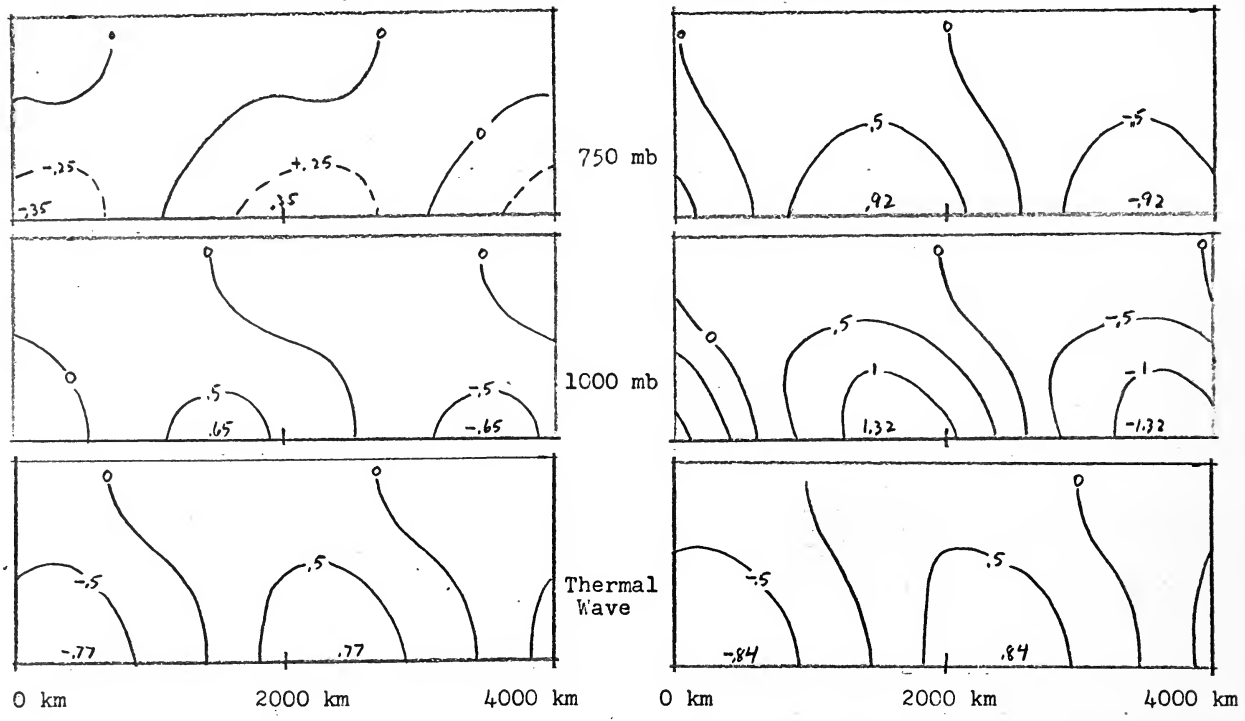

Figure 12.2. Case 12 (λ = 4000 km), Perturbation Stream Function (Ψ').

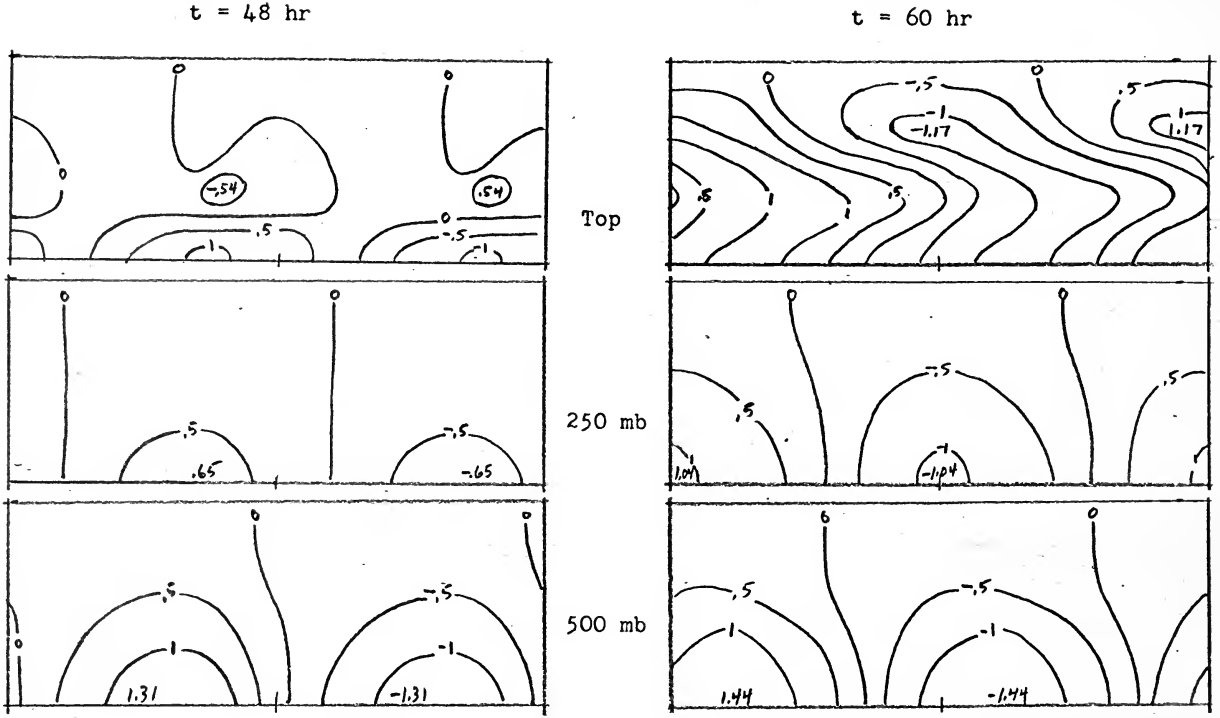
t = 48 hr
t = 60 hr
Top
250 mb
500 mb
0
.5
-.5
-1
-.54
.54
.65
-.65
1.31
-1.31
1.17
1.04
-1.04
1.44
-1.44

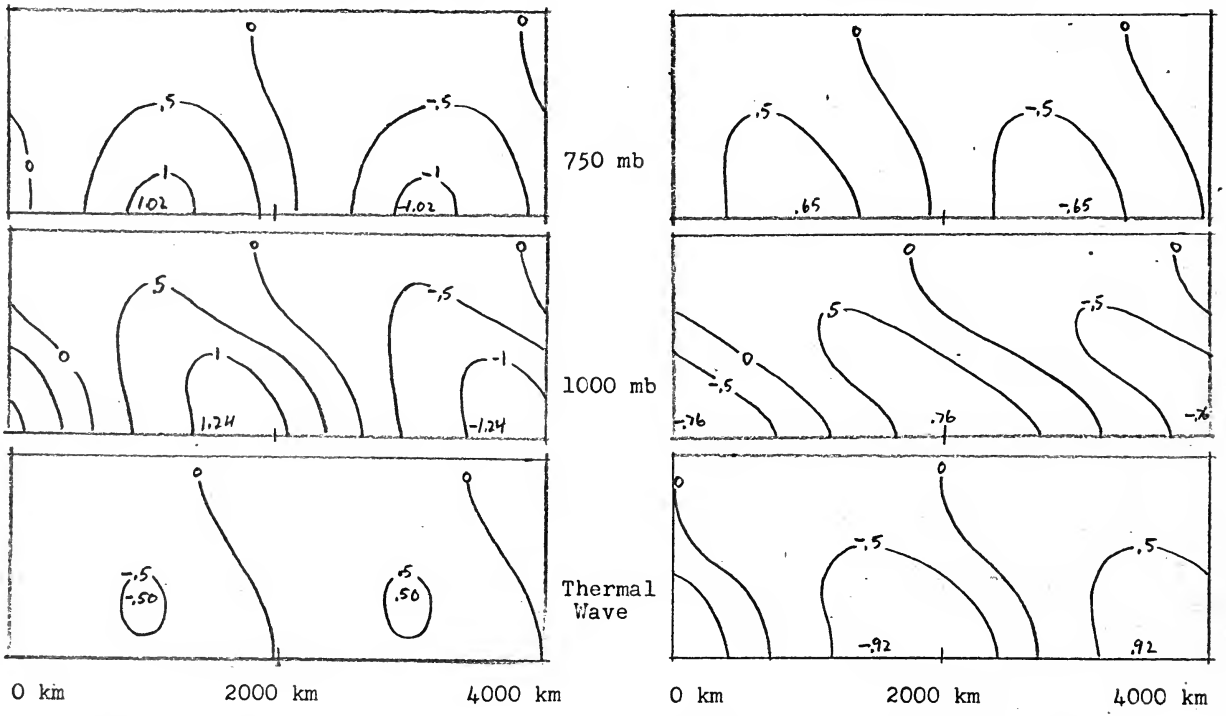

Figure 12.3. Case 12 (λ = 4000 km), Perturbation Stream Function (Ψ').

t = 72 hr

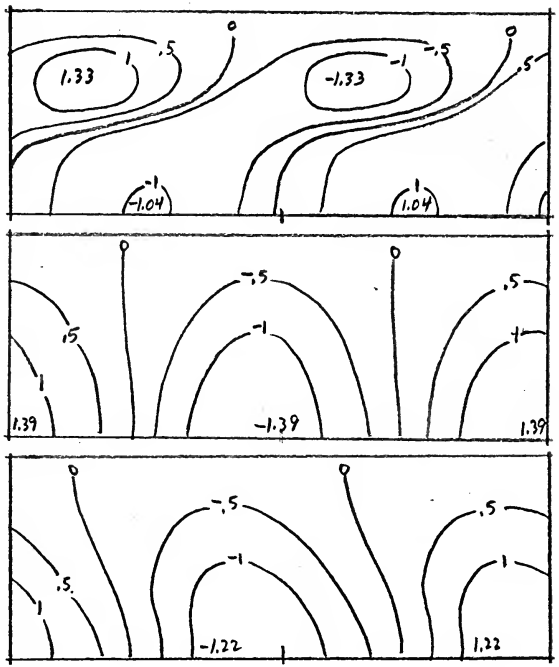

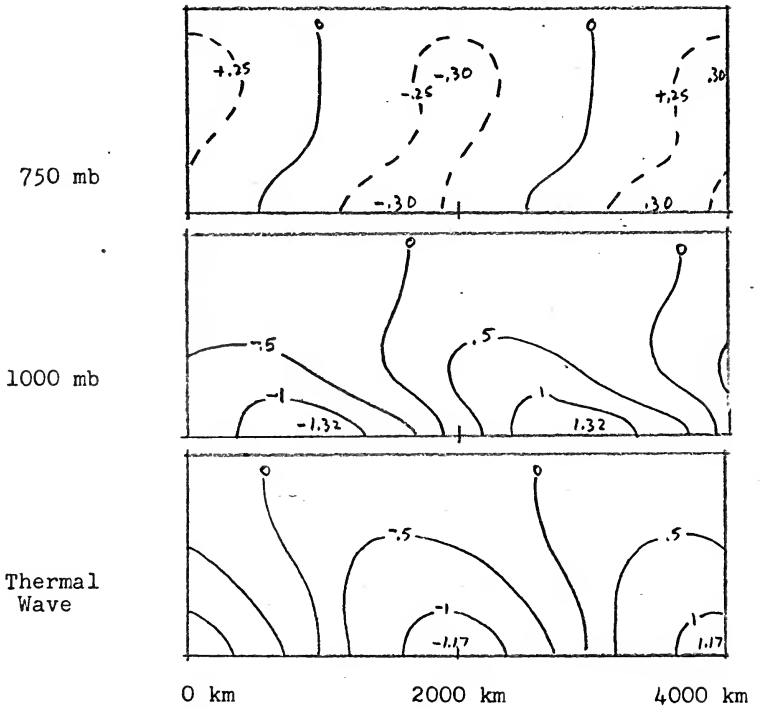

Figure 12.4. Case 12 (λ = 4000 km), Perturbation Stream Function (Ψ').

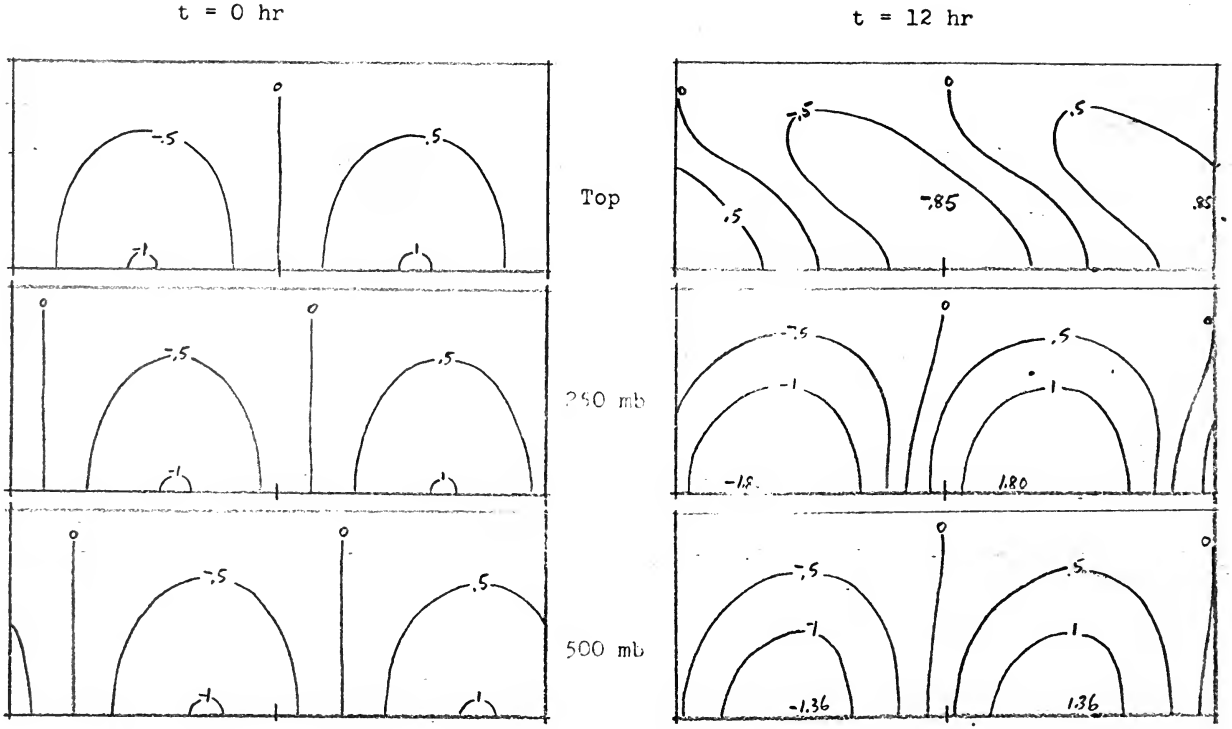
t = 0 hr
t = 12 hr
Top
250 mb
500 mb
-.5
.5
-1
1
0
-.85
.85
-1.8
1.80
-1.36
1.36

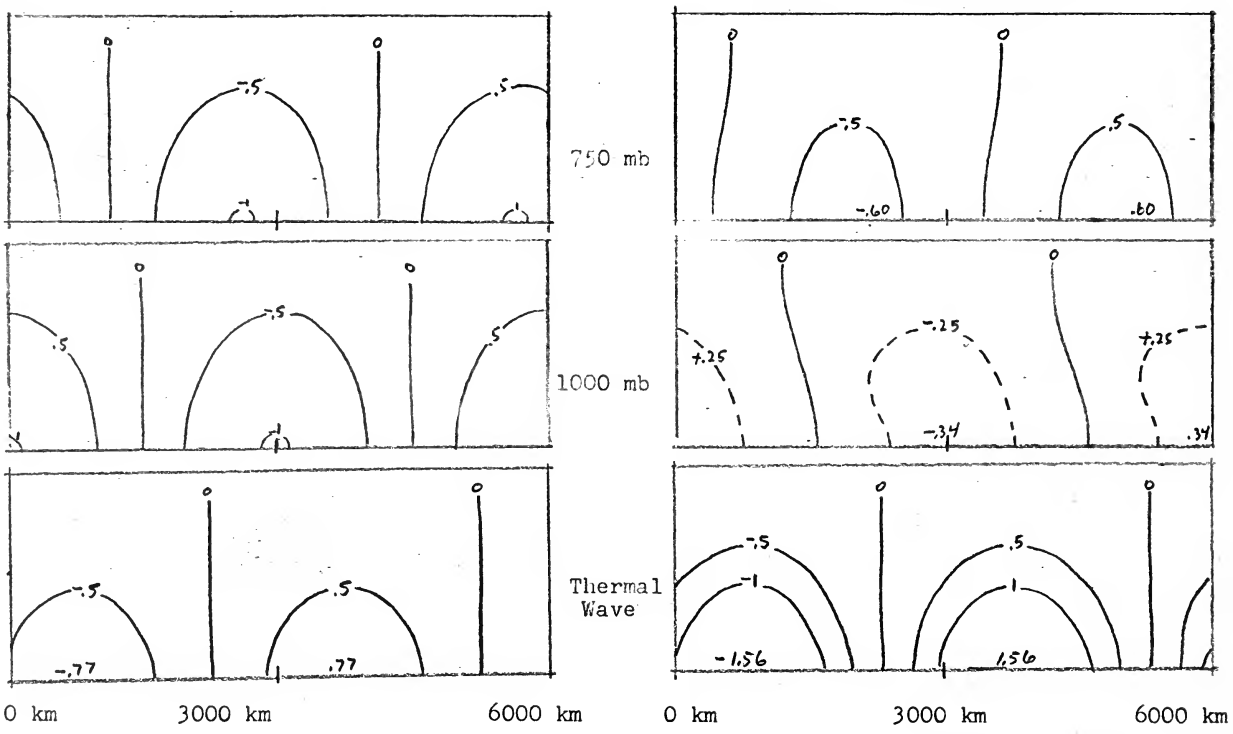

Figure 13.1. Case 13, (λ = 6000 km), Perturbation Stream Function (Ψ').

t = 24 hr

t = 36 hr

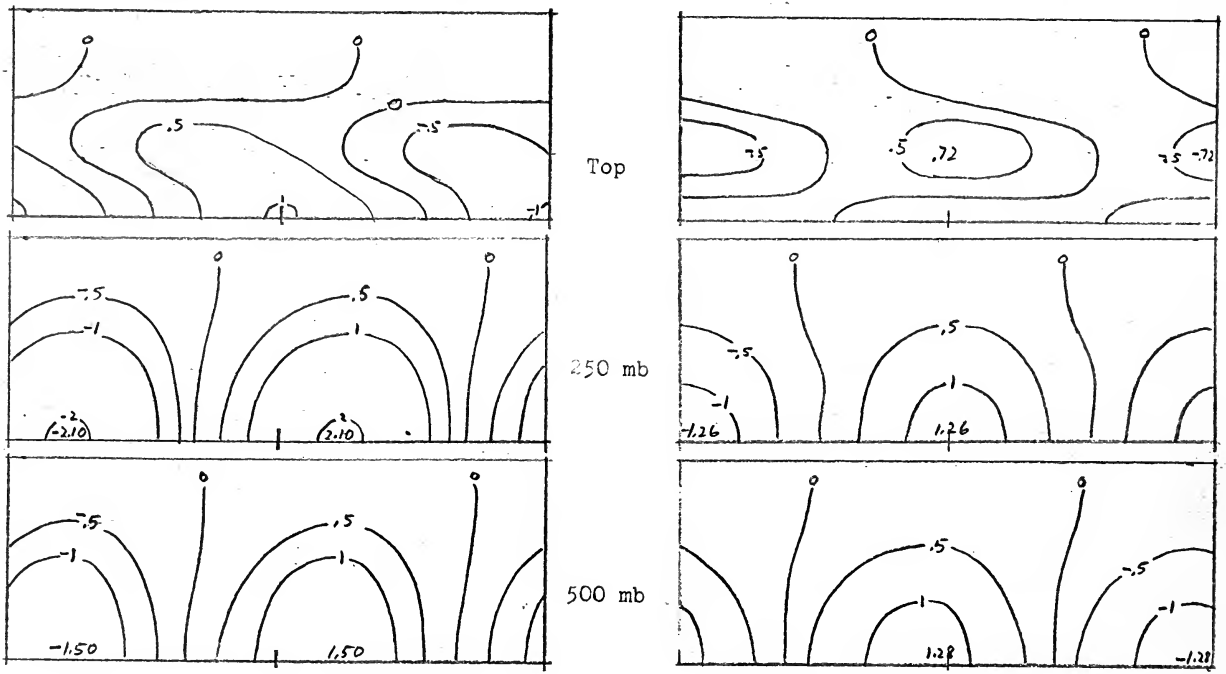

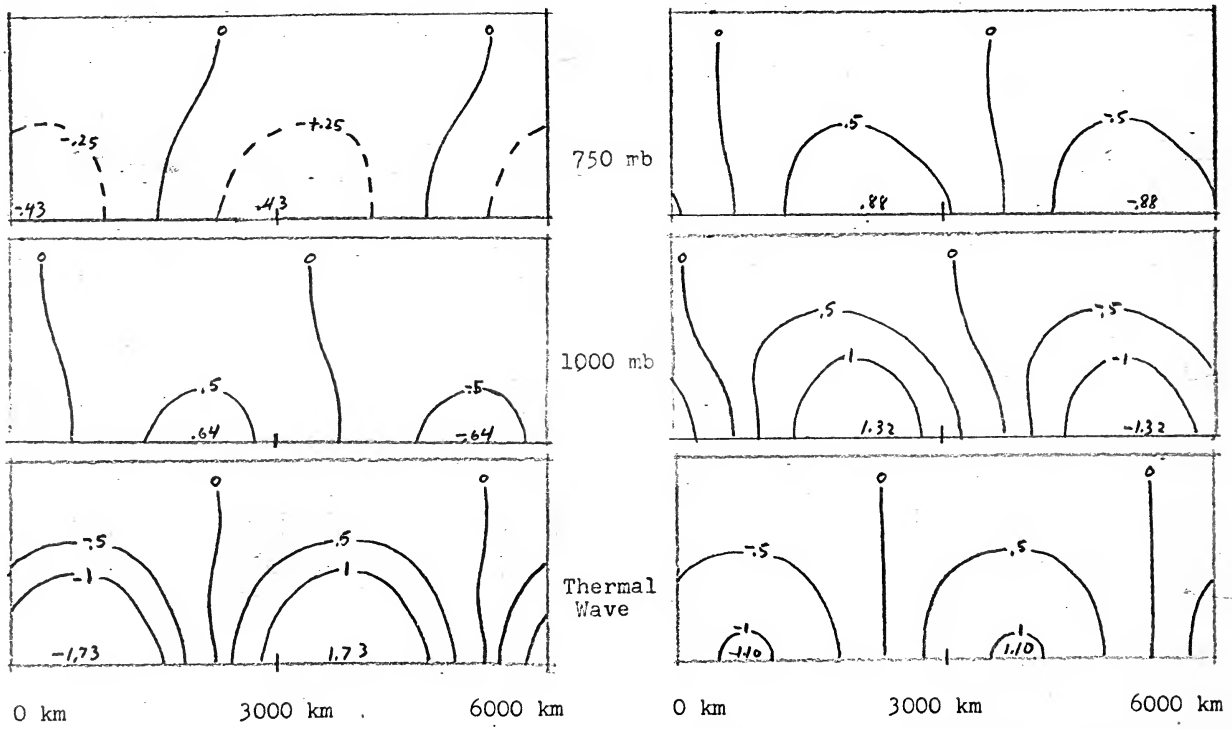

Figure 13.2. Case 13 (λ = 6000 km), Perturbation Stream Function (Ψ').

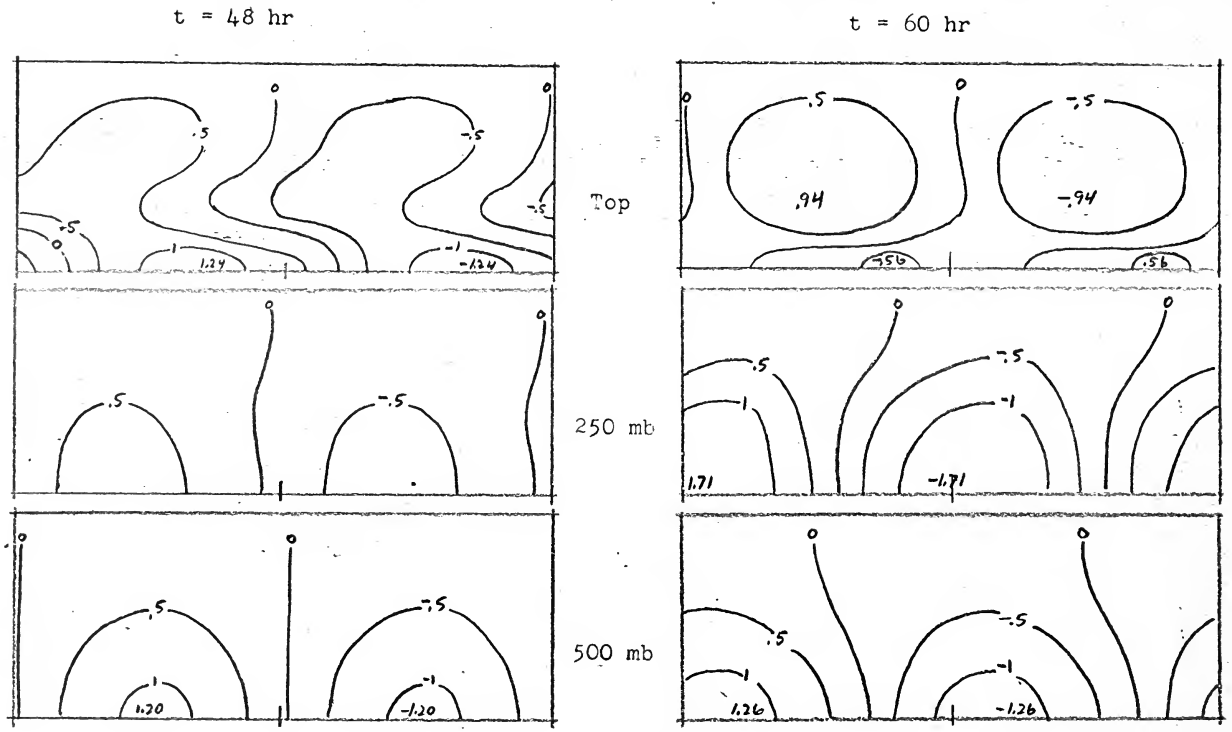
t = 48 hr
t = 60 hr
Top
250 mb
500 mb
.5
0
-.5
1
-1
1.24
-1.24
.94
-.94
.56
-.56
1.71
-1.71
1.20
-1.20
1.26
-1.26

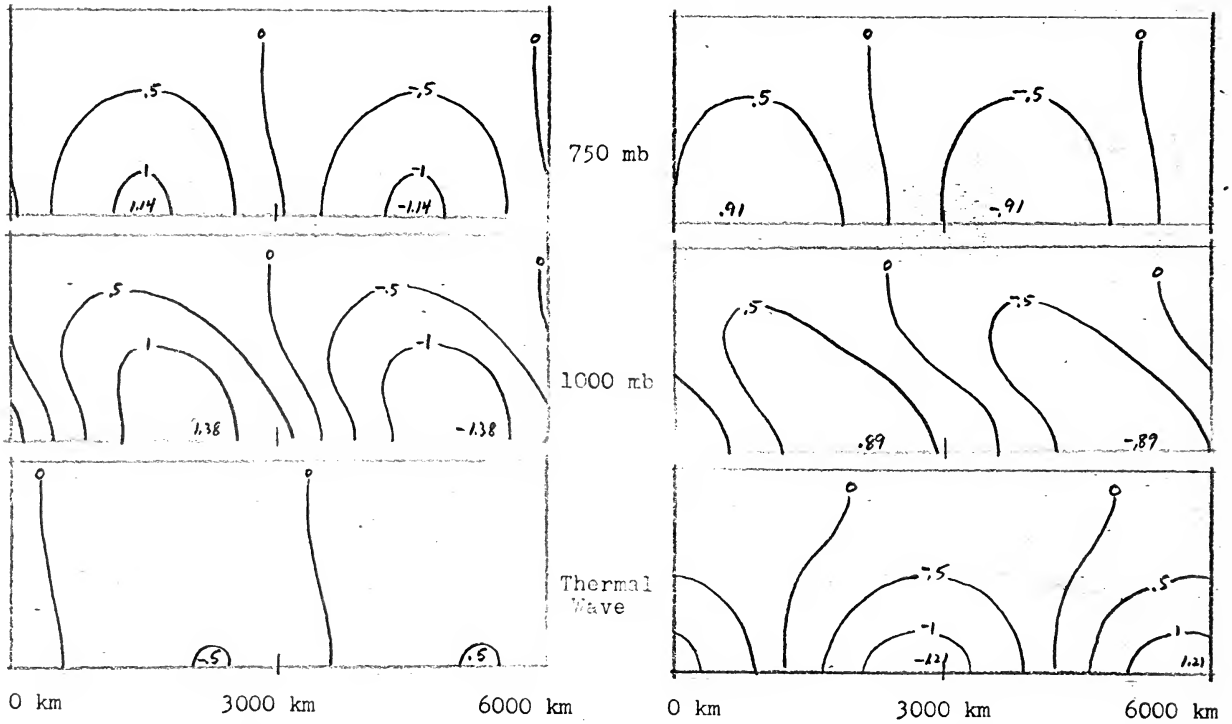

Figure 13.3. Case 13 (λ = 6000 km), Perturbation Stream Function (Ψ').

t = 72 hr

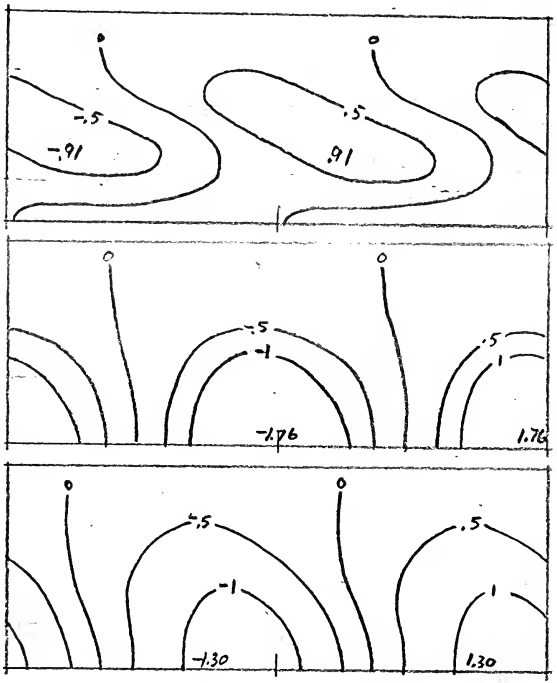

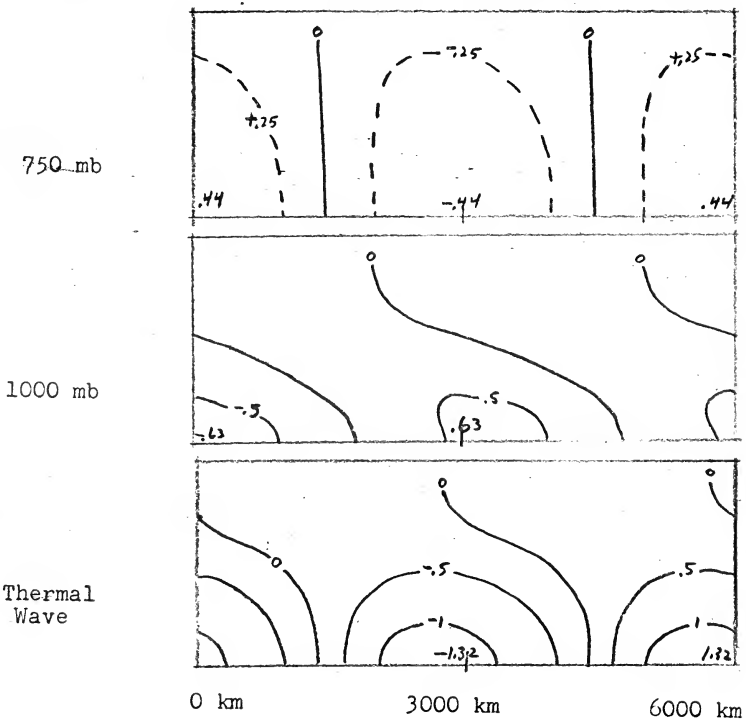

Figure 13.4. Case 13 (λ = 6000 km), Perturbation Stream Function (Ψ').

thesL615
Morphology of unstable waves in a barocl
3 2768 002 11895 2
DUDLEY KNOX LIBRARY